THE ROLE OF ER STRESS IN LIPOGENESIS AND INSULIN RESISTANCE IN RESPONSE TO OVER NUTRITION

A Thesis Submitted in Fulfilment of the Requirements for the Degree of Doctor of Philosophy

Ruoqiong Sun
Master of Science

Supervisors:

Professor Jiming Ye, PhD

Dr Juan Carlos Molero

School of Health Science

College of Science, Engineering and Health

RMIT University

July 2014

DECLARATION

I, the candidate, Ruoqiong Sun, certify that:

a) except where due acknowledgement has been made, the work is that of the candidate alone;

b) the work has not been submitted previously, in whole or in part, to qualify for any other academic award;

c) the content of the thesis is the result of work which has been carried out since the official commencement date of the approved research program;

d) any editorial work, paid or unpaid, carried out by a third party is acknowledged;

e) ethics procedures and guidelines have been followed.

Signature of the candidate

Ruoqiong Sun

Molecular Pharmacology for Diabetes Group

School of Health Science

RMIT University

Bundoora Victoria 3083

Australia

PUBLICATIONS AND PRESENTATIONS

Publications originating from this thesis:

SM Chan, **RQ Sun** (co-first author), XY Zeng, ZH Choong, H Wang, MJ Watt and JM Ye, Activation of PPARalpha ameliorates hepatic insulin resistance and steatosis in high fructose-fed mice despite increased ER stress. Diabetes, 2013. 62: 2095-105 (Chapter 4)[1].

RQ Sun, H Wang, XY Zeng, SP Li, SL Leung, JC Molero and JM Ye, IRE1 initiates the impairment of insulin signal transduction in the liver of high fructose-fed mice via JNK activation independent of lipid accumulation (submitted on July 2014) (Chapter 3).

SM Chan, **RQ Sun**, XY Zeng, H Wang, X Zhou, SL Leung, SP Li, AM Xu, JC Molero, MJ Watt and JM Ye, UPR associated diacylglycerol repartitioning by fenofibrate protects against hepatic insulin resistance independent of steatosis in high fat-fed mice (submitted on July 2014) (Chapter 6)[2].

Contribution to other publications

LP Ren. SM Chan, XY Zeng, DR Laybutt, TJ Iseli, **RQ Sun**, EW Kraegen, GJ Cooney, N Turner and JM Ye. Differing endoplasmic reticulum stress response to excess lipogenesis versus lipid oversupply in relation to hepatic steatosis and insulin resistance. PLoS One. 2012, 7, e30816.

H Wang, **RQ Sun**, XY Zeng, SM Chan, X Zhou, SP Li, E Jo, JC Molero and JM Ye, Restoration of autophagy alleviates ER stress and impaired insulin signaling transduction in high fructose fed mice. Endocrinology. 2014 Oct 24:en20141454.

---

[1] SM Chan designed the study, contributed to the research data, and wrote the manuscript. RQ Sun contributed to the research data and wrote the manuscript. XY Zeng, ZH Choong and H Wang contributed to the research data. MJ Watt. contributed to the research data and provided reagents, materials, and analysis tools. JM Ye conceived and designed the study, provided reagents, materials, and analysis tools, and wrote the manuscript.

[2] SM Chan designed the study, contributed to the research data, and wrote the manuscript. RQ Sun contributed to the research data and wrote the manuscript. XY Zeng, H Wang, X Zhou, SL Leung and SP Li contributed to the research data. AM Xu, JC Molero and MJ Watt contributed to the research data and provided reagents, materials, and analysis tools. JM Ye conceived and designed the study, provided reagents, materials, and analysis tools, and wrote the manuscript.

Presentations at Conferences (National and International):

Oral Presentation:

RQ Sun, SM Chan, XY Zeng, H Wang, JC Molerol and JM Ye. Differential involvement of unfolded protein response pathways in the onset of *de novo* lipogenesis and insulin resistance in the liver. *The Annual Scientific Meeting of the Australia Diabetes Society and the Australia Diabetes Educators Association (ADS & ADEA)*, Gold Coast, Australia, 2012.

Posters:

RQ Sun, SM Chan, XY Zeng, H Wang, X Zhou, SP Li and JM Ye, Fenofibrate eliminates hepatic insulin resistance in high hat feeding while activating unfolded protein response pathways. *World Diabetes Congress (by International Diabetes Federation)*, Melbourne, Australia, 2013.

ACKNOWLEDGEMENTS

LIST OF ABBREVIATIONS

ACC	Acetyl-CoA carboxylase
AGPAT	Sn-1-acyl-glycerol-3-phosphate acyltransferase
Akt/PKB	Protein kinase B
apoB	Apolipoprotein B
APR	Acute-phase response
AR	Aldose reductase
ASK	Apoptosis-signaling kinase
ATF	Activating transcription factor
BSA	Bovine serum albumin
CHOP	C/EBP-homologous protein
ChREBP	Carbohydrate response element binding protein
DAG	1,2-diacyglycerol
DGAT	Sn-1,2-diacylglycerol acyltransferase
DHAP	Dihydroxyacetone phosphate
DNL	*De novo* lipogenesis
eIF2α	Eukaryotic translation initiator factor 2α
ER	Endoplasmic reticulum
ERAD	ER-associated protein degradation
ERSE	ER stress-response element
F1P	Fructose-1-phosphate
FAS	Fatty acid synthase
FoxO	Forkhead box protein
G3P	Glycerol-3-phosphate
GA3P	Glyceraldehyde-3-phosphate
GADD34	Growth arrest and DNA damage-inducible protein 34
GLUT	Glucose transporter
GPAT	Sn-1-glycerol-3-phosphate acyltransferase
GRP	Glucose-regulated protein
GSK3	Glycogen synthase kinase-3
HFCS	High fructose corn syrup
iAUC	Incremental area under curve
IKK	IκB kinase-β
IL-23	Interleukin 23
Insig	Insulin-induced gene
IR	Insulin receptor
IRE1	Inositol-requiring protein 1
IRS	Insulin receptor substrate
JNK	C-Jun NH2-terminal kinase
LPA	Lysophosphatidic acid
LXR	Liver X receptor
mTOR	Mammalian target of rapamycin
MTTP	Microsomal triglyceride transfer protein
NADP	Nicotinamide adenine dinucleotide phosphate
NAFLD	Non-alcoholic fatty liver disease
NF-κB	Nuclear factor kappa-light-chain-enhancer of activated B cells
NRF2	NF-E2-related factor 2
PDK	Phosphoinositide-dependent kinase

PERK	PKP-like endoplasmic reticulum kinase
PFK	Phosphofructokinase
PI3K	Phosphatidylinositol-3-kinase
PIP2	Phosphatidylinositol-4,5-bisphosphate
PIP3	Phsphoinositide-3,4,5-trisphosphate
PKC	Protein kinase C
PPAR	Peroxisome proliferator-activated receptor
PSG	Penicillin-Streptomycin-Glutamine
RER	Respiratory exchange ratio
S1P	Site-1 protease
S2P	Site-2 protease
SCAP	SREBP-cleavage activating protein
SCD	Stearoyl-CoA desaturase
SHP	Small heterodimer protein
SPT	Serine palmitoyltransferase
SREBP	Sterol regulatory element binding protein
TBST	Tris Buffered Saline plus 0.1% Tween-20
Thr	Threonine
TNF	Tumour necrosis factor
TRAF2	TNF receptor-associated factor 2
TRB3	Tribbles homolog 3
TUDCA	Tauroursodeoxycholic acid
Tyr	Tyrosine
UPR	Unfolded protein response
VLDL	Very low density lipoprotein
VO2	Oxygen consumption rate
XBP1	X-binding protein 1

TABLE OF CONTENTS

LIST OF FIGURES

LIST OF TABLES

ABSTRACT

Insulin resistance is one of the major defects of type 2 diabetes. Liver, muscle and adipose tissue are the major sites responsive to the regulation of glucose homeostasis in response to insulin action. It has been demonstrated that hepatic insulin resistance occurs prior to peripheral insulin resistance. Excess lipid accumulation from dietary fat and *de novo* lipogenesis (DNL) has been suggested to be a trigger of hepatic insulin resistance. In the past decade, endoplasmic reticulum (ER) stress emerges to play a role in lipid metabolism and insulin resistance in the liver. However, the mechanisms of the development of insulin resistance that related to either lipid accumulation or ER stress remain unclear. Several pathways have been proposed to link lipid accumulation, ER stress and insulin resistance in the liver, such as JNK which is suggested to be activated by ER stress and affect insulin sensitivity negatively.

The aims of the thesis were to investigate: 1) the role of ER stress in lipid synthesize (lipogenesis) and the development of lipid-related insulin resistance in the liver and, 2) the effect that lipogenesis and ER stress have on each other.

The first study was designed to determine the contribution of either ER stress or lipid accumulation to the onset of hepatic insulin resistance induced by high fructose (HFru) feeding in mice. After feeding with high fructose for one day, ER stress was activated only in inositol-requiring protein 1 (IRE1)/X-box protein 1 (XBP1) branch of the unfolded protein response (UPR) pathways. Simultaneously, the expression of lipogenic transcription factors and enzymes was upregulated and the lipid content in the liver was increased. Besides the absence of glucose intolerance, insulin-stimulated phosphorylation of Akt was suppressed. Blocking IRE1 activity with the chemical chaperone tauroursodeoxycholic acid (TUDCA) abolished fructose-dependent increases in JNK activity and IRS serine phosphorylation, and protected insulin-stimulated Akt phosphorylation without altering hepatic steatosis or protein

kinase C (PKC) ε, a key enzyme involved in lipid-induced insulin resistance. These data together suggest that activation of JNK rather than lipid accumulation is a key early trigger of ER stress related insulin resistance induced by HFru feeding in the liver. In addition, activation of ER stress and lipogenesis closely correlated in response to HFru feeding.

To interrogate the role of either increasing lipid accumulation or activation of JNK and IKK in hepatic insulin resistance induced by high fructose, a hepatic steatosis-independent ER stress model was developed. Animals were fed with high fructose diet for 2 weeks. Fenofibrate, a peroxisome proliferator-activated receptor α (PPARα) agonist, was administrated to reduce lipid accumulation while maintaining elevated DNL in the liver. Fenofibrate administration completely eliminated HFru-induced glucose intolerance and hepatic steatosis and insulin signal transduction. Both IRE1/XBP1 and PKP-like endoplasmic reticulum kinase (PERK)/ Eukaryotic translation initiator factor 2α (eIF2α) branches were activated. Fenofibrate treatment markedly increased fatty acid oxidation and eliminated the accumulation of diacyglycerols (DAG) which is known to have a negative impact on insulin signaling. Despite the marked activation of UPR signaling, neither c-Jun NH2-terminal kinase (JNK) nor IκB kinase (IKK) was activated. These data suggest that lipid accumulation, rather than JNK or IKK activation, is pivotal for ER stress to cause hepatic insulin resistance when the mice were challenged with HFru diet for a long time.

In a different series of studies, mice were fed with a high fat (HFat) diet for either 1 day or 2 weeks. Hepatic DAG content was increased in the HFat-fed animals, indicating that the hepatic insulin resistance could result from elevated DAG level. Interestingly, unlike HFru-fed mice, HFat-fed mice did not show ER stress activation. The HFat-fed mice showed that insulin resistance was induced via different mechanisms in the face of fatty acid influx. These finding indicate that ER stress is unlikely to result from lipid accumulation.

To investigate the interaction between ER stress and lipogenesis, we utilized fructose to induce ER stress in cultured cells, aimed to mimic the HFru-feeding model in animals. Betulin, which can suppress the activity of lipogenic transcription factor sterol regulatory element binding protein (SREBP1c) was applied to cells treated with fructose. With the presence of betulin, lipogenic enzymes levels were significantly diminished. However, the magnified fructose-induced phosphorylation of IRE1 and eIF2α was not altered, suggesting that increasing lipogenesis does not contribute to the activation of IRE1 and PERK branches under the condition induced by fructose oversupply.

In summary, ER stress and DNL both contribute to HFru-induced hepatic insulin resistance. It seems that ER stress is more important in the early stage of the development of insulin resistance in the liver. Accordingly, lipid accumulation plays a critical role later on. The predominantly negative effect of JNK activation induced by IRE1 might be overcome by the persistently increasing lipid accumulation, possibly becomes a secondary inducer of insulin resistance in the long term. However, the relationship between these two mechanistic pathways and its implication in insulin resistance seems very complex and more studies are required.

The significance of these studies not only lies in bridging gaps in the current literature, but also in providing the basis for drug design and discovery towards preventing and treating type 2 diabetes.

Chapter 1

Introduction

1.1 Diabetes and insulin resistance

1.1.1 Diabetes

Diabetes is characterized by hyperglycemia (fasting blood glucose level ≥ 7.0 mmol/L) [1] that results from defects in the body's ability to produce and/or use insulin. It is estimated that 347 million people suffer this chronic disease by 2011 [2] and the population with diabetes is continuing to increase. Diabetes remarkably increases the risk of cardiovascular events and death and many complications such as retinopathy, neuropathy and nephropathy [3]. There are two major types of diabetes, namely type 1 diabetes (also known as juvenile or insulin-dependent diabetes) and type 2 diabetes (also known as adult-onset or non-insulin dependent diabetes). In the type 1 diabetes, little or no insulin that produced by β cell from pancreas stimulates glucose uptake into cells, resulting in an elevation of blood glucose. As the dysfunction of the β cell is due to the body's own immune system [4], type 1 diabetes is mainly regarded as autoimmune diseases. In contrast, type 2 diabetes is the most common form of diabetes which comprises 90% of people with diabetes. Type 2 diabetes derives from insulin resistance that leads to high blood glucose levels (hyperglycemia) [5]. Under physiological condition, blood glucose level is maintained by the circulating insulin. However, when the body becomes insulin resistant, the insulin at normal level is no longer able to keep the blood glucose homeostasis. To compensate for this disorder, more insulin is released from the pancreas, leading to a high concentration of insulin in the plasma (hyperinsulinemia). As the β cell becomes exhausted, circulating insulin levels decrease. Consequently, the body develops glucose intolerance and hyperglycemia. Thus, oral drugs and/or insulin injection is applied to maintain blood glucose levels. Type 2 diabetes is commonly diagnosed in the aged population [6]. However, there is an increased population of diabetic patients in younger people, even children. A healthy lifestyle including regular physical activity, healthy food and losing excess body weight can decrease the risk of the development of type 2 diabetes [7].

Diabetes is associated with a number of complications. These complications are wide ranging [8-11] and are due at least in part to chronic elevation of blood glucose levels, which leads to damage of blood vessels [12]. The complications resulting from the damage of blood vessels are termed as "microvascular disease", including eye disease (retinopathy) [13], kidney disease (nephropathy) [14] and neural damage (neuropathy) [15]. This thesis focused on the early events in the development of type 2 diabetes particularly, insulin resistance.

1.1.2   Insulin resistance

1.1.2.1   Physiological role of insulin in fuel metabolism

Insulin is a hormone secreted by pancreatic β cells and affects a wide range of physiological processes. Liver, muscle and adipose tissue are the three major tissues responsible for insulin action to regulate blood glucose level. High blood glucose levels after a meal promotes insulin secretion. After being taken up by the skeletal muscle and to a less extent by the liver, glucose is catalyzed to glycogen as energy storage, promoted by the insulin. At the same time, glycogenolysis and gluconeogenesis in the liver are suppressed. However, when glycogen levels in the liver are high, glycogen synthesize is suppressed. In this case, additional glucose taken up by liver cells is shunted into the synthesis of fatty acids, which are then transported from the liver into other tissues. Meanwhile, the rate of fatty acid oxidation is reduced. In the muscle, insulin increases the rate of glucose transport across the cell membrane, leading to enhanced glucose uptake from the bloodstream. Simultaneously, it stimulates the glycogen synthesize in the muscle to store glucose [16]. In adipose tissue, insulin stimulates the uptake of triglyceride from the blood and decreases lipolysis to maintain the plasma fatty acid level. Together with other hormones such as glucagon, insulin plays major roles in the regulation of

blood glucose concentration and overall flow of fuels. Insulin is also implicated in protein

metabolism, cell growth and survival [17].
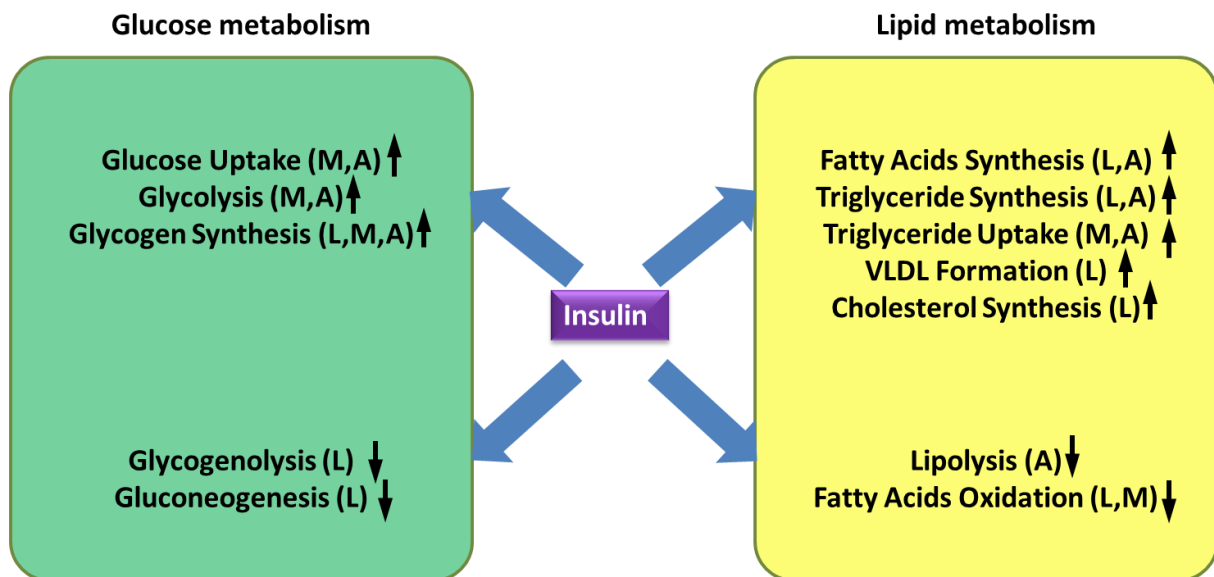
Figure 1.1 The effects of insulin on glucose metabolism and lipid metabolism.

Insulin is able to enhance glucose uptake and glycolysis in the muscle and adipose tissue. Besides these effects, insulin also enhances glycogen synthesize in the liver, muscle and adipose tissue. Glycogenolysis and gluconeogenesis in the liver are suppressed by insulin. Fatty acids and triglyceride synthesize in the liver and adipose tissue is upregulated by insulin as well as triglyceride uptake in the muscle and adipose tissue. VLDL formation and cholesterol synthesize can be elevated by insulin. Lipolysis in the adipose tissue and fatty acids oxidation in the liver and muscle are downregulated in response to insulin (L: liver; M: muscle; A: adipose tissue).

1.1.2.2 Insulin signaling cascade

The secretion of insulin is stimulated in response to increasing level of glucose, fatty acids

or/and to a less extent of amino acids, in the bloodstream. Insulin binds to insulin receptors

(IR) embedded in the plasma membrane [16]. The IR is composed of two α subunits and two

β subunits. The α units are located in the outside membrane and house insulin binding

domains, while the linked β units penetrate through the plasma membrane. The IR is a

tyrosine kinase receptor such that the binding of insulin to its α units leads to the

autophosphorylation of β units at the tyrosine residues to activate the receptor [18, 19]. The activated IR then phosphorylates intracellular insulin receptor substrate (IRS), to provide a docking side to recruit phsphoinositide-3,4,5-trisphosphate (PIP3). IRS is recruited to the receptor at the cell membrane, and includes four isoforms: IRS1, IRS2, IRS3 and IRS4. IRS1 serves as a docking center for recruitment and activation of downstream enzymes that ultimately mediate insulin effects. IRS2 serves as the primary protein to mediate the effect of insulin on hepatic glucose production, gluconeogenesis and glycogen formation in the liver [20]. The phosphorylation on tyrosine residues of IRS allows it to initiate downstream responses. However, there are other phosphorylation residues of IRS that are induced by other enzymes, and do not response to insulin. The negative regulation of insulin action will be discussed in the next section. Downstream of IRS, phosphatidylinositol-3-kinase (PI3K) is composed of an adaptor/regulatory subunit (p85) and a catalytic subunit (p110). The former interacts with activated IRS, leading to the induction of PI3K, while the latter catalyzes phosphatidylinositol-4, 5-bisphosphate (PIP2) to PIP3, a second messenger in the plasma membrane [21]. The increased PIP3 recruits a subset of signaling proteins with pleckstrin homology (PH) domains, including protein kinase B (PKB, or Akt) and phosphoinositide-dependent kinase 1 (PDK1) [22]. PDK1 phosphorylates Akt at threonine (Thr) 308, leading to stabilization of the activation loop in an active conformation. The Ser473 phosphorylation of Akt that may be induced by protein kinase C α (PKCα), or by PDK2 [23]. Thr308 and ser473 phosphorylations are required for the activation of Akt to induce diverse signaling cascades downstream [24].

Activation of Akt leads to a range of cellular responses. The review here will focus on its role on glucose and lipid metabolism. The mechanism by which Akt might contribute to insulin-mediated suppression of glycogenolysis in the liver as well as muscle is mainly by driving glycogen synthesize [16]. Glycogen synthase kinase-3 (GSK3) plays a negative role to link

Akt and glycogen synthesize. Phosphorylation of GSK3 dephosphorylates glycogen synthase to suppress glycogen synthesize [25, 26]. Thus, under physiological condition, GSK3 is inhibited in its phosphorylation form by activated Akt. In order to reduce blood glucose levels in response to insulin, Akt also stimulates glycolysis. It is suggested that Akt might indirectly induce the glycolysis rate-limiting enzyme, phosphofructokinase-1 (PFK1) by directly phosphorylating phosphofructokinase-2 (PFK2) [27]. Meanwhile, Akt also plays an important role in glucose transport in skeletal muscle and adipose tissue, by mediating the translocation of glucose transporter type 4 (GLUT4) [28]. In terms of its role in lipid metabolism, Akt is considered to link to the sterol-regulatory element binding proteins (SREBPs) which are transcription factors regulating lipid metabolism. The potential mechanisms by which Akt influences SREBPs could be through GSK3 by preventing the mature SREBP degradation [29]. Another possible mechanism is related to the mammalian target of rapamycin (mTOR). The effects of mTOR on modulating SREBPs cleavage is through Akt activation [30].
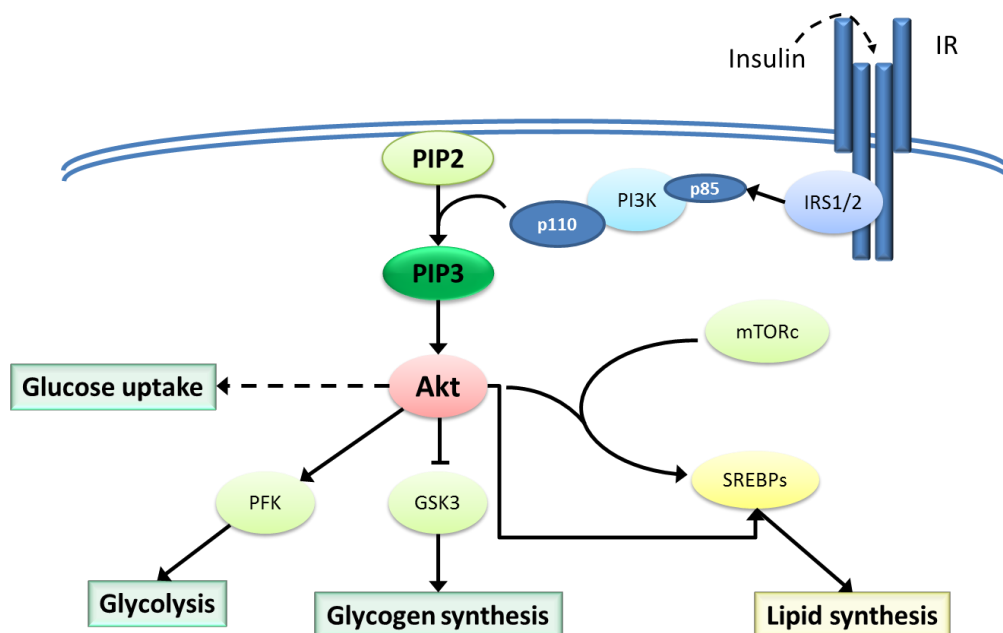
Figure 1.2 Simplified insulin signaling cascade and its role in glucose and lipid metabolism.

The details are described in 1.1.2.2.

1.1.2.3   Negative feedback control of insulin signaling transduction

Control over insulin signaling pathways can be achieved by negative feedback from downstream components [31, 32]. Signals from other pathways can inhibit insulin signaling. However, the IRS proteins are also subject to the negative feedback control mechanisms. Phosphorylation of IRS proteins at serine residues is a key step in the feedback control processes [33, 34]. For example, the Ser/Thr phosphorylation of IRS proteins by PKCζ leads to the dissociation of IR: IRS [35] and IRS: PI3K [36] complexes. This dissociation then inhibits the ability of IRS to undergo further insulin-stimulated tyrosine (Tyr) phosphorylation. Desensitization of insulin signaling could also trigger by inflammatory signal. C-Jun NH$_2$-terminal kinase (JNK), which is mediated by stress, promotes the phosphorylation of Ser^{307}. Ser^{318} of IRS1 is also a potential target for JNK, as well as PKCζ [37].

1.1.2.4   Insulin resistance

Insulin resistance is the inability of the body to response to, and to use, insulin it produces and it is one of the major disorders of type 2 diabetes [38, 39]. Insulin action is defective in the liver, skeletal muscle and adipose tissue when there is insulin resistance [40]. Insulin resistance is also considered as a key link between type 2 diabetes and obesity [41]. In the pre-diabetic stage, blood glucose is maintained relatively normal due to a compensatory increase of insulin secretion while body already becomes insulin resistant [42]. However, prolonged insulin resistance could lead to β-cell failure and circulating insulin levels become insufficient to maintain blood glucose concentrations, resulting in hyperglycemia and the development of diabetes.

Insulin resistance is a characteristic feature of glucose intolerance, involving both liver and skeletal muscle, in type 2 diabetic individuals [43]. Deficiency in insulin-stimulated glycogen

synthesize and increased gluconeogenesis in the liver are major characteristics of hepatic insulin resistance and fasting hyperglycemia [44]. Kraegen and colleagues performed hyperinsulinemic-euglycemic clamps in high fat fed mice and their results showed that the insulin resistance in muscle is a later occurrence than hepatic insulin resistance in the high fat fed rat [45]. Therefore, the present project will focus on hepatic insulin resistance which occurs prior to peripheral insulin resistance.
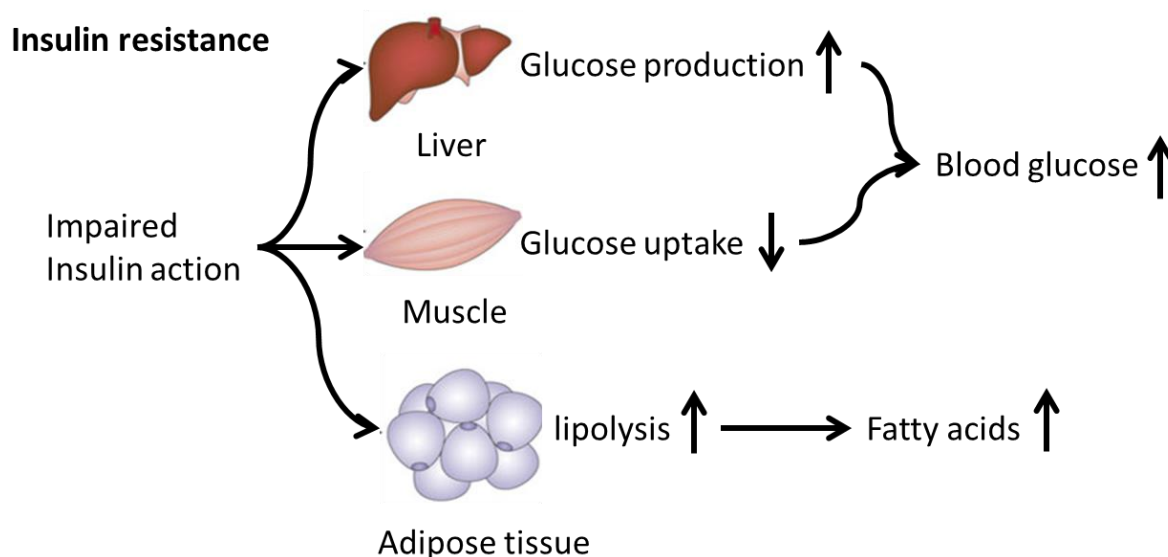
Figure 1.3 Insulin resistance in different tissues.

Under the insulin resistant state, insulin is unable to suppress glucose production by the liver and decrease glucose uptake in the muscle, which together lead to elevated blood glucose levels. Meanwhile, lipolysis in the adipose tissue increases, resulting in upregulation of plasma fatty acids levels [46].

1.2 Lipid metabolism

Lipids are one of the major energy resources for the body. Adipose tissue has been considered as a major site for storage of extra fuel. After increased food intake and/or decreased energy expenditure, excess energy is deposited efficiently in adipose tissue [47, 48]. Abnormal lipid

metabolism leads to excess lipid accumulation in adipose tissue and other non-adipose tissues such as skeletal muscle and liver. These detrimental effects are important pathogeneses of metabolic disorders such as diabetes, obesity and fatty liver disease. More than 90% of the lipid is in the form of triglyceride. Triglycerides come from three primary sources: 1) absorption from the diet; 2) storage depots in adipocytes and 3) *de novo* synthesize (DNL) [49].

Fat from diet is dissolved by bile salts that can cope with the insolubility of lipids and is transported through the blood and lymph partly by lipoproteins. Triglycerides are broken to a mixture of glycerol, free fatty acids, monoacylglycerols, and diacyglycerols by a lipase secreted from the pancreas. Triglyceride is resynthesized after absorption from the hydrolysis products and then transported to tissues with lipoproteins as the form of chylomicrons [50]. In current thesis, we focused on lipid synthesis (lipogenesis). Fatty acid oxidation will also be reviewed in this part.

1.2.1   Lipogenesis

1.2.1.1   Lipid synthesis

DNL is the process of formation of lipids from non-fat precursors such as carbohydrates to fatty acids [51, 52]. Adipose tissue and liver are the major sites of DNL [53]. The first committed step of DNL is the formation of malonyl-CoA from bicarbonate and acetyl-CoA which is a central metabolite from either the pyruvate dehydrogenase reaction or fatty acid β-oxidation, catalyzed by acetyl-CoA carboxylase (ACC). Malonyl-CoA is used mostly as a substrate by fatty acid synthase (FAS) for DNL. Fatty acid chain which contains successive additions of two carbon units needs to be built up from malonyl-CoA. In animals, all of the activities of adding carbon units are linked to a highly-structured multienzyme complex, FAS.

The resultant product, including mainly 16C palmitic acid and minor amounts of 18C stearic acid[54], are either elongated or desaturated. The elongation of fatty acid chains is essential for many membrane lipids. Unsaturated fatty acids are necessary for lipid storage, membrane synthesize and maintenance. Monounsaturated fatty acids are formed by direct oxidative desaturation with oxygenase type of enzyme that associated with the endoplasmic reticulum (ER) in the liver, mammary gland, brain, testes and adipose tissue. The stearoyl-CoA desaturase (SCD) is the predominant desaturation enzyme for saturated acids in these tissues and is rate-limiting in the formation of 18:1 n-9. There are two isoforms of SCD which are SCD1 that expresses exclusively in the liver whereas brain, spleen, heart and lymphocytes express only SCD2 [55].

Fatty acids, together with glycerol-3-phosphate, are resources of triglyceride that is mainly synthesized in the liver and adipose tissue [56]. Glycerol-3-phosphate is either from the reduction of the glycolytic intermediate dihydroxyacteone phosphate or from ATP-dependent phosphorylation of glycerol. Lysophosphatidic acid is the first product catalyzed by sn-1-glycerol-3-phosphate acyltransferase (GPAT) from glycerol-3-phospate and acyl-CoA. It is further catalyzed by sn-1-acyl-glycerol-3-phosphate acyltransferase (AGPAT) to the formation of phosphatidic acid which is then metabolized to produce 1,2-diacyglycerol (DAG). DAG is further acylated by sn-1,2-diacylglycerol acyltransferase (DGAT) to form triglyceride [50].
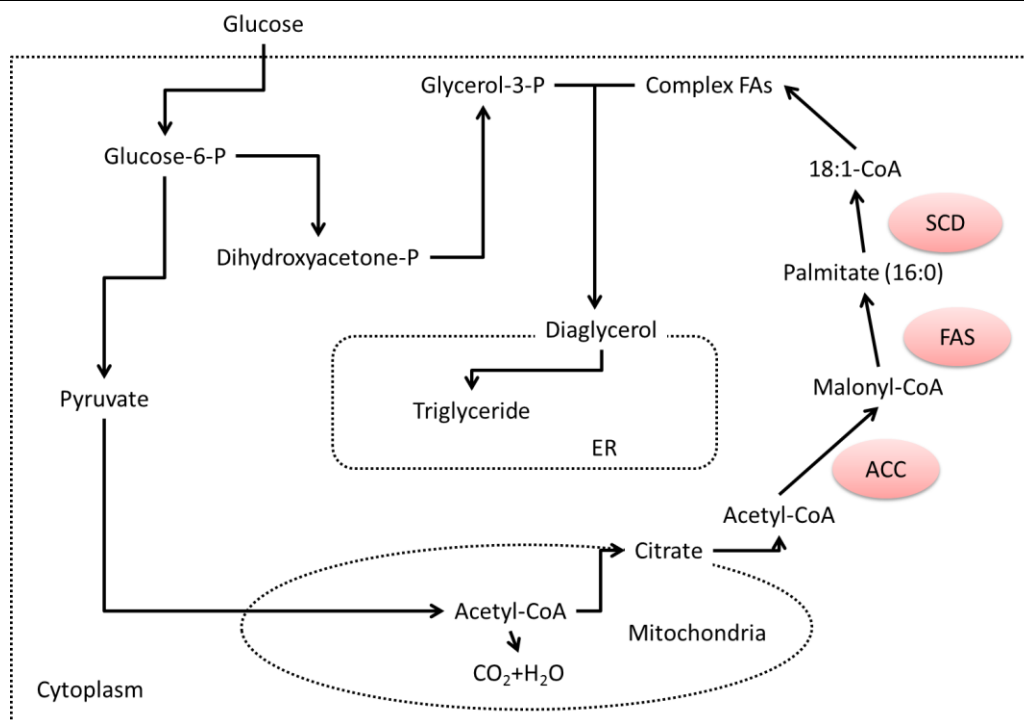
Figure 1.4 Lipid synthesize pathway.

The details are described in 1.2.1.1.
Glucose-6-P: glucose-6-phosphate; Dihydroxyacetone-P: dihydroxyacetone-phosphate; Acetyl-CoA: Acetyl coenzyme A; Glycerol-3-P: glycerol-3-phosphate; ER: endoplasmic reticulum; ACC: Acetyl-CoA carboxylase; FAS: fatty acid synthesis; SCD: Stearoyl-CoA desaturase; Complex FAs: complex fatty acids.

1.2.1.2   Regulation of lipogenesis

Lipogenesis can be stimulated by a high carbohydrate diet via up-regulating the enzymes that are involved in triglyceride biosynthesize. Depending on insulin and glucose levels, this process can be regulated by specific transcription factors. SREBP1c [57] and carbohydrate response element binding protein (ChREBP) [58] are two critical transcription factors of lipogenesis.

SREBP1c

SREBPs are a family of transcription factors that regulate lipid synthesize by controlling a range of enzymes required for lipid metabolism. There are three isoforms of SREBP:

SREBP2, SREBP1a and SREBP1c, of which the last one is closely related to lipogenesis and expressed in most tissues in humans and mice, with especially high levels in the liver, white adipose tissue and brain [59]. SREBP1c is considered as a major transcriptional factor involved in the insulin regulation of lipogenic protein expressions [60]. SREBPs are synthesized as an inactive form in the ER membrane where they reside in a complex with SREBP-cleavage activating protein (SCAP) and the insulin-induced gene (Insig). When SCAP is activated by low sterol levels, it undergoes a conformational change and disassociates from Insig. The precursors of SREBPs are then transported to the Golgi apparatus with the assistance of SCAP to undergo proteolytic cleavage by site-1 protease (S1P) and site-2 protease (S2P) to release the N-terminal domain which constitutes the mature transcription factor [61, 62]. Once SREBPs in the nucleus are in the mature form, they are subject to a number of post-translational modifications that regulate the transcriptional activity of the active transcription factor [63]. Insulin is a potent activator of SREBP1c. The effect of insulin has been shown by *in vivo* studies. SREBP1c expression and nuclear abundance are low in the liver of diabetic animals and increase remarkably after an insulin treatment [64]. The effect of insulin on SREBP1c is mediated by a PI3K-dependent pathway [65]. However, the downstream mechanism is not clear. Another potent activator is liver X receptor (LXR). Although the LXR has been reported to play vital roles in regulating cholesterol metabolism, it has been identified to be able to target on SREBP1c [66]. The stimulation of LXR by its agonist increases gene and protein expression of SREBP1c [67]. Besides insulin and LXR, it is suggested that SREBP1c can be regulated by other effectors. Forkhead box protein 1 (FoxO1) is another regulator that can suppress SREBP1c transcriptional activity in HepG2 cells [68]. In addition, nutritional regulation of SREBP1c is demonstrated to be independent of insulin as long as sufficient carbohydrates are available

[69]. ER stress is also able to modify the expression of SREBP1c, which will be reviewed in 1.6.1.

The target enzymes of SREBP1c include ACC, FAS and SCD1, which are rate-limiting enzymes in lipogenesis. The down-regulation of SREBP1c leads to the reduction of lipogenesis. The inhibition of SREBP1c in high-fat diet induced obese mice resulted in a decrease in total plasma triglycerides and total liver fat. The inhibition of SREBP1c can also lead to a reduction of levels of lipogenic proteins such as ACC, FAS and SCD1[70]. Notably, hepatic SCD1, unlike the other two critical targets enzymes (ACC and FAS) of SREBP1c is proposed be upregulated by dietary carbohydrates in both SREBP1c-dependent and SREBP1c-independent pathways. The other regulator of this pathway other than SREBP1c is suggested to be the thyroid hormone [71].

ChREBP

ChREBP is a member of the basic helix-loop-helix/leucine zipper (bHLH/ZIP) family of transcription factors. It can be activated by high glucose and inhibited by cAMP [72]. Like SREBP1c, ChREBP is a key determinant of lipid synthesize as a glucose-responsive transcription factor in the liver [73]. ChREBP stays in the cytoplasm when the glucose concentration is low and moves into the nucleus when the glucose concentration is high [72]. Besides the regulation of its subcellular location by glucose concentrations, ChREBP is also regulated at post-translational level for its activities, e.g. via phosphorylation and dephosphorylation [74]. It is also likely that ChREBP activity is dependent secondarily on SREBP1c, because of activation of glucokinase by SREBP1c [63].

The role of ChREBP in the regulation of lipid and glucose metabolism is complex. It has been reported that the liver-specific inhibition of ChREBP affected the rate-limiting enzymes in lipogenesis which are ACC, FAS and SCD1 [75]. ChREBP knockdown significantly restores insulin sensitivity in the liver, in agreement with the concept that excessive hepatic lipid accumulation leads to insulin resistance [76]. However, another study demonstrated that increased ChREBP can dissociated hepatic steatosis from insulin resistance, with beneficial effects on both lipid and glucose metabolism in a ChREBP overexpression model [77].

1.2.2   Fatty acids oxidation and lipid transportation

Besides of lipid synthesize, fatty acids oxidation and transport also contribute to the lipid homeostasis as discussed here.

1.2.2.1   Fatty acids oxidation

Fatty acid oxidation is a major component of lipid metabolism. Liver and muscle are two major sites of fatty acid oxidation. Types of oxidation include: β-oxidation, α-oxidation, ω-oxidation and peroxisomal-oxidation. β-oxidation in the mitochondria is the major mechanism of fatty acid oxidation [78]. It is the process of breaking down a long chain acyl-CoA to acetyl-CoA, via the sequential removal of 2-carbon units by oxidation at the β-carbon position of the acyl-CoA molecule. Each round of β-oxidation involves four steps, oxidation, hydration, oxidation and cleavage. The final products enter into TCA cycle, where they are further oxidized to CO_2.

The oxidation of fatty acids yields significantly more energy per carbon atom than does the oxidation of carbohydrates. The degradation of palmitoyl CoA (C16-acyl CoA) requires seven

reaction cycles. In the last cycle, the C_4-ketoacyl CoA is thiolyzed to two molecules of acetyl CoA. The stoichiometry of oxidation of palmitoyl CoA is described in **Table 1**. The equivalent of 2 molecules of ATP are consumed in the activation of palmitate. Hence, the complete oxidation of a molecule of palmitate yields 106 molecules of ATP [79].

Table 1 Energy yields of palmitoyl CoA.

C 16:0-CoA +7 FAD + 7 NAD+ +7H$_2$O +7 CoA→8 Acetyl-CoA+7 FADH$_2$+ 7 NADH + 7 H$^+$	
7 NADH	17.5 ATP
7 FADH$_2$	10.5 ATP
8 Acetyl-CoA	80 ATP

For the complete oxidation of palmitic acid (16:0), seven β-oxidation cycles are required. 8 Acetly-CoA are generated. 7 mol of FADH$_2$ and 7 mol of NADH and H$^+$ are produced as well. Every 8 Acetyl-CoA generate 80 molecules of ATP while 7 FADH$_2$ generate 17.5 molecules of ATP and 7NADH generate 10.5 molecules of ATP.

1.2.2.2 Lipid transport

Triglycerides are transported in body fluids in the form of lipoprotein particles [80]. Lipoproteins are responsible for carrying lipids via the bloodstream to other parts of the body [81]. Multiple enzymes and proteins are involved in the transport process. Dietary (exogenous) fat can be formed into large chylomicron particles in the Golgi complex of intestinal cells to other tissues such as liver. Assembly and secretion of chylomicrons is dependent of the present of apolipoprotein (apo) B. Liver is a major site of triglyceride synthesizes. Excessive endogenous triglycerides are assembled as the form of very low density lipoprotein (VLDL)

for export. In the liver, microsomal triglyceride transfer protein (MTTP) is involved in the formation of VLDL [82].

1.2.3 Other fates of intracellular lipids

Besides oxidation, the majority of fatty acids are incorporated into glycerolipids [83]. The first committed step is the acylation of sn-glycerol-3-phophate to form lysophosphatidic acid catalyzed by GPAT. Subsequent lysophosphatidic acid (LPA) acylation results in the production of phosphatidic acid that is dephosphorylated to produce DAG. This reverses lipogenesis to form triglyceride (TG).

Another fate of intracellular fatty acids is involvement in the biosynthesize of sphingolipids. Palmitoyl-CoA and serine are catalyzed by serine palmitoyltransferase (SPT) to produce 3-oxoshpinganine. The following pathways result in the production of sphinganine, dihydroceramide and ultimately ceramide. Ceramide is the precursor of most active sphingolipids [83].

1.3 ER stress and the unfolded protein response

1.3.1 Endoplasmic reticulum

The endoplasmic reticulum (ER) exists in all eukaryotic cells. The ER membrane forms a continuous sheet enclosing a single internal, convoluted space, called the ER lumen [81]. The ER plays an important role in lipid biosynthesize and is the site for producing phospholipids, cholesterol, triacylglycerol and ceramides. The ER is also a central coordinator of protein synthesize, folding and processing [84]. Another key function of ER in maintaining cellular homeostasis is as an intracellular Ca^{2+} storage site.

1.3.2 ER stress and the unfolded protein response (UPR)

A number of pathological and physiological conditions can directly or indirectly disturb ER function and lead to ER stress. ER stress is triggered by excess unfolded or misfolded proteins accumulating in the ER lumen [85, 86]. For example, Ca^{2+} depletion has been reported to suppress protein folding, affecting retention of ER-resident proteins [87], ER-Golgi trafficking [88] and chaperone function [89]. Overload of protein and excess lipid accumulation are also suggested [78] to trigger ER stress. The mechanisms of how these two factors are involved in ER stress will be reviewed in 1.6.2. To deal with ER stress, cells develop an adaptive signaling pathway called the unfolded protein response (UPR). The physiological role of the UPR is to relieve ER stress by either increasing ER folding capacity or suppressing protein loading [90, 91]. However, under more severe conditions, UPR can interfere with the normal function of other pathways, and can even lead to cell apoptosis [91]. The UPR is mediated by three ER-resident transmembrane proteins that sense ER stress and mediate downstream signaling pathways. Under normal conditions, the three sensors bind ER chaperones, such as glucose-regulated protein 78 (GRP78) and glucose-regulated protein 94 (GRP94) [92]. However, due to increased protein loading, the ER chaperones are moved to deal with misfolded or unfolded proteins [93, 94]. The release of the chaperones from their bound complexes activates sensors known as inositol-requiring protein 1 (IRE1), PKP-like endoplasmic reticulum kinase (PERK), and activating transcription factor 6 (ATF6). The activation of these signals may not occur simultaneously. For example, it has been reported that PERK is the first sensor to be activated once released from GRP78, and is rapidly followed by ATF6, whereas IRE1 is activated last[95]. Activation of these three sensors leads to activation of downstream signalling pathways such as chaperone synthesis, lipid synthesis and apoptosis.

1.3.2.1   IRE1 branch of the UPR

IRE1 branch is the oldest branch of the UPR in an evolutionary sense and is conserved from yeast to humans [96]. The yeast UPR is entirely dependent on ER-resident, transmembrane endoribonuclease Ire1p [97]. In the mammal, IRE1 includes two subunits, IRE1α and IRE1β [98]. IRE1α is suggested to play a role in ER stress-induced hepatic steatosis [99] while IRE1β may play a role in lipid metabolism, especially in intestinal cells [100]. IRE1 consists of an N-terminal domain, a single-pass transmembrane spanning segment, a cytosolic region subdivided into a Ser/Thr protein kinase domain, and a C-terminal endoribonuclease domain [101]. After dissociation from its chaperones, the luminal domain of IRE1 dimerizes, allowing associated cytoplasmic domains to be close to the other side of the ER membrane. This change facilitates transautophosphorylation of the kinase domain, which results in activation of the endoribonuclease domain [102, 103]. The kinase activity of IRE1α can activate JNK in response to ER stress by interacting with the adaptor protein tumour necrosis factor (TNF) receptor-associated factor 2 (TRAF2) [104]. The endoribonuclease activity of IRE1α cleaves a 26-base fragment from mRNA encoding X-binding protein 1 (XBP1), leading to its spliced form sXBP1, and its subsequent translocation to the nucleus. Active sXBP1 can be regulated by ATF6 and is intimately associated with the ATF-controlled ER stress-response element (ERSE) [105, 106]. In addition, spliced XBP1 upregulates a number of UPR target genes that are related to protein folding, ER-associated protein degradation (ERAD) and protein quality control [107] . Moreover, IRE1α may regulate apoptosis by cleaving premature microRNAs [108]. IREβ, in turn, may directly bind misfolded proteins, similarly to yeast IRE1 [109].

1.3.2.2   PERK branch of the UPR

The activation of PERK is similar to IRE1α and it involves dimerization and autophosphorylation and the formation of large clusters [110].

Activation of the PERK pathway attenuates general protein synthesize by phosphorylation of eukaryotic translation initiator factor 2α (eIF2α). EIF2α activation is able to suppress protein synthesize, to decrease the number of proteins then entering the ER [107, 111]. Therefore PERK activation has an important pro-survival effect on the cell. The eIF2α phosphorylation also leads to the selective translation of the ATF4 mRNA. ATF4 regulates the expression of genes that encode proteins related to amino acid metabolism and ER chaperones [112]. ATF4 also controls the expression of genes involved in apoptosis, including the transcription factor C/EBP-homologous protein (CHOP) and GADD34 [107].

1.3.2.3   ATF6 branch of the UPR

The activation of ATF6 is different from the other two branches of UPR. Similarly to SREBP1c, ATF6 is an ER membrane-bound transcription factor, and its activation is dependent on cleavage. The proteases that respond to this cleavage are the same as SREBP1c [113]. During ER stress, ATF6 translocates to the Golgi complex where it is processed to release a fragment to the cytoplasm. The cytosolic p50 fragment is the active form of ATF6, which then relocates to the nucleus where it regulates the expression of gene products [114]. The ATF6 branch of the UPR is reported to contribute to protein folding, protein secretion and ERAD, thereby supporting the cell's effort to cope with ER stress and excessive misfolded/unfolded proteins [115, 116].
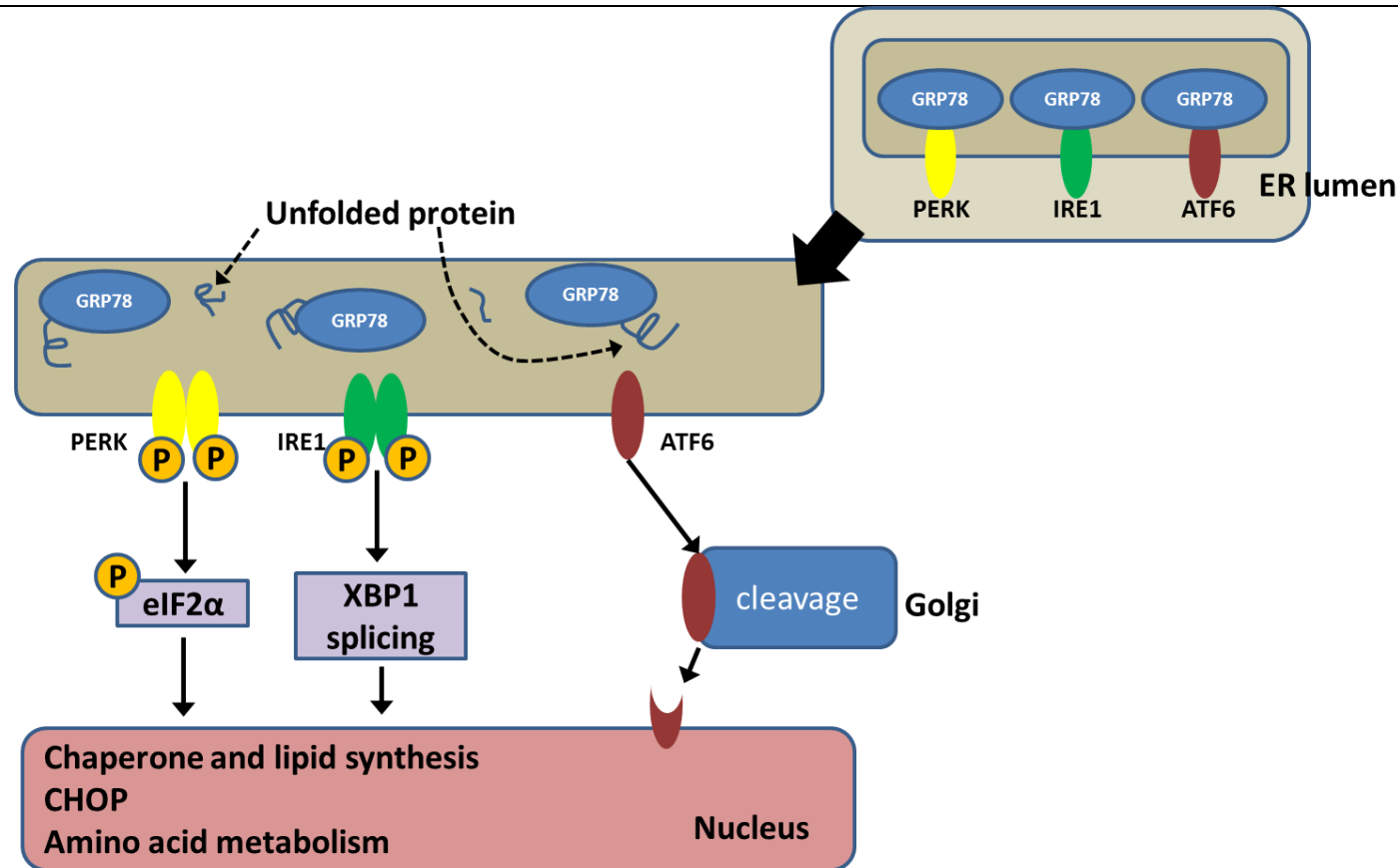
Figure 1.5 The unfolded protein response (UPR).

In UPR, three ER membrane transducers are activated by release from GRP78 (BIP) binding. IRE1 is a ribonuclease that splices and religates XBP1 transcripts for the synthesize of active transcription factor. Spliced XBP1 exerts the induction of expression of genes that relate to chaperone and lipid synthesize in the nuclear. PERK is a kinase that phosphorylates eIF2α and suppresses protein synthesize. ATF6 is a transcription factor that once released from ER will travel to the Golgi, cleaved and translocated to the nucleus, to activate the transcription of chaperone genes (Adapted from Schonthal, A. H., Scientifica (Cairo) 2012).

1.4   Role of inflammation

Inflammation is the first response to infection or irritation of the immune system, after referred to as the innate cascade. It has been implicated in the pathogeneses of arthritis, cancer and stroke, as well as in cardiovascular disease. Inflammation is an intrinsically beneficial event that induces the remove of detrimental factors and restoration of tissue structure and physiological function [117].

1.4.1   Inflammation and insulin resistance

The clues to the involvement of inflammation in diabetes were indicated more than a century ago. However the role of inflammation in the pathogenesis of insulin resistance was not well studied until late of 20th century and the early 21st century, by re-examining the hypoglycemic actions of salicylates and confirming that the molecular target was the IκB kinase-β (IKKβ)/ nuclear factor kappa-light-chain-enhancer of activated B cells (NF-κB) axis [118, 119]. After the study of the induction of insulin resistance by TNFα, the concept of lipid as a site for cytokine production and other bioactive substances quickly extended to include leptin, IL-6, resistin and others [120].

1.4.2   Inflammation in the liver

Non-alcoholic fatty liver disease (NAFLD) is often associated with the presence of abdominal adiposity and its prevalence is increasing and related with T2D and hyperlipidaemia. Inflammation clearly plays a role in the progression of NAFLD. Inflammation gene expression shows increasing in the liver with enhanced adiposity [121]. This indicates that hepatic steatosis might induce a subacute inflammatory response in the liver. It is suggested that proinflammatory factors in the portal circulation might initiate hepatic inflammation.

Regardless, NF-κB can be activated in the hepatocyte. Cytokines including IL-6, TNFα and IL-1β are overexpressed in fatty liver [122].

1.4.3   Inflammation and ER stress

Besides nutritional excess, and the related metabolic factors triggered by both metabolic dysfunction and inflammation, ER stress has been suggested to be activated and to mediate both metabolic and immune responses [103]. ER is the place where the majoring of proteins are processed, and the role of the ER tends to be particularly vital in immune cells as they produce a very large amount of protein. Communication governed by ER stress usually results in inflammation, to control tissue damage and aid in tissue repair [123].

Following ER stress, the cytosolic domain of IRE1α can bind to TRAF2. The IRE1-TRAF2 complex then activates IKK and consequently leads to IκB degradation to release NF-κB, to induce the proinflammatory process [104] [124]. In addition, the IRE1-TRAF2 complex may also activate JNK and this activation can be induced independently of XBP1 splicing [125]. Activated JNK then phosphorylates and activates AP-1, which induces its own inflammatory gene program [126]. PERK-activated eIF2α results in translational arrest, which leads to decreased content of IκB protein and consequently increases the ratio of NF-κB to IκB. This change causes the release of NF-κB which exerts the proinflammatory transcriptional role in the nucleus [127]. While inducing CHOP, PERK may also activate transcription of interleukin 23(IL-23), a proinflammatory cytokine [128]. CHOP activation is suggested to negatively regulate the inflammatory response by activating both NF-κB and JNK. By contrast, ATF6, which leaves the ER to relocate to Golgi complex under ER stress, can lead to the acute-phase response (APR). APR is a group of organism-level physiological processes that are initiated soon after an inflammatory insult, trauma, or infection [103] [129].
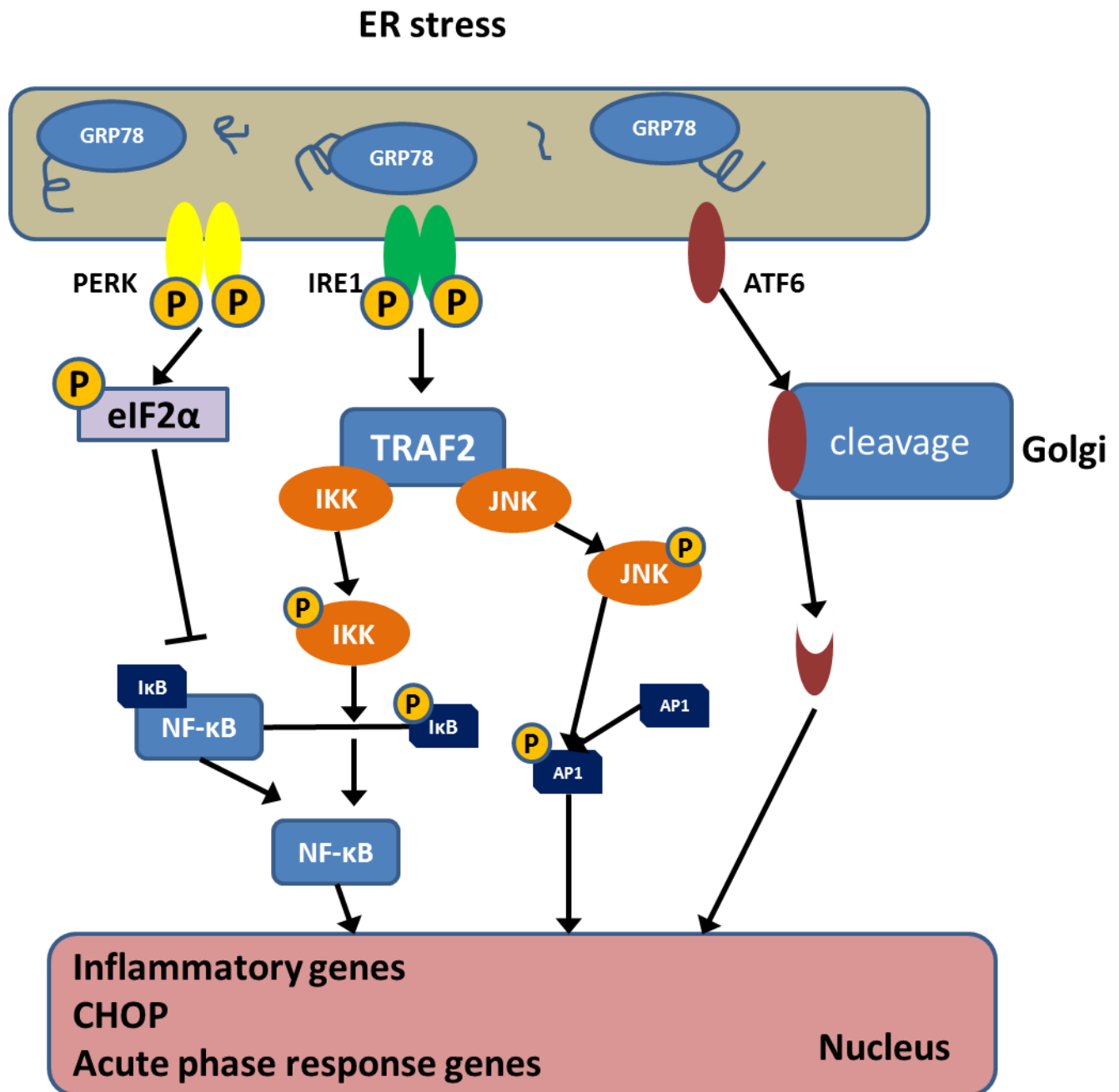
Figure 1.6 The URP-mediated inflammatory transcriptional program.

The details are described in 1.4.3 (Adapted from Garg, A. D, et al., Trends Mol Med, 2012).

1.5 Relationship between lipid accumulation, UPR and insulin resistance

Understanding the molecular mechanisms of insulin resistance is a major medical challenge in the 21st century. Over the last half-century, many hypotheses have been proposed to interpret insulin resistance. Since the early 1980s, excess lipid content and improper lipid location have been considered to be associated with insulin resistance [130]. As reviewed in 1.4.1, a chronic low degree of inflammation has been revealed to play a role in insulin resistance in liver, muscle and adipose tissues. During the last decade, a number of studies have pointed to an important role of ER stress/UPR in the development of insulin resistance [131, 132]. A number of studies have suggested a link between obesity, ER stress, insulin resistance and type 2 diabetes. These mechanisms have largely been explored in isolation, resulting in competing reductionist and compartmentalized proposals. Here we review current understanding of the complex relationships between lipid metabolism, UPR and insulin resistance are complicated.

1.5.1 Lipid accumulation and insulin resistance

The liver and skeletal muscle is the two major organs responsible for insulin action to maintain normal blood glucose levels. The livers of obese insulin resistant individuals are characterized by severe hepatic insulin resistance, which significantly contributes to hyperglycemia. However, insulin-dependent lipogenesis is paradoxically active. SBPRE1c levels in the liver are over-induced in ob/ob animals [133, 134]. The failure of insulin to suppress gluconeogenesis while lipogenesis is strongly stimulated could reflect a selective insulin resistance. A considerable number of studies have shown the detrimental effects of excess lipid level in insulin resistance [83, 135, 136]. In rats, high-fat feeding remarkably enhances hepatic DAG and TG content, without alteration in muscle lipid content [130]. Although there was no effect of fat feeding on insulin receptor tyrosine phosphorylation,

insulin-stimulated IRS1 and IRS2 tyrosine phosphorylation was blocked in these animals. Consistently, the downstream insulin effectors, Akt2 and GSK3 were suppressed. Interestingly, the blunted insulin signaling was observed only in liver, not in peripheral tissues [130]. The results suggest a link between hepatic steatosis and hepatic insulin resistance. However, the changes of lipogenesis transcriptional factors did not show detrimental effect on insulin signaling. Overexpression of ChREBP in mice fed a high-fat diet presented normal insulin levels, improved insulin signaling and glucose tolerance compared with controls, despite greater hepatic steatosis [77]. The absence of SREBP1c in leptin deficient mice ameliorated fatty liver but not insulin resistance [137]. The results from these studies demonstrate that hepatic steatosis could disassociate from hepatic insulin resistance under certain conditions. However, the excessive lipid accumulation remains a key factor in the development of insulin resistance.

1.5.1.1 Diacyglycerol (DAG)

DAG is an intermediate in lipid metabolism and an important second messenger in controlling cell division. The most common pathological cause of high intracellular DAG content in the liver is overnutrition [43]. Rats fed a high-fat diet exhibited high hepatic DAG content, which is associated with protein kinase C ε (PKCε) activity and decreased IRS tyrosine phosphorylation [130]. PKCε, a novel isoform of the protein kinase C family, is thought to play key roles in fat-induced hepatic insulin resistance. When DAG is present in sufficient concentrations, it binds to the C1 domain of PKCε and recruits PKCε from the cytosol to membrane to be activated [138]. Activated PKCε further leads to IRS serine phosphorylation to inhibit insulin signal transduction. PKCε-specific antisense oligionucleotide-treated rats are protected from fat-induced hepatic insulin resistance, despite similar levels of hepatic DAG

and TG levels [139]. Inhibition of hepatic DAG synthesizes by knocking out the gene encoding mitochondrial glycerol-3-phosphate acyltransferase protects mice from fat-induced hepatic insulin resistance [140]. In addition, enhanced fatty acid oxidation and mitochondrial uncoupling by knockdown of ACC, or the use of 2,4-dinitrophenol, reduces DAG content, consequently decreasing PKCε activation and protection from fat-induced hepatic insulin resistance [141]. A similar mechanism of DAG induced insulin resistance operates in the skeletal muscle. PKCθ activation in the muscle, rather than PKCε, could decrease IRS1-associated PI3K activity to block insulin signal transduction [43].

1.5.1.2 Ceramides

As mentioned in 1.2.3, ceramide is the precursor of sphingolipid, where synthesize is largely dependent on *de novo* biosynthesize. The rate of ceramide synthesize is predominantly dependent upon the availability of palmitate (16:0) CoA, which participate in the initial, rate-limiting step in *de novo* ceramide synthesize [142]. The first analysis of ceramide levels in insulin resistance animals was performed prior to the observation that ceramide was a potent antagonist of insulin signaling [143]. Several subsequent studies have evaluated the increasing level of ceramides in muscle or liver of insulin resistant rodents [144] or humans [145]. It has been demonstrated that ceramide is able to block activation of Akt, a serine/threonine kinase that is required for insulin and factor activation of anabolism and cell survival [146]. This regulation is accomplished by at least two mechanisms. First, ceramide inhibits translocation of Akt from the cytoplasm to the plasma membrane [147]. The key intermediate is PKCζ, which is activated by ceramide in vitro [148]. PKCζ inhibits Akt translocation by phosphorylating threonine-34 [149]. The second mechanism involves the dephosphorylation of Akt by protein phosphatase 2A (PP2A) [150, 151]. Ceramides have been indicated to

directly activate PP2A, the primary phosphatase responsible for dephosphorylation of Akt. This has been demonstrated in C2C12 myotubes [152], PC12 cells [153], brown adipocytes [150] or a human glioblastoma cell line [151], using a PP2A inhibitor.

1.5.2 The UPR and insulin resistance

In the past decade, UPR triggered by ER stress has emerged as a new player in type 2 diabetes, due to its detrimental effects on β-cells in the pancreas [154] and insulin action in the liver [155]. A number of studies have demonstrated the role of UPR in the progression of insulin resistance because it can transduce some effects of lipid metabolites and cytokines into an activation of these stress sensors. In addition, UPR has been proved to modulate key pathways including lipogenesis and gluconeogenesis [156]. It is commonly thought that UPR could contribute to the development of insulin resistance in the liver in three different ways: (i) transcription factors activated by UPR can directly modify transcription of critical lipogenic and gluconeogenic enzymes to lead to abnormal activation of these pathways under insulin resistance conditions [157-160], (ii) activation of UPR by stimulating stress kinases that interfere with insulin signaling can directly promote insulin resistance [161], and (iii) UPR may contribute to insulin resistance by promoting lipid accumulation in hepatocytes [131, 158, 160].

1.5.2.1 IRE1 branch and insulin resistance

IRE1 activation upon ER stress induces JNK and IKK, of which both can impair insulin signaling by phosphorylation of IRS1 on serine 307 residues, as described above. Shulman's group showed that IRE1-mediated JNK activation can be independent of hepatic insulin

resistance in XBP1 knockout mice fed a fructose diet [162]. This study hypothesised that the hepatic insulin resistance in models of ER stress could be secondary to lipid accumulation triggered by ER stress activated lipogenesis. JNK could be activated by different pathways, not always involving ER stress. In addition to IRE1 phosphorylation, ER stress can also activate JNK via calcium/calmodulin-dependent protein kinase II (CaMK II) [163].

XBP1, a downstream effector of IRE1, is thought to stimulate hepatic lipogenesis, either dependently or independently of SREBP1c [158, 160]. XBP1 knockout mice exhibit reduced lipogenesis with decreased serum levels of triglycerides, cholesterol and free fatty acids [160]. Intriguingly, XBP1 splicing can be stimulated by insulin. Insulin increases the nuclear concentration of spliced XBP1 by promoting its binding to the p85 regulatory subunit of PI3 kinase [164].

1.5.2.2   PERK branch and insulin resistance

Activated PERK is able to phosphorylate NF-E2-related factor 2 (NRF2), involved in the transcriptional regulation of lipogenic gene expression. Deletion of NRF2 in mice leads to reduced hepatic triglyceride levels and downregulation of genes involved in lipid synthesize and uptake [165]. NRF2 regulates lipid metabolism in the liver, either by upregulating the transcription of lipogenic enzymes such as FAS, SBPRE1c and SCD1, or by inducing the expression of small heterodimer protein (SHP) indirectly. Tribbles homolog 3 (TRB3) is involved in apoptosis and has been suggested to be involved in insulin resistance in obese subjects [166]. Knockdown of hepatic TRB3 improves glucose tolerance, whereas its overexpression leads to insulin resistance [167]. It has been demonstrated that TRB3 inhibits the insulin-induced activation of Akt. TRB3 has been considered as an ER stress-induced protein which is induced by ATF4 and CHOP by PERK branch [168]. Studies by Cohen's

group indicated that the activation of PERK as a conserve signaling mechanism may have negative effects on insulin responsiveness at the level of FoxO activity. They demonstrated that PERK can act directly on FoxO to increase FoxO activity in human cells. The active FoxO subsequently suppress hepatic glucose production [169].

1.5.2.3   ATF6 branch and insulin resistance

It has been suggested that overexpression of ATF6 is able to restore insulin-stimulated insulin receptor phosphorylation [170]. HEK293 cells treated with tunicamycin to induce ER stress and were then transfected with ATF6. Insulin receptor tyrosine phosphorylation was attenuated by tunicamycin, whereas overexpression of AFT6 protected against insulin resistance as a result of tunicamycin treatment [170]. Intriguingly, Hisamitsu's group [171] observed that ATF6 contributes to both prevention and promotion of diabetes in mice. In their study, ATF6α knockout mice displayed higher insulin sensitivity, but lower pancreatic insulin content, in response to high fat-feeding.

1.6   Lipid metabolism and ER stress

1.6.1   ER stress induced lipid synthesize

It has been shown that ER stress/UPR activation plays a crucial role in lipid metabolism and homeostasis [160, 172, 173]. Here, it is likely that ER stress-dependent dysregulation of lipid metabolism may result in dyslipidemia, insulin resistance, type 2 diabetes, and obesity. ER stress has been observed in several tissues from obese mice [125, 174] and humans [175, 176]. ER stress-induced UPR activation may also be relevant to fatty liver disease, where lipid droplets accumulate in the liver cells. The mechanisms by which UPR pathways mediate the

development of fatty liver disease has been under intense investigation. Werstuck and colleagues demonstrated that ER stress induced by homocysteine promotes hepatic steatosis, and triglyceride biosynthesize, both *in vitro* and in the livers of hyperhomocysteinemic mice [177]. Overexpression of GRP78, which improves ER stress and inhibits UPR activation, has been shown to alleviate hepatic steatosis by reducing SREBP1c activity [157].

The IRE1 branch of ER stress has been shown to play a critical role in lipid metabolism. Zhang and colleagues [99] generated hepatocyte-specific Ire1α –null mice to elucidate the physiological roles of IRE1α-mediated signaling in the liver. They demonstrated that hepatocyte-specific Ire1α deletion increased hepatic lipid and reduced plasma lipid content upon ER stress. In addition, IRE1α was indicated to suppress expression of lipogenic transcriptional activators, including PPARγ, LXR and ChREBP. When treated with tunicamycin, hepatocyte-specific Ire1α –null mice exhibited a deficient adaption to ER stress and modified lipid metabolism in the absence of the IRE1α. Moreover, ATF4 and CHOP, downstream proteins of the PERK pathway were increased in tunicamycin treated hepatocyte-specific Ire1α –null mouse liver [99]. However, another study in the same knockout mice fed a high fructose diet for 12 weeks did not show altered DNL, as indicated by unchanged expression of lipogenic enzymes (i.e. SCD1, FASN and ACC) and hepatic fatty acid synthesize as shown by labelling with [178] acetic acids [179].

XBP1, the downstream effector of IRE1, is reported as sufficient to induce phospholipid biosynthesize and ER expansion in mammalian cells [180]. The regulation of phospholipid synthesize is dependent on the cellular needs for ER membrane components. The most definitive study of the critical role of XBP1 in hepatic lipid regulation comes from Lee's group [160]. In this study, deletion of hepatic XBP1 led to lower lipid levels in the liver and reduced the expression of lipogenic genes such as DGAT2, SCD1 and ACC. XBP1

deficiencies led to profound compromise of *de novo* hepatic lipid synthesize, resulting in concomitant decreases in serum triglycerides and free fatty acids, in the absence of hepatic steatosis in high fructose feeding. Interestingly, IRE1α was activated in XBP1-deficient mouse liver, whereas the ATF6 processing, Bip and CHOP was absence [160]. In another study, IRE1α expression in the liver was silenced using siRNA in XBP1-deficient mice. IRE1α siRNA led to increased plasma triglyceride and cholesterol content in XBP1 knockout mice, suggesting that hyper-activated IRE1α contributes to the reduction of plasma lipids in the absence of XBP1 [179]. Furthermore, it has been demonstrated that XBP1 deficiency results in a feedback activation of IRE1α, inducing the degradation of mRNAs of a group of lipid metabolism genes (Dgat2, Acacb, Pcsk9, Angptl3 and Ces1) which regulate triglyceride and cholesterol metabolism at multiple levels [179].

In summary, the IRE1/XBP1 branch of UPR can regulate hepatic lipid metabolism via two distinct mechanisms. 1) IRE1α promotes the degradation of mRNAs encoding lipid metabolism genes involved in DNL, hydrolysis of triglyceride and lipoprotein catabolism. 2) IRE1α activates the XBP1 splicing, which can directly activate certain lipid metabolism genes.

The eIF2α is a downstream target of PERK, involving in UPR signaling pathways. The attenuation of eIF2α by overexpression of GADD34 in the liver results in impaired glucose tolerance and diminished hepatosteatosis in animals fed a high-fat diet. This attenuation correlated with levels of PPARγ, an adipogenic nuclear receptor, and the transcription factor C/EBP [181].

CHOP plays an important role in ER stress-induced apoptosis, and has been suggested to suppress the genes involved in lipid homeostasis, likely by negatively affecting C/EBP [173]. ATF6 and SREBPs are ER membrane bound transcription factors that share the same proteases for cleavage by the Golgi [182]. A close investigation of the relationship between

ATF6 activity and SREBP2-mediated lipogenesis suggested that nuclear ATF6 interferes with the mature form of SREBP2 in the nucleus and therefore antagonizes SREBP2-regulated transcription of lipogenic genes and lipid accumulation in cultured hepatocytes [183]. Additional studies have also examined the role of ATF6 on liver disease and lipid droplet formation *in vivo* [173, 184]. ATF6 knockout mice presented no apparent phenotype under physiological conditions, however when challenged with an ER stress insult by injection of tunicamycin, the livers of knockout mice failed to recover [184, 185]. The phenotypic outcome of the ER stress insult in ATF6 knockout mice was hepatic steatosis, caused by induction of lipid droplet formation due to the reduced β-oxidation of fatty acids and suppressed VLDL formation [185].

1.6.2   ER stress induced by lipids

Excess lipid accumulation and protein overload are two triggers of ER stress. Under physiological conditions, one of the roles of lipids on ER function is to maintain the ER capacity as phospholipids are an important component of the ER membrane. The composition of lipid affects many membrane-associated functions. Saturated fatty acid has been demonstrated to be a detrimental lipid in ER stress in cultured cells [186, 187]. It has been reported in contrast that unsaturated fatty acids led to a reduction of palmitate-induced upregulation of GRP78, GADD34 and CHOP in cultured cells. It has also been reported that hepatic steatosis caused by saturated fatty acid-enriched diets is associated with ER stress and liver injury, despite similar accumulation of triglycerides [188]. The negative effect of saturated fatty acids in ER stress was confirmed using SCD1-deficiency. Knockdown of SCD1 expression caused increased saturation of fatty acids and induced UPR [189]. Increased saturated fatty acids in the blood are also linked to insulin resistance and the risk of diabetes

in humans [190-192]. This phenomenon was also demonstrated in animal models, where treatment of animals with palmitate, a saturated fatty acid, induced acute ER stress and cytotoxicity [172]. These indicate a potential correlation between ER stress and insulin resistance. In addition, exposure to excess fatty acids over long periods of time may lead to overload, especially of nonadipose cells, resulting in chronic ER stress and lipotoxicity, as demonstrated in cell culture. When cells were incubated with oleic acid for a short time, both VLDL and triglyceride secretion were increased, while extended incubation led to ER stress and suppression of VLDL secretion [188]. This disorder of ER stress and suppression can be restored both *in vivo* and *in vitro* by 4-phenylbutyrate (PBA), a chemical chaperone, indicating that the chronic effects of fatty acids on ER function are related to compromised chaperone function [188]. Moreover, other studies have observed a chronic state of ER stress in obese subjects, in both mice or humans [156], which has allowed researchers to presume that the mechanism relates, at least in part, to a long term exposure to lipids.

Overload of proteins, the same as excessive lipid, is an endogenous trigger of ER stress. Another study from our group suggested that ER stress is involved in DNL *per se* rather than resulting from steatosis in the liver and insulin resistance, by comparing the HFru and HFat diets [193]. Studies by Hotamisligil's group [194] found that during ER stress in ob/ob mice, although ER-associated protein synthesize was suppressed in the liver, an augmention was detected of genes involved in DNL. When phosphatidylethanolamine N-methyltransferase (Pemt), responsible for phospholipid synthesize was suppressed, ER stress was an improved. However, in addition to the reduction of lipid content, a remarkable decrease in lipogenic genes was also detected. Whether or not increasing pecific proteins in lipogenesis are able to initiate ER stress, is not yet clear.

1.7 PPARα and lipid metabolism

PPARα belongs to the family of peroxisome proliferator-activated receptors (PPARs). Transcriptional regulation of PPARα is achieved by direct binding to specific nucleotidic sequences, in the promoter region of target genes or in an intronic sequence of a gene [195-197], such as PPARα can be activated by both endogenous and synthetic ligands. The increased fatty acid influx into the cell resulting from fasting or high fat feeding is able to activate PPARα [198, 199]. PPARα is also a molecular target for fibrates. Fenofibrate is a derivative of a fibric acid used for the treatment of mixed dyslipidaemia and hyper-triglyceridaemia in adults [200]. These effects are mediated by the activation of PPARα. PPARα activation induces the expression of multiple genes involved in lipid metabolism, including both fatty acid oxidation and other lipid metabolic processes [201, 202]. The first report of the relationship between PPARα and fatty acid oxidation was published in 1992 [203]. The authors reported that activation of PPARα upregulates the expression of peroxisomal acyl-CoA oxidase, a key enzyme involved in peroxisomal fatty acid β-oxidation. Further studies have demonstrated that the mitochondria fatty acid β-oxidation is also regulated by PPARα as well as peroxisomal fatty acid β-oxidation [201].

Although most of the PPARα target genes are involved in fatty acid catabolism, some genes involved in lipogenesis has also been identified as PPARα targets [204-206]. The malate NADP oxidoreductase catalyzes the oxidative decarboxylation of malate into pyruvate, generating the energy required for fatty acid synthesize. PPARα knockout mice show decreased malate NADP oxidoreductase in the liver, indicating a potential link with PPARα [204]. In addition, SCD1 is a direct target gene of PPARα, as it catalyzes saturated fatty acids to unsaturated fatty acids [205]. Other desaturases have also been found to be upregulated by

PPARα [206]. These findings suggest that PPARα may play an important role in the conversion of saturated fatty acids to unsaturated fatty acids.

Regulation of PPARα can be complex in physiological conditions. For example, PPARα-mediated upregulation of some desaturases may serve to counteract excess fatty acid breakdown caused by the induction of oxidation [207]. Alternatively, the induction of desaturases serves to provide endogenous ligands for PPARs, as unsaturated fatty acids may be better PPARα ligands [208]. It has also been suggested that PPARα and SREBP1 regulate desaturases, where SREBP1 is responsible for feeding periods, and PPARα exerts regulation during fasting [207].

While several pharmacological agents are commonly used as PPARα specific agonists, including WY14643 [209] and GW7647 [210], only fibrates (often fenofibrate) are used clinically to treat dyslipidemia. Fenofibrate is a fibric acid derivative and is a pharmacological PPARα agonist that is used clinically to treat dyslipidemia. In primary dyslipidemia, fenofibrate monotherapy consistently reduced triglyceride content, significantly increased high density lipoprotein cholesterol levels while suppressed the low-density lipoprotein cholesterol and total cholesterol levels [200].

1.8   Tauroursodeoxycholic acid

Tauroursodeoxycholic acid (TUDCA) is an ambiphilic bile acid. It is the taurine conjugate form of ursodeoxycholic acid (UDCA) [211]. TUDCA has been safely used as a hepatoprotective agent in humans with cholestatic liver diseases; it ameliorates ER stress in cells and whole animals by blocking calcium-mediated apoptotic pathways [212]. It is also a chemical chaperone that can modulate ER function by protecting against UPR induction and ER-stress induced apoptosis [213]. Consequently, TUDCA is often used to attenuate ER

stress in animal studies. When treated with TUDCA, obese mice present reduced expression of UPR transducers such as p-PERK and p-IRE1. IRS^{ser307}, which can be activated by JNK, also decreased as did JNK itself in TUDCA treated animals. Moreover, blunted insulin signal transduction was observed [212, 214].

1.9 Role of dietary fructose

1.9.1 Fructose consumption

There is a dramatic increase in dietary sugar consumption in the world over the past four decades. The increased consumption is paralleled by epidemics in obesity and metabolic syndrome, suggesting a causal relationship [215]. A character of most Western diets is the utilization of high levels of carbohydrate, especially sugar [216]. A growing body of evidence demonstrates that in addition to overall sugar intake, fructose is especially harmful to metabolic health as a risk factor for obesity and type 2 diabetes [217-221]. The rapid increase in fructose consumption is mainly due to the use of high fructose corn syrup (HFCS) in food and beverage production, as a sweetener. The typical form of HFCS-55 has 10% more fructose than sucrose [222]. It has been reported that countries with HFCS as a second sweetener exhibit an elevated risk of diabetes beyond the effects of sugar itself and of BMI, possibly due to its higher content of fructose (Table 2) [222]. One study in healthy subjects shows a significant increase in fasting blood glucose level after ingestion of 20% fructose solution as part of the three main daily meals for the 6 days before the test [223]. These subjects developed insulin resistance in the liver and adipose tissue, but not in muscle, when assessed by hyperinsulinemic-euglycemic clamp combined with the use of ^{3}H-glucose [223, 224]. Only fructose consumption led to a significant increase in hepatic *de novo* lipogenesis in

overweight and obese subjects who consumed either glucose- or fructose-sweetened beverages for 10 weeks. Moreover, fasting blood glucose and insulin levels were upregulated, while insulin sensitivity was downregulated in the subjects consuming fructose, but not in those consuming glucose [225]. These indicators of diabetes were higher in countries that use HFCS as compared to those that do not, and this trend was significant for International Diabetes Federation estimates of diabetes prevalence and fasting plasma glucose [222].

Table 2 Comparison of countries with low vs. high availability of HFCS.

	Countries not using HFSC (n=22)	Countries using HFSC (n=21)	p-Value
Prevalence of Diabetes (IDF) (%)	6.3±1.5	7.8±2.1	0.013
Fasting glucose (mmol)	5.23±0.17	5.33±0.17	0.046
BMI (kg/m^2)	25.5±1.6	25.9±1.4	NS
Total intake (Kcal/day per capita)	3230±377	3221±365	NS
Cereals (kg/year per capita)	129.8±30.1	137.0±36.2	NS
Total sugar (kg/year per capita)	38.2±12.8	39.9±11.3	NS
Other sweeteners (kg/year per capita)	5.5±7.1	6.1±8.3	NS

IDF: International Diabetes Federation.
(Adapted from Goran, M. I., et al. Glob Public Health, 2013)

1.9.2   Fructose metabolism

Although fructose has the same molecular formula and molecular weight as glucose, it is chemically distinct. The substitution of a hemiketal group for the hemiacetal group of glucose

results in a markedly different fate. The absorption of fructose in the intestines is regulated by GLUT5 while glucose uptake is through GLUT4 [226]. Once fructose is absorbed, it is delivered to the liver through the portal vein [227]. In the liver, fructose is largely transported via GLUT2 and rapidly phosphorylated by fructokinase to form fructose-1-phosphate (F1P). Unlike phosphofructokinase, fructokinase activity is not suppressed by ATP [228]. Consequently this reaction might be less responsive to cellular energy states, leading to poorer regulation of fructolysis [229]. F1P is then metabolised to glyceraldehyde and dihydroxyacetone phosphate (DHAP) by aldolase B. Both products can be converted to glyceraldehyde-3-phosphate (GA3P). The carbons in GA3P can proceed further down the glycolytic pathway into acetyl-CoA, which is either oxidized in the TCA cycle or committed towards fatty acid synthesize. The glyceraldehyde can also contribute to lipid synthesize by forming glycerol-3-phosphate (G3P) [229]. Hence, the carbons of fructose are fated to end up in triglyceride within the hepatocytes.

Unlike fructose-6-phosphate in glucose metabolism, fructose-1-phosphate can bypass a critical regulatory step in glycolysis, generating fructose-1, 6-bisphosphate via the action of the energy-sensitive enzyme phosphofructokinase. As a result, fructose is converted into lipid unconstrainedly from the cellular control [218, 225]. In addition, Lanaspa and his colleagues have demonstrated that mice with fructokinase-deficiency are protected from the adverse effects of excessive glucose consumption. It is believed that the polyol pathway in the liver converts the excess glucose by aldose reductase (AR) into fructose, which is stored as lipid, but only in the presence of fructokinase (Figure 1.7)[215]. As high consumption of fructose could cause excess lipid accumulation in the liver, it is hence considered as a "fat sugar".

Diet

Glycolysis

Glucose → AR → Fructose

Polyol pathway

Fructokinase

G-1-P ↔ G-6-P

F-1-P

F-6-P

ATP or citrate

Glyceraldehyde

DHAP

Glycogen

F-1,6-P

GA3P

Fructose metabolism

ATP and citrate

G3P

FA and TG biosynthesis
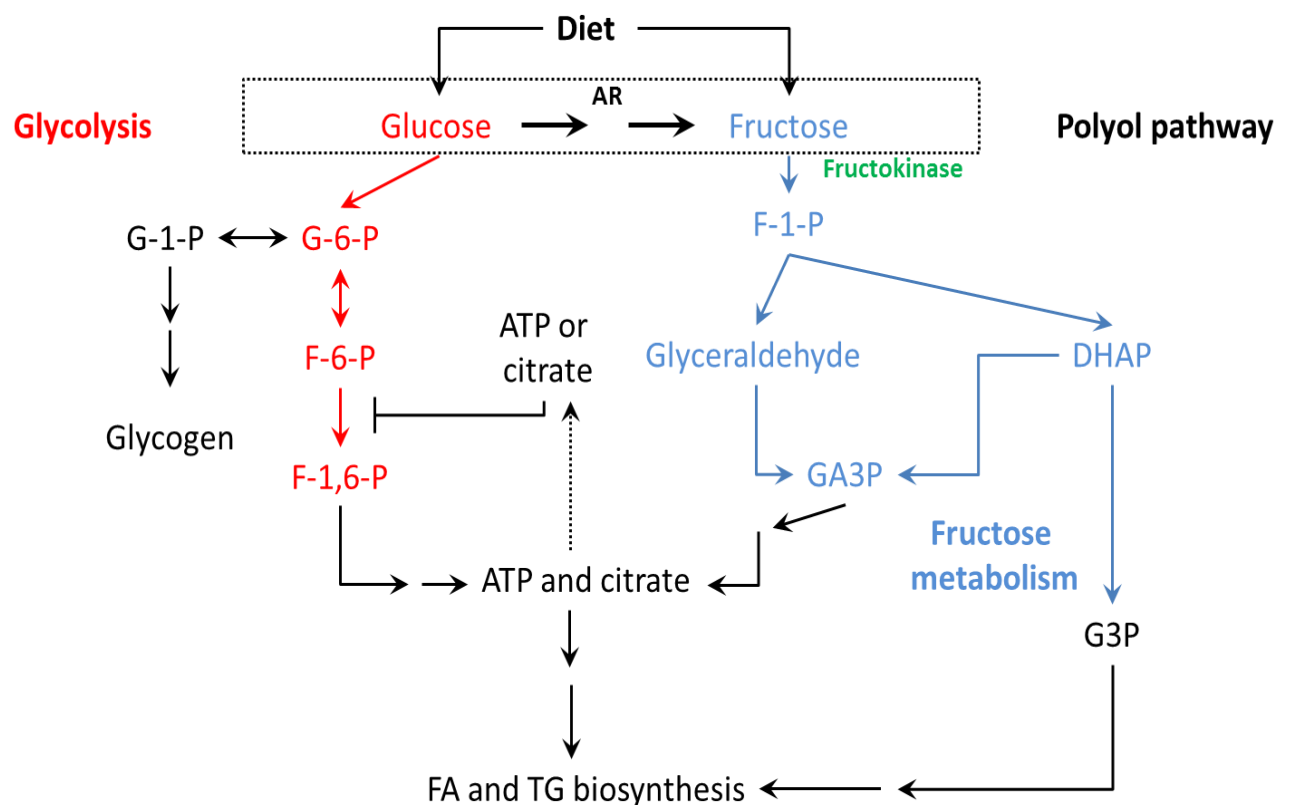
Figure 1.7 Carbohydrate metabolism.

Glucose and fructose are dietary sugars. Glucose is most metabolized by glycolysis and can be inhibited by ATP or citrate as a feedback response. In the liver, fructose is metabolized to glyceraldehyde-3-phosphate (GA3P) or glycerol-3-phosphate (G3P) to form fatty acids or triglyceride. It is a biosynthetic pathway that is not regulated by the ATP- or citrate-feedback mechanisms. Glucose can also be converted into fructose by the polyol pathway. AR, aldose reductases; G-1-P, glucose-1-phophate; G-6-P, glucose-6-phosphate; F-6-P, fructose-6-phosphate; F-1,6-P, fructose-1,6-bisphosphate; F-1-P, fructose-1-phosphate; DHAP, dihydroxyacetone phosphate; FA, fatty acids; TG, triglyceride (Modified from Lyssiotis, C. A., et al., Nature, 2013)

1.10 Aims of the thesis and summary of outcomes

Although enormous progress has been made in our understanding of the role of dietary

fructose in lipid metabolism and insulin resistance, the mechanisms involved are not

completely clear. Based on the published literature and preliminary data, the overall aim of

this project is to understand the role of lipid accumulation and ER stress on the development of insulin resistance in response to different levels of nutrition.

The experimental models chosen for this research were the high fructose, or high fat fed, mice, which show hepatic lipid accumulation and insulin resistance. High fructose fed mice exhibited activated UPR while high fat fed mice did not present any ER stress during the feeding periods (<8 wk). These models allow the investigation of the effects of lipid- or ER stress-reducing strategies on insulin sensitivity. The method chosen to reduce lipid content was the oral intake of fenofibrate, to induce PPARα activation. The method chosen to reduce ER stress was the i.p. injection of the chemical chaperone, TUDCA to ameliorate ER stress.

The first aim, discussed in Chapter Chapter 3, was to investigate the role of lipid accumulation and ER stress on the initial insulin resistance when the whole body remained glucose tolerant. The second aim, discussed in Chapter Chapter 4, was to confirm whether the negative effects of ER stress-induced JNK activation on insulin sensitivity remained as a predominant trigger when insulin resistance became more developed over time in response to over-nutrition consumption. Chapter Chapter 5 discussed the relationships between lipogenesis and ER stress *in vitro*. Chapter Chapter 6 presented the results of the high fat model study. However, these data were not completed to understand the different mechanisms by which high fructose contributes to insulin resistance.

Dietary effects on whole-body metabolism are considered to play one of the central roles in the pathogenesis of metabolic syndromes. The outcome of this project will provide the principle of concept to target lipogenesis and ER-stress, to screen new drugs for the treatment of insulin resistance and the metabolic syndrome. This project will also establish a new platform for the discovery of new drugs for the treatment of type 2 diabetes. The significance

of these studies not only lies in bridging gaps in the current literature, but also in providing the basis for drug design and discovery towards preventing and treating type 2 diabetes.

Chapter 2

General Methods

2.1   Studies in animals

All experimental procedures were approved by the Animal Ethics Committees of the RMIT University in accord with to the Australia National Health and Medical Research Council guidelines.

Male C57BL/6J mice, obtained from the Animal Resources Center (Perth, Australia), were communally housed at $22 \pm 1^{\circ}C$ on a 12 hours light/dark cycle in the Research Animal Facility at RMIT University. All animals were given free access to food (standard pellet diet) and water ad libitum. In different studies, animals were fed with either high fat or high fructose diets which will be described later. Bodyweight and food intake were measured daily.

After the acclimatization for approximately 1-2 weeks, the mice were fed either chow (CH), high fructose (HFru) or high fat (HFat) diets. Chow-fed mice, with normal insulin sensitivity, were maintained in the chow diet during the study period, with free access to food and water.

The insulin resistance/ER stress/DNL models consist of mice fed either HFru or HFat for the relative period. The details will be described in following chapters. Both HFru and HFat diet were prepared weekly from the ingredients presented in **Table 3** and kept in the fridge until use. The composition of the chow diet as percentage of total calories was 23% protein, 71% carbohydrate, and 6% fat. The composition of the HFru diet as percentage of total calories was 21% protein, 70% carbohydrate, and 9% fat. The composition of the HFat (60%) diet as percentage of total calories was 20% protein, 23% carbohydrate, and 60% fat. These diets were with the equal quantities of fiber, vitamins, and minerals to the standard diet [193].

Table 3 Composition of the diets.

	Component g/kg		Component g/kg		Digestible energy kcal/kg
HFru diet	Casein	169.0	Methionine	1.7	3.569
	Fructose	295.8	Gelatine	12.7	
	Cornstarch	295.8	Choline Bitartate	3.9	
	Mineral Mix	44.8	Safflower Oil	5.2	
	Trace Minerals(ICN)	12.5	Lard	32.0	
	BRAN	33.8	AIN Vitamins	8.5	
HFat diet (60%)	Casein	255.6	Methionine	2.6	5.397
	Sucrose	85.6	Gelatine	19.2	
	Cornstarch	170.0	Choline Bitartate	4.5	
	Mineral Mix	44.7	Safflower Oil	47.8	
	Trace Minerals(ICN)	12.8	Lard	293.4	
	BRAN	51.1	AIN Vitamins	12.8	
Chow diet	The standard chow diet (CH; Meat Free Rat and Mouse Diet) was purchased from Specialty Feeds, Western Australia.				3.34

2.1.1 Determination of whole-body energy expenditure and fat oxidation

The oxygen consumption rate (VO_2) and carbon dioxide production rate was assessed using comprehensive laboratory animal measurement system (CLAMS, Columbus Instruments, USA). Mice were weighed and placed in the metabolic chamber at 5 pm. After overnight acclimation, VO_2 and CO_2 production were measured in individual mice at 18 min intervals

over a period of 24 hours period at a constant environmental temperature (22 $^{\circ}$C). Respiratory exchange rate (RER) was calculated from VO_2 and CO_2 production and the values are in reverse proportion to whole-body fat oxidation.

2.1.2 Glucose tolerant test (GTT)

Glucose tolerant test (GTT) is a standard procedure to assess how quickly exogenous glucose can be cleared from blood. Glucose intolerance is an indication of impaired glucose homeostasis such as insulin resistance and diabetes.

Mice were fasted for 4 hours with free water supply before experiment. After basal blood glucose level was measured, glucose (3 g/kg bodyweight) dissolved in saline was injected intraperitoneally. Mice were then put back into the cages. Blood glucose level was measured at 15, 30, 60, 90 minutes and blood samples were collected at each time point. The incremental area under curve (iAUC) was calculated to assess the glucose tolerance.

2.1.3 Plasma measurements and assays

Blood samples were collected by reopening the tail wound using a heparin capillary tube (Hirschmann Laboratory, Germany) to prevent clotting and haemolysis. Blood glucose level was measured using a glucometer (AccuCheck Proforma Nano; Roche, Victoria, Australia). Plasma samples were derived from supernatant of the blood samples after centrifuging at 13000 rpm for 2 min. 5 μl of plasma sample was added into 96 well plates with a Peridochrom Triglyceride GPO-PAP kit (Roche Diagnostics, Australia). Plasma insulin level was determined using a commercial insulin radioimmunoassay kit (Merck Millipore, #SRI-

13K). This method is based on a double antibody technique, using ^{125}I-labelled insulin and specific mouse insulin antiserum.

2.1.4 Tissue assay methods

2.1.4.1 Tissue fractionation

Approximate 70 mg of fresh liver tissue was homogenized in 350 μl of HES (HEPES/EDTA/sucrose) buffer [230]. Then samples were centrifuged at 25,000 g for 10 min at 4 $^{\circ}$C. The supernatant plasma was collected into new tubes for analysis. The pellet was suspended with 100 μl of HES buffer and centrifuged under the same condition as before and the supernatant was discarded. The pellet which was the nucleus was resuspended with 100 μl of HES buffer and then homogenized with a 25-G7/8 needle.

100 mg of fresh tissue was homogenized in 1 ml of homogenization buffer A. 400 μl of 3% sucrose was layered on top of the homogenate and samples were centrifuged at 100,000 g for 1 h at 4 $^{\circ}$C. The lipid layers were removed with a 23-G1 needle and the plasma was removed. The pellet was resuspended in 700 μl Buffer A for DAG analysis or 700 μl Buffer B and other reagents for protein analysis. The samples were then homogenized with a 25-G7/8 needle, and centrifuged at 20,800 g for 15 min at 4 $^{\circ}$C. The remaining floating lipid was removed with a 23-G1 needle and Triton-X was added (2%) to the supernatant of the samples for protein analysis, or the supernatant was completely removed and the pellet was suspended in 700 μl Buffer A for DAG analysis. Membrane samples were then passed through a 28-G1/2 needle and stored at -20 $^{\circ}$C for DAG analysis. The supernatant membrane fraction was removed and saved. Proteins in the lipid fraction were precipitated in acetone at -20 $^{\circ}$C overnight, and then

centrifuged at 20,800 g for 30 min at 4 ºC. The protein pellet was then dried under N_2 and resuspended in Buffer B with 2% Triton-X [231].

Table 4 Composition of the buffers for tissue fractionation.

HES buffer	20 mM Hepes, pH 7.4, 1 mM EDTA, 250 mM sucrose and protease and phosphatase inhibitors
Buffer A	20 mM Tris- HCl (pH 7.4), 1 mM EDTA, 0.25 mM EGTA, 250 mM sucrose, protease and phosphatase inhibitors
Buffer B	20 mM Tris- HCl (pH 7.5 at 4 ºC)
Reagents with Buffer B	150 mM NaCl, 50 mM NaF, 5 mM NaPPi, 1 mM EDTA, 1 mM EGTA, 1 mM PMSF, protease and phosphatase inhibitors

2.1.4.2   Tissue triglyceride content

Frozen tissue samples were homogenized in $CHCl_3$: MeOH (2:1) using a hand-held glass homogenizer to extract triglycerides. The homogenate was then transferred to a clean tube. The homogenizer was rinsed with a further $CHCl_3$: MeOH, which was added to the homogenate. The tube were tightly capped and rotated at room temperature overnight to ensure the solubilisation of the triglyceride. 1 mM of NaCl was added afterwards, thoroughly mixed and the tubes were centrifuged at 450 g for 15 min to separate the aqueous from organic phases. The lower organic layer, containing the triglyceride, was carefully transferred to a glass vial and dried completely under air at 45 ºC. The pellet was redissolved in an appropriate amount of ethanol depending of the tissue. The tissue triglyceride level was determined using a commercial kit (Peridochrom Triglyceride GPO-PAP kit, Roche Diagnostics, Australia), against a standard curve [193].

2.1.4.3   Determination of tissue diacylglycerol and ceramide

Lipids were extracted from liver homogenates that were mentioned in 0 using $CHCl_3$: MeOH : PBS+0.2% SDS (1:2:0.8). Diacylglycerol kinase and ^{32}P-labelled ATP (0.55 GBq/mmol cold ATP) were added to the lysates pre-incubated with cardiolipin/octylglucoside. During the reaction, DAG and ceramide were converted in to ^{32}P-phophatidic acid and ^{32}P-ceramide-1-phosphate respectively. The reaction was stopped after 2.5 hours by the addition of $CHCl_3$: MeOH (2:1) and 1% perchloric acid. To separate the radioactive products, the tubes were centrifuged at 2000g for 2 min. The upper aqueous layer containing unreacted ^{32}P-ATP was discarded and the organic payer was washed twice with $CHCl_3$, centrifuged and upper phase discarded. The organic layer was dried under N_2 and stored at -20 ^oC overnight.

To separate and quantify of ^{32}P-phosphatidic acid and ^{32}P-ceramide-1-phosphate, the samples were spotted onto thin-layer chromatography (TLC) plates. For the accurate comparison between plates, each plate contained one blank, one DAG and one ceramide standards. The plates were placed in the pre-saturated TLC tanks containing $CHCl_3$: MeOH: ammonium hydroxide (65:35:7.5 v/v/v), until the solvent reached the top of the plate. Following approximately 30 min drying period, the plates were place in the pre-saturated TLC tank containing $CHCl_3$: MeOH : acetic acid : acetone : water (10:2:3:4:1 v/v/v/v/v) until the solvent reached the top of the plate. This procedure optimized the separation of ^{32}P-phosphatidic acid and ^{32}P-ceramide-1-phophate. The plates were dried for 30 min and placed in black phosphorimager cassettes overnight. The plates were then developed. ^{32}P-labelled phosphatidic acid and ceramide-1-phosphate were identified by autoradiography, dried, scraped from the TLC plates and counted in a liquid scintillation analyser (LS6500, Beckman Counter Inc, USA) [232].

2.1.4.4 Measurement of hepatic fatty acid oxidation

Fatty acid oxidation was measured in liver homogenates. Liver samples were homogenized in ice-cold 250 mmol/l sucrose, 10 mmol/l Tris-HCl, and 1 mmol/l EDTA, pH 7.4. For assessment of substrate oxidation, 50 μl of liver homogenate was incubated with 450μl reaction mixtures (pH 7.4). Final concentration of the reaction mixture were: 100 mmol/l sucrose, 80 mmol/l KCl, 10 mmol/l Tris-HCl, 5 mmol/l KH_2PO_4, 1 mmol/l $MgCl_2$, 2 mmol/l malate, 2 mmol/l ATP, 1 mmol/l dithiothreoitol, 0.2 mmol/l EDTA and 0.3% fatty acid free BSA. The homogenate was incubated at 30 ℃ for 90 min in the reaction mixture containing 0.2 mM [178]-palmitate (0.5 μCi), 2 mM L-carnitine and 0.05 mM Coenzyme A. The reaction was stopped by the addition of 100 μl of ice-cold 1 M perchloric acid. CO_2 produced from the reaction was captured in 1 M NaOH. [14]C counts in the acid-soluble fraction were combined with the CO_2 values to give the total palmitate oxidation rate [232].

2.1.4.5 Measurement of hepatic de novo lipogenesis

Hepatic *de novo* lipogenesis was assessed by measuring the incorporation of [44, 45, 178]-H_2O into triglyceride in the liver. Mice were injected with [44, 45, 178]-H_2O (20 μCi/g BW, ip) before tissue collection. Liver samples were collected at 90 minutes for the measurement of radioactivity in liver triglyceride against the count in plasma using a β-scintillation counter (Tricarb, Bio-Rad, USA).

2.1.4.6 Citrate synthase assay

Citrate synthase is a critical enzyme in the Krebs cycle. It is localized in the mitochondrial matrix and commonly used as a quantitative marker enzyme for the capacity of intact

mitochondria [233]. Mitochondria proliferation is normally associated with an increase of citrate synthase activity. Citrate synthase catalyzes the reaction of 2 carbon acetyl CoA to form 6 carbon citrate and hence to regenerat coenzyme A [234]. The citrate synthase assay is a spectrophotometric enzyme assay. The optical density of the liquid sample is related to the absorbance. The rate of increase of the absorbance appears to be the slope which is proportional to enzyme activity. In the spectrophotometer, the reaction catalyzed by citrate synthase is coupled to the irreversible chemical reaction. The product of the reaction (thionitrobenzoic acid) is an absorbing substance with intense absorption at 412nm. The absorbance increases linearly with time.

Frozen samples were homogenized in 165 mmol/l KCL and 1.98 mmol/l EDTA-containing buffer (pH 7.4) with a glass homogenizer before being subjected to three freeze-thaw cycles. Samples were added to 96 well plates with working solution that shown in **Table 5** for blank reaction which was red at 412 nm over 2 min at room temperature. Then oxaloacetic acid was added to each well to initiate the main reaction and the change of the absorbance was recorded [235].

Table 5 Working solution of citrate synthase assay.

Reagent (10 ml)		
100 mM Tris buffer	7	ml
1 mM DTNB	1	ml
3 mM acetyl CoA	1.5	ml
10% Triton X-100	250	μl
dH_2O	250	μl

Equation for calculation:

$$\text{Acitivity} = \frac{\text{Change in absorbance per minute } \times \text{Volume}_{\text{total}} \times \text{dilution factor}}{\text{Extinction coefficient } \times \text{Volume}_{\text{sample}} \times \text{Optic path} - \text{length}}$$

Where:

Change in absorbance per min = Δ Abs./min

Volume $_{\text{Total}}$ = 0.5 ml for cuvette, 0.2 ml for microplate

Dilution factor = 40 for 1:50 dilution or 100 for 1:100 dilution

Extinction Coefficient = 6.22 μmol/cm^2

Optical path-length= 1 cm for cuvette, to be determined for microplate

Volume $_{\text{Sample}}$ = 0.02 ml for microplate

2.1.4.7   β3-hydroxyacyl-CoA dehydrogenase activity assay

β3-hydroxyacyl-CoA dehydrogenase (β-HAD) is an oxidoreductase which catalyzes the third step of β-oxidation, converting the hydroxyl group to a keto group and forming the end product 3-ketoacyl CoA [236]. The β-HADIRE1 assay is based on the reverse reaction. Enzyme activity is calculated according to the disappearing rate of NADH over time.

The sample preparation was the same as mentioned in 2.1.4.6. The supernatents were then added into 96 well plates with the assay solution. The plate was then incubated in the spectrophotometer for 5 minutes at room temperature and red the blank reaction at 340 nm. Additional 4 μl acetoacetyl-CoA was added to each well. The decrease in absorbance was recorded in spectrophotometer for at least 3 minutes.

Table 6 Assay solution of β-HAD assay.

Reagent	volume (ml)
[63] Tris-HCl	1.25
[200 mM] EDTA	0.25
[5 mM] NADH	1.25
H_2O	22.25

For 96 well plate method, 10% Triton X need to be added to the assay solution.

Equation for calculation:

$$\beta - HAD_{activity} \ (\mu mol/g/min)$$

$$= \frac{(\text{Rate of disappearance of NADH} \times \text{Volume}_{total}) \times \text{dilution fator}}{\text{Extinction coefficient} \ \times \text{Optical path} - \text{length} \times \text{Volume}_{Sample}}$$

Where:

Rate of disappearance of NADH = Δ Abs./min

Volume $_{Total}$ = 0.5 ml for cuvette, 0.2 ml for microplate

Dilution factor = 40 for 1:50 dilution or 100 for 1:100 dilution

Extinction Coefficient = 6.22 $\mu mol/cm^2$

Optical path-length= 1 cm for cuvette, to be determined for microplate

Volume $_{Sample}$ = 0.01 ml for microplate

2.2 Cell culture procedures

2.2.1 General procedures

Cells were cultured in Dulbecco's modified Eagle's medium (DMEM) supplemented with 10% (v/v) fetal bovine serum (FBS) and 1% (v/v) penicillin-streptomycin-glutamine (PSG) or 1% (v/v) penicillin-streptomycin (PS) at 37 °C in 5% CO_2. All above culture reagents were obtained from Invitrogen (Melbourne, Australia). The cell culture medium was changed every two or three days. Cell passages of 5 to 20 were used for all experiments. Briefly, cells were sub-cultured at 1 in 5 dilutions when cells reached 70-80% of confluence. Subculture was made by rinsing the cells first with 1x phosphate buffered saline (PBS) buffer (0.2 M NaCl, 10 mM Na_2HPO_4, 3 mM KCl, 2 mM KH_2PO_4, pH 7.4), then adding 1~2 ml of 1x trypsin-EDTA solution (Sigma-Aldrich, Melbourne, Australia) to detach the cells from the T75 flask (usually within 1 min). Cells were then centrifuged at 100 g for 5 mins and re-suspended in ~5 ml of fresh culture medium and were transferred with desired amount into a new T75 flask containing fresh growth medium.

2.2.2 Storages of cells

Cells were washed with 1x PBS, trypsinized with 1x trypsin-EDTA solution and incubated at 37 °C for 1~2 mins. Cells were then rinsing with 5 ml normal culture media per T75 flask and centrifuged at 100 g for 5 mins. Supernatant was aspirated. The remaining cell pellet was re-suspended in 0.5 ml of DMEM / 20% FBS / 15% DMSO / 1% PS or PSG to re-suspend cells, mixed. Then 1 ml aliquots were prepared in each cryovial. Cryovials were then wrapped in a clean paper towel and transferred to a Nalgene® cryo 1°C freezing container (Thermo Fisher Scientific, Australia) filled with 100% isopropanol (Sigma-Aldrich, #I9516), and stored

overnight at -80 ℃. The next day, one of the frozen vials was defrosted to test cell viability while the rest of vials were placed in liquid nitrogen for long-term storage.

2.2.3 Counting of cells number

Cell numbers were counted using haemocytometer (Grace Davison Discovery Sciences, Australia). In general, 100 μl of well-mixed cells suspension was placed into the counting area of a clean haemocytometer and counted under a microscope (10x or 20x objectives) and counted (4 x 16 corner squares). Cell concentration were calculated by dividing the total number of counted cells by 4 and multiplying by 2, from all 4 corners of the haemocytometer (Figure 2.1)
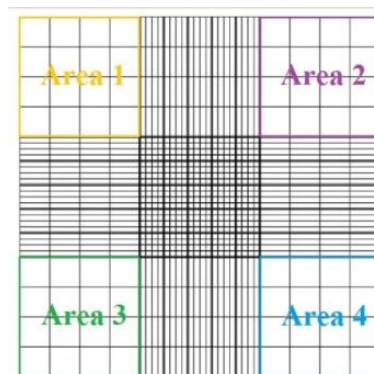
Figure 2.1 Hemocytometer.

The calculation formula of counting cells using hemocytometer is:

$$Cell\ number/ml = \ Counted\ cells\ number/4 \times 10^4$$

Where:

Counted cells number = Cells number of Sum (Area1 + Area2 + Area3 + Area4)

After cells number reached a desired confluence, the cells were seeded into suitable plate for further experiments.

2.3 Western Blotting

2.3.1 Protein extraction

Frozen tissues were kept on ice and homogenised with ice-cold RIPA buffer (pH 7.4, Table 7) with a pestle mixer. After incubating with lysis buffer for 2 hours at 4 $^{\circ}$C, the samples were centrifuged at 13,000 rpm for 10 min at 4 $^{\circ}$C. The supernatant was collected for further experiments or stored at -80 $^{\circ}$C.

Table 7 RIPA buffer.

Stock		Fresh	
Tris	65 mM	NaF	10 mM
NaCl	150 mM	NA_3VO_4	1 mM
EDTA	5 mM	PMSF	1 mM
NP-40	1%		
Na-deoxycholate	0.50%	protease/phosphatase inhibitors	10 ul/ml
SDS	0.10%		
glycerol	10%		

2.3.2 Protein assay

The protein concentration of homogenate was determined by the BCA protein assay using a commercial kit (Sigma-Aldrich, #B9643). Samples were diluted from 1:5 to 1:50, depending on the specific tissues being assayed, with lysis buffer and added into 96-well plate with duplications. The standard was the bovine serum albumin (BSA) which was diluted to different concentration. Working reagent was made following the manufacturer's instructions and pipetted to the plate to start the reaction. The plate was incubated at 37 $^{\circ}$C for 30 minutes

and read in the spectrophotometer. Protein concentration of the samples was calculated from the standard curve. An aliquot of the samples was dissolved in the Laemmli buffer to obtain equal amounts of protein in all samples. The samples were heated at 37 ºC for 30 minutes or 90 ºC for 10 minutes to denature, depending on the specific protein being assayed.

2.3.3   SDS-PAGE and immunodetection of protein

Plates were assembled following the manufacturers' instruction (Biorad, Sydney, NSW, Australia). The 8%, 10% or 12% Tris-glycine based gels (1.5 M Tris, pH 8.8, 30% acrylamide, 10% SDS, distilled water, 10% ammonium persulfate and TEMED) were prepared and transferred to the glass plates as running gels. The EtOH was added on the top of the gels to remove bubbles. The solution in the plate was left to set at room temperature. Once the running gel had set, the EtOH was removed and a 4% stacking solution (0.5 M Tris, pH 6.8, 30% acrylamide, 10% SDS, distilled water, 10% ammonium persulfate and TEMED) was layered on top of the running gel. The comb was inserted the solution was left to polymerize at room temperature. Gels were stored in running buffer at 4 ºC until use.

Equal amounts of protein samples were loaded into wells on the gels and run with the protein ladder (Biorad, Sydney, NSW, Australia) in a tank filled with running buffer (25mM Tris, 192 mM glycine, 0.1% SDS, pH 8.9). Electrophoresis was performed at 130 V until the separation was completed.

The gels were then carefully removed from the plates and stored in ice-cold transfer buffer (25 mM Tris, 192 mM glycine, 20% MeOH) temporarily. When the preparation of sponges and blotting papers was ready, the gel and membrane were sandwiched between sponge and paper and were clamped tightly together after checking air bubbles between the gel and

membrane. The whole set was then placed in a tank filled with transfer buffer and protein was transferred from gels to activated PVDF membranes (Biorad, Sydney, NSW, Australia) at 90 V for 2 hours. Ponceau red staining was used to confirm the transfer of protein.

Non-specific binding was blocked with 3% bovine serum albumin in Tris Buffered Saline plus 0.1% Tween-20 (TBST) for 1 hour at room temperature or overnight at 4°C. The membranes were washed with TBST and incubated with the primary antibody (**Table 8**) for 2 hours at room temperature or overnight at 4°C. The membranes were then washed with TBST several times to remove the unbound antibody. The wash was followed by the incubation with a respective secondary antibody for at least 2 hours at room temperature. After washing with TBST for 6 times, chemiluminescence reagent was used to detect the bound antibody to visualise the protein bands. The protein bands of interest were quantified using commercial software (Image Lab v4.1, Biorad Laboratories, 2012).

After the development of specific proteins, membranes were stripped with a stripping buffer (1 M Tris-HCl, pH 6.7, 20% SDS) at 60°C for 30 minutes. To confirm whether the membrane was stripped completely or not, the membrane was blocked with 3% BSA in TBST solution and incubated with secondary antibody for 1 hour at room temperature. The membrane then was developed with chemiluminescence solution and the loss of protein bands indicated that stripping was successful. The stripped membrane can be used to probe for other proteins.

Table 8 List of antibodies.

Name	Company	Name	Company
p-Akt (Ser 473)	Cell Signaling	p-IRS1(Ser307)	Cell Signaling
t-Akt	Cell Signaling	CHOP	Santa Cruz
p-GSK3β	Cell Signaling	p-IRE1	Abcam

Name	Company	Name	Company
t-GSK3β	Cell Signaling	XBP1	Santa Cruz
SREBP1c	Santa Cruz	ATF6	Santa Cruz
FAS	Cell Signaling	p-IKKα/IKKβ	Cell Signaling
ACC	Cell Signaling	IκBα	Cell Signaling
SCD1	Cell Signaling	p-JNK	Cell Signaling
ACOX1	Santa Cruz	t-JNK	Cell Signaling
p-PERK	Cell Signaling	p-cJun	Cell Signaling
p-eIF2α	Cell Signaling	t-cJun	Cell Signaling
GADD34	Cell Signaling	PKCε	Cell signaling

2.4   Statistical analysis

Results were expressed as mean $\pm$ SE throughout the thesis. For the comparison of more than two groups, one-way analysis of variance (ANOVA), followed by Tukey-Kramer multiple comparisons test, were performed to assess statistical significance between groups. A Student's t test was used where only two groups were compared. The analysis was performed using a commercial software package (GraphPad Prism, 5.01, GraphPad Software Inc. USA). $P<0.05$ was considered statistically significant.

Chapter 3

Induction of

Acute Insulin Resistance

3.1   Introduction

For the past three decades, the consumption of fructose has increased in parallel with the increasing prevalence of obesity [237]. Experimental evidence has demonstrated that consumption of diets high in fructose (HFru) results in increased *de novo* lipogenesis (DNL), ectopic lipid accumulation, insulin resistance, and obesity in animals [160, 232, 238, 239], as well as in humans [224, 225, 240, 241]. In line with this, we [193] and others [161] have detected increased DNL, and ectopic lipid accumulation along with activated UPR signaling and impaired insulin sensitivity in the liver of mice after feeding for one week on a HFru diet. This supports the role of the liver being the unique organ that is capable of metabolising fructose as an energy source [242], and such metabolism can rapidly lead to the development of insulin resistance with the liver being the first tissue to be affected.

Under the state of insulin resistance, the liver becomes less responsive to the regulatory effects of insulin on glucose production and glycogen synthesize leading to the subsequent manifestation of fasting hyperglycemia [243]. Although the cause of hepatic insulin resistance can be multifactorial [244], excessive lipid accumulation from DNL and prolonged UPR signaling appears to be the key mechanism during HFru feeding [160, 232] as reviewed in detail in 1.5.1. However, mice harbouring overexpression of diacylglycerol acyltransferase 2 (DGAT2) in the liver, which catalyzes the esterification of DAGs to triglyceride, did not manifest with insulin resistance, despite marked hepatic steatosis associated with increased DAG content [245]. This suggests additional factors other than lipid accumulation *per se* might be crucial for the development of insulin resistance in the liver.

The unfolded protein response (UPR) is increasingly recognized to be a major theme implicated in the pathogenesis of hepatic insulin resistance [244]. This has been reviewed in 1.5.2.

Alhough β cell failure-induced imapired insulin secretion and insulin resistance are both characteristics of type 2 diabetes, insulin resistance is the earliest detectable defect in pre-diabetic individuals under most situations [246]. Elevated blood glucose concentration can be overcome by increasing insulin secretion. However, persistent elevated glucose levels above the physiological range leads to β cell failure and hyperglycemia. The subsequent impaired glucose tolerance can be diagnosed and is a precursor of type 2 diabetes. To our best knowledge, most current *in vivo* models achieved the phase of glucose intolerance in insulin resistance. It still remains unclear the respective implication of these cellular events in the onset of the process to develop hepatic insulin resistance by HFru feeding.

The present study sought to investigate the changes in DNL and UPR signaling, and to identify the initiating mechanism for hepatic insulin resistance, in response to acute HFru feeding. Our findings demonstrated that enhanced hepatic DNL and UPR signaling are detectable as early as 3 days, which were maintained throughout the course of HFru-feeding with no signs of critical protein deterioration of either DNL or UPR in the liver. Acute HFru feeding was able to impair hepatic insulin signaling along with promoting DNL and the activation of only the IRE1 branch of UPR signaling pathway. Inhibition of IRE1 was accompanied by attenuation of JNK-mediated serine phosphorylation of IRS and preservation of hepatic insulin signaling, despite increased hepatic DNL and marked steatosis. These findings suggest the activation of IRE1/JNK is a predominant trigger at the onset of hepatic insulin resistance induced by HFru feeding.

3.2 Methods

3.2.1 Animal Studies

Male C57BL/6J mice (12 weeks old) from the Animal Resources Centre (Perth, Australia) were kept at 22 ± 1 °C on a 12h light/dark cycle. After 2 weeks of acclimatization, mice were fed for either 1 day, 3 days, 1 week or 8 weeks with either normal chow diet (70% calories from starch, ~10% calories from fat, and ~20% calories from protein; Gordon's Specialty Stock Feeds, Yanderra, Australia) or high fructose (HFru; containing 35% fructose, 35% starch, ~10% fat and ~17% protein) as described in our previous studies [193]. HFru diet was provided to the mice from 6pm to 2pm (20 hrs) on the following day when they were sacrificed. The chemical chaperone TUDCA (Sigma Aldrich Pty Ltd, Australia) was applied by *i.p.* injection (300 mg kg^{-1} body weight) 4 hours prior to HFru feeding [193, 232, 247]. The betulin-treated animals were first fed with chow mixed with betulin (30 mg kg^{-1} body weight) for 1 week and fed with HFru diet mixed with betulin (30mg kg^{-1} body weight) for overnight as HFru diet. All experiments were approved by the Animal Ethics Committee of RMIT University.

Body weight and food intake were measured before and after experiments. After one day of feeding, the mice were fasted for four hours before the collection of plasma samples for the measurement of insulin levels by radioimmunoassay (Linco/Milipore, Billerica, MA) [232, 238, 248] and glucose levels using a glucometer (AccuCheck II; Roche, Australia). Tissues of interest were collected and freeze-clamp immediately for subsequent analyses. Glucose tolerance test (GTT; 2g kg^{-1} BW, *i.p.*) was conducted in a separate group of mice following a four hours fasting and blood glucose levels were measured at 0, 15, 30, 60 and 90 minutes using a glucometer (AccuCheck II; Roche, Australia). The area under curve (AUC) was

calculated to estimate glucose intolerance. For the assessment of insulin signaling in the liver, 5-7 hour-fasted mice were injected with insulin (2U kg^{-1} BW, *i.p.*) 20 min prior to tissue collection [193, 232]. Insulin tolerance test (ITT; 0.75U kg^{-1} BW, *i.p.*) was performed in a separate group of mice and blood glucose levels were measured at 0, 15, 30, 60 and 90 minutes using a glucometer (AccuCheck II; Roche, Australia). The area under curve (AUC) was calculated to estimate glucose intolerance. Mice fed with HFru diet for 3 days, 1 week and 8 weeks were performed tissue collection following 4 hours fasting.

3.2.2 Measurement of triglyceride levels

The details were described in 2.1.4.2.

3.2.3 Western blotting

The details were described in 2.3.

3.2.4 Statistical Analyses

Data are presented as means $\pm$ SE. One-way analysis of variance was used for comparison of relevant groups. When significant variations were found, the Tukey-Kramer multiple comparisons test was applied. Differences at $p<0.05$ were considered to be statistically significant.

3.3 Results

3.3.1 Time course of hepatic DNL and UPR signaling induced by HFru feeding

We first examined the expression of key regulating proteins of UPR and DNL signaling in the liver in relation to changes in glucose tolerance over a range of different feeding periods. Mice fed an HFru diet displayed greater caloric intake starting at day 3 ($p<0.05$ vs. CH) and manifested with glucose intolerance from day 7 as evidenced by the greater area under curve (AUC, $p<0.05$ vs. CH, Table 9). As shown in Figure 3.2Figure **3.2** Time course of hepatic UPR and DNL induced by HFru feeding., HFru feeding also resulted in the activation of two UPR signaling pathways as indicated by significant increases in phosphorylated-IRE1 (p-IRE1) and -eIF2α (p-eIF2α, ~2-fold, both $p<0.05$). Concomitant to the induction of UPR, the expression of ACC and FAS, which catalyze the formation of malonyl-CoA and long chain fatty acids, respectively, were markedly elevated 3 days after the commencement of HFru feeding (5-folds, both $p<0.01$). These data indicate that both activations of UPR signaling and the elevated DNL have reached their maximal levels within 3 days and these changes are maintained to week 8.

Table 9. Changes in metabolic parameters of HFru-fed mice over time

	CH	HFru
Body mass(g)		
Day 0	26.5 ±0.5	26.9 ±0.4
Day 1	27.1 ±0.4	27.4 ±0.4
Day 3	26.5 ±0.6	27.0 ±0.3
Week 1	26.6 ±0.4	26.9 ±0.4
Week 8	27.1 ±0.6	27.2 ±0.5
Caloric intake (kcal/g/day) Day 1	12.6 ±1.9	14.0 ±1.3
Day 3	10.1 ±0.5	15.6 ±0.6 *
Week 1	11.8 ±0.3	18.4 ±0.9 **
Week 8	14.8 ±0.4	18.4 ±0.8 *

	CH	HFru
Blood glucose (mM)		
Day 1	9.2 ± 0.2	9.2 ± 0.4
Day 3	9.3 ± 0.9	9.0 ± 0.5
Week 1	8.4 ± 0.3	9.5 ± 0.2 **
Week 8	9.2 ± 0.2	11.7 ± 0.6 *
Plasma insulin (pg/ml)		
Day 1	1267 ± 131	1841 ± 244 **
Day 3	1345 ± 150	1474 ± 146
Week 1	NA	NA
Week 8	1276 ± 116	1450 ± 174
AUC for GTT[+]		
Day 1	1136 ± 62	953 ± 76
Day 3	1044 ± 48	1098 ± 73
Week 1	1046 ± 32	1256 ± 986 *
Week 8	1020 ± 39	1394 ± 70 **

Male C57BL/6J mice were fed either a CH or HFru diet for a period of up to 8 weeks. The calculation of caloric intake was based on food intake. AUC stands for the area under curve for glucose tolerance tests. Data are means ± SE of 8-10 mice per group. * $p < 0.05$, ** $p < 0.01$ vs CH-fed mice. +: The curves of glucose tolerance is presented below.
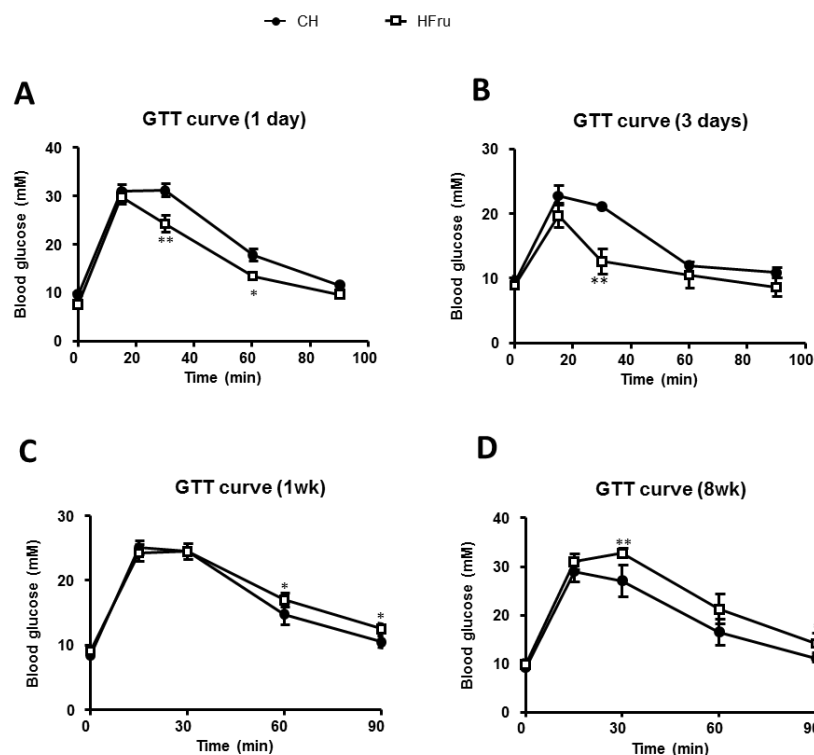
Figure 3.1 The curves of glucose tolerance test.

Glucose tolerance test (GTT) was performed with an injection of glucose (2.5 g/kg, *ip*) after 5-7 hours of fasting in HFru-fed mice for one day (A), 3 days (B), 1 week (C) and 8weeks (D).
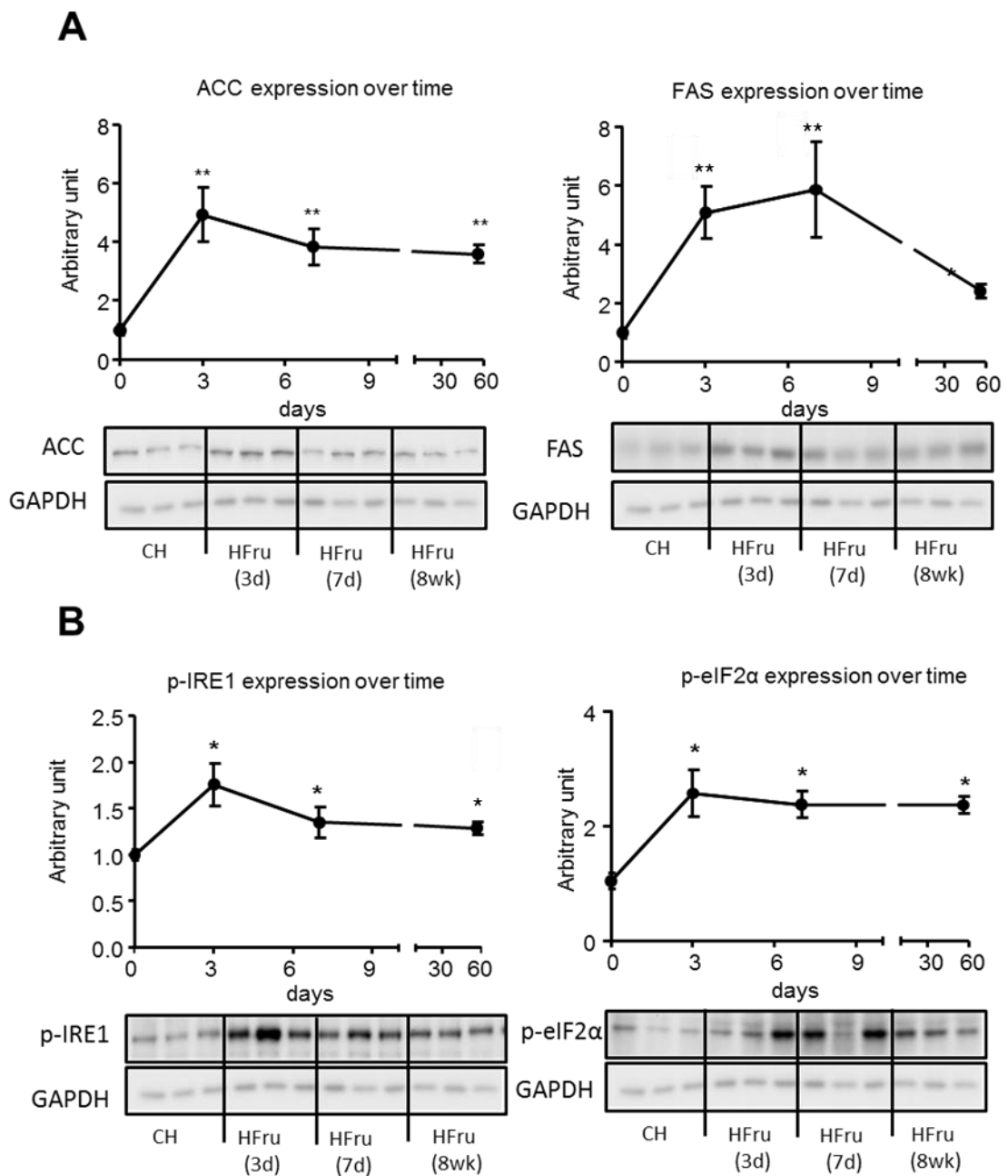
Figure 3.2 Time course of hepatic UPR and DNL induced by HFru feeding.

Male C57BJ/6J mice (10-12 weeks old) were fed a high fructose (HFru) diet for up to 8 weeks. Liver tissues were collected after 3 days, 1 week and 8 weeks and immunoblotted for key markers of UPR signaling: phosphorylated-IRE1 and -eIF2α and fatty acid synthesis: ACC and FAS. The day 0 refers to the chow-fed mice. The fold changes of proteins are calculated against housekeeping proteins (GAPDH). * $p<0.05$; ** $p<0.01$ compared with the baseline (Day 0). Data are mean ± SE of 6-8 mice per group.

3.3.2 One day feeding of HFru diet stimulated DNL and lipid accumulation in the liver but not in muscle or adipose tissue

As both DNL and UPR signaling pathways were induced in parallel by HFru feeding from 3 days onwards, we next examined the effect of one day feeding of HFru diet in an attempt to identify which of these cellular events was triggered earlier. One day feeding of HFru was able to increase the expression of key regulators of DNL in the liver, namely ACC (2.3-fold), FAS (2.3-fold), mSREBP-1c (1.5-fold) and SCD1 (2.5-fold, all $p<0.05$ vs. CH, Figure 3.3A). Consistent with this, hepatic TG content was also increased by 2.1-fold ($p<0.01$ vs. CH, Figure 3.3A right hand panel). In contrast, no significant differences were detected for any of these key regulators for DNL in skeletal muscle (Figure 3.3B) and white adipose tissue (Figure 3.3C). Accordingly, the content of TG remained unaltered in skeletal muscle following one day feeding of HFru (Figure 3.3B). These results suggest that one day feeding of HFru diet is sufficient to trigger DNL and such effect is confined to the liver.
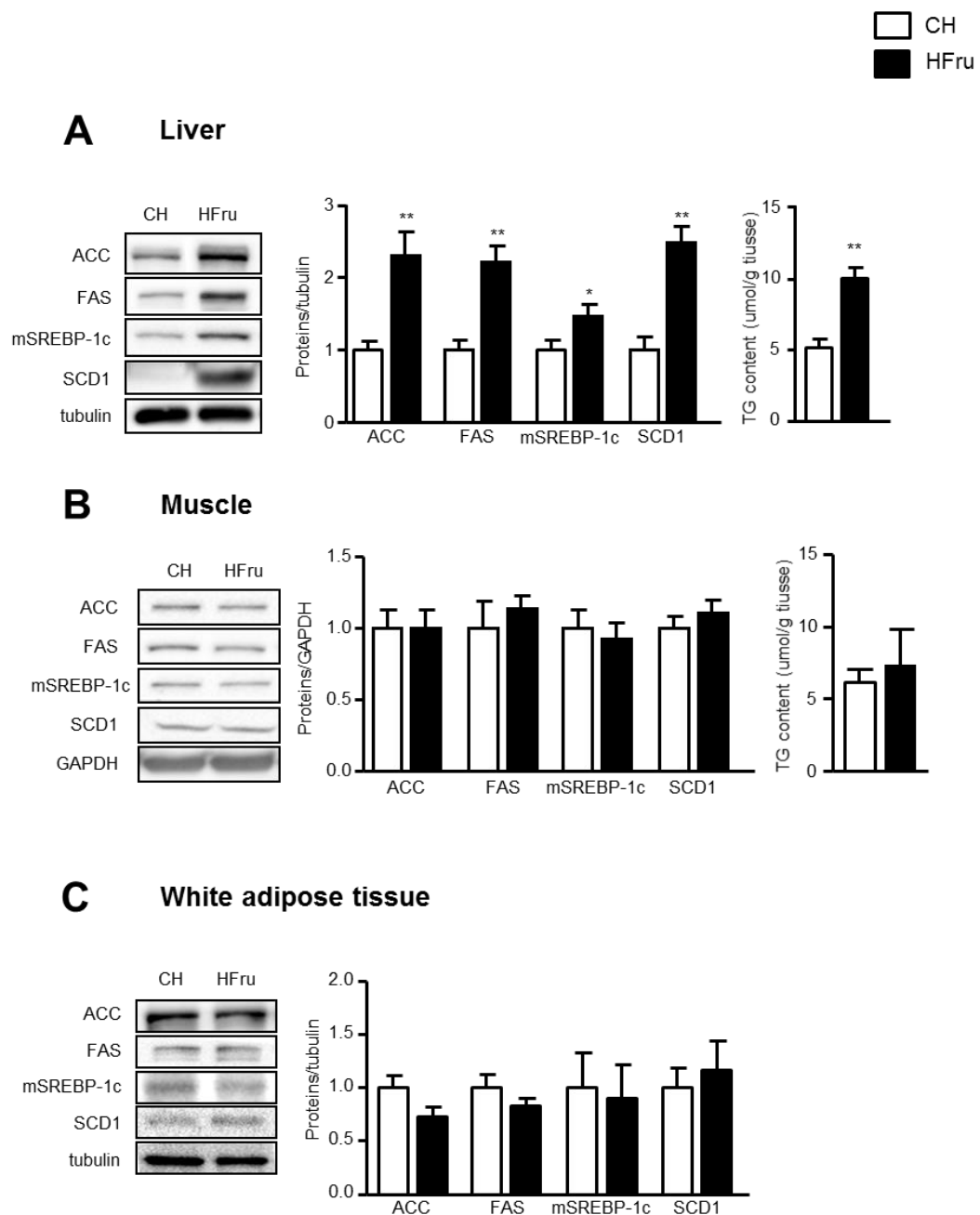
Figure 3.3 Hepatic DNL and lipid accumulation induced by one day feeding of HFru diet.

Mice were exposed for one day feeding of HFru diet. The expression of lipogenic enzyme: ACC, FAS, matured SREBP-1c and SCD1 were determined by immunobloting of whole cell lysate from liver **(A),** skeletal muscle **(B)** and epididymal white adipose tissue **(C)**. Representative western blots are shown. Tissue triglyceride (TG) content was determined following 4 hours of fasting. Data are mean $\pm$ SE of 6-8 mice per group. * $p<0.05$ compared with CH; ** $p<0.01$ compared with CH.

3.3.3 One day feeding of HFru diet activated the IRE1 and XBP1 splicing in the liver

As the PERK and IRE signaling arms (but not the ATF6 arm) of the UPR pathways were both activated after 3 days HFru feeding, we next examined whether both or only one of these two arms of UPR may be activated in the liver following one day feeding of HFru diet. As shown in Figure 3A, the p-IRE1and the splicing of its downstream effector XBP1 (sXBP1) were significantly augmented following one day feeding of HFru diet (2 to 2.5 fold, respectively, both $p<0.01$ vs. CH). However, no significant differences were found in the phosphorylation of eIF2α (p-eIF2α) or the expression level of CHOP, a downstream protein of the PERK branch [249]. Similarly, the maturation of ATF6 in the liver remained unaffected by one day feeding of HFru diet (Figure 3.4A). Consistent with the lack of changes in DNL in skeletal muscle and white adipose tissue, no significant differences were found in any of the measured UPR protein markers in these tissues (Figure 3.4B, C) compared to CH-fed mice. These data indicate that one day feeding of HFru diet is able to trigger the activation of specific UPR signaling in the liver involving the IRE1 arm.
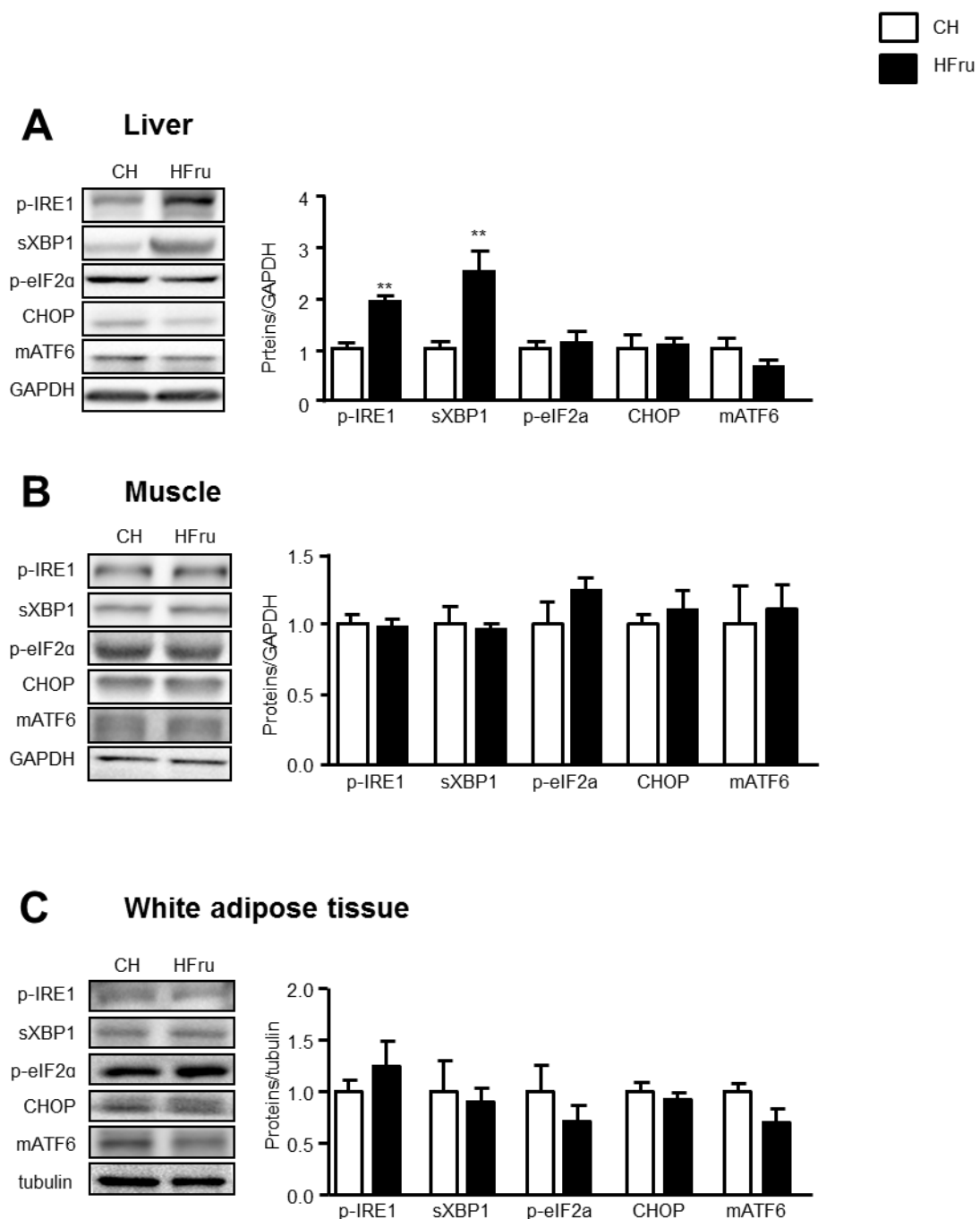
Figure 3.4 Activation of IRE1/XBP1 branch in the liver by one day feeding of HFru diet.

Mice were exposed to one day feeding of HFru diet. Protein expression of key UPR signal transducers: phosphorylated-IRE1, spliced XBP1, phosphorylated-eIF2α, CHOP and matured ATF6 were determined by immunobloting of whole cell lysate from liver (A), skeletal muscle (B) and epididymal white adipose tissue (C). Representative western blots are shown. Data are mean $\pm$ SE of 6-8 mice per group. * $p<0.05$ compared with CH; ** $p<0.01$ compared with CH.

3.3.4 One day feeding of HFru diet impaired hepatic insulin signal transduction

We next questioned whether insulin signal transduction might be affected by the one day feeding of HFru diet. This was associated with an increased activity of JNK, as evidenced by the increased phosphorylation of JNK (p-JNK, 1.6-fold, p<0.05 vs CH) and its downstream effector c-Jun (p-c-Jun, 1.5-fold, p<0.05 vs. CH). Consistent with enhanced JNK activation we also observed a 50% increase in serine phosphorylation of IRS (p-IRS, $p<0.05$ vs. CH, Figure 3.5A) in the liver. As expected, the insulin-stimulated phosphorylation of Akt (p-Akt) was markedly reduced by 30% in the liver (p<0.05 vs. CH insulin stimulated) following one day feeding of HFru diet. Consistently, HFru-fed mice showed insulin intolerance as indicated by decreased reversed-AUC of ITT (Figure 3.9A). In addition, mTOR which can be enhanced by either insulin or HFru [250] showed a significant reduction with the presence of insulin in HFru-fed mice compared with relative control (Figure 3.9B). No detectable defects in the insulin-stimulated phosphorylation of Akt were found in response to one day feeding of HFru diet in skeletal muscle and white adipose tissue (Figure 3.5B and C). These results indicate that HFru diet is sufficient to impair hepatic insulin sensitivity and this impairment is closely correlate with the activation of IRE1 pathway.
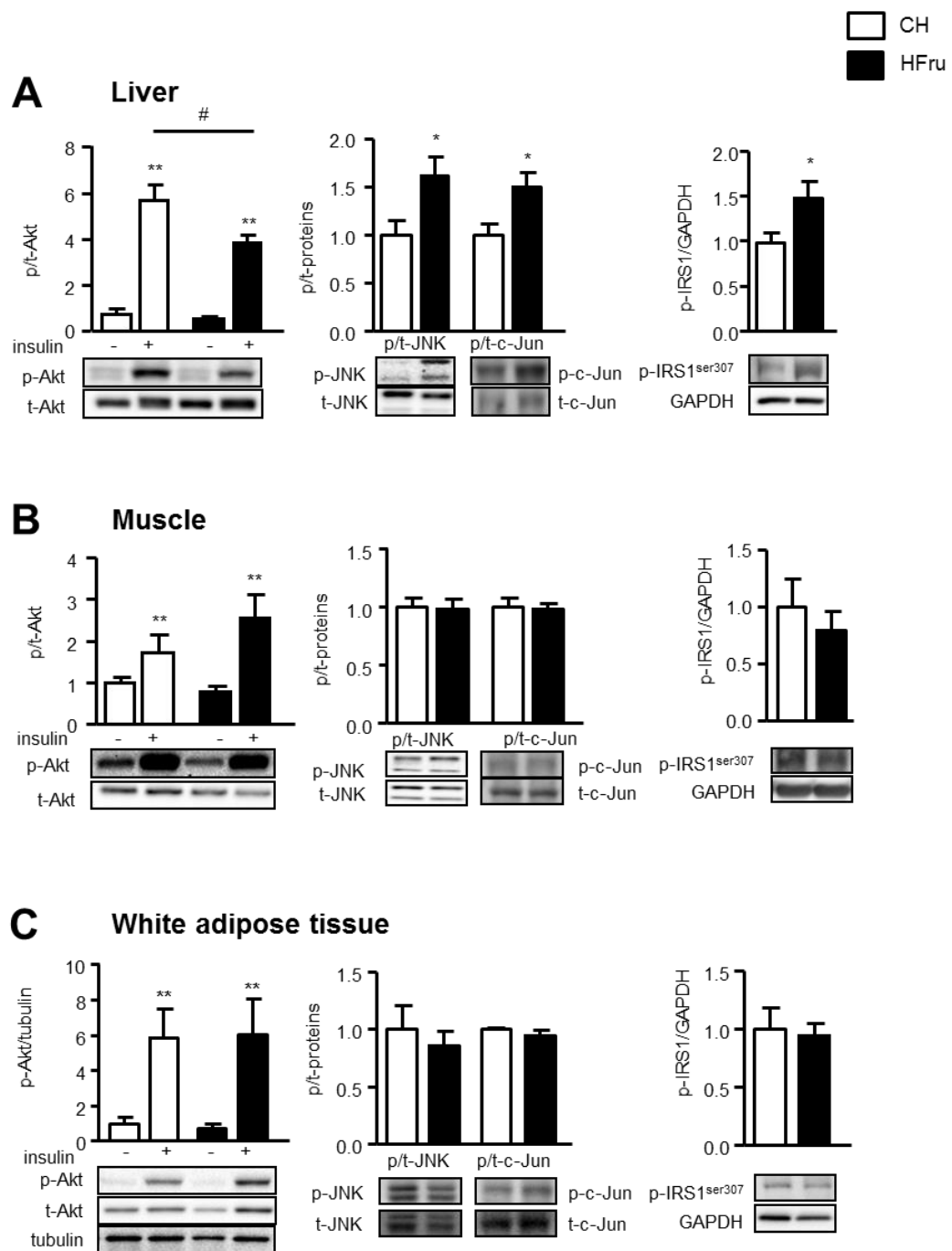
Figure 3.5 Impaired hepatic insulin signal transduction by one day feeding of HFru diet.

Mice were fed for HFru diet for one day. Insulin signal transduction was assessed by immunoblotting of key proteins: phosphorylated-Akt (serine 473), -JNK (Threonine 183/ Tyrosine 185) and -c-Jun (serine 63) and p-IRS1 (serine 307) in whole cell lysate of liver (A), skeletal muscle (B) and epididymal white adipose tissue (C). Representative western blots are shown. Data are mean ± SE of 6-8 mice per group. * $p<0.05$ compared with CH; # $p<0.05$ compared with CH+ insulin.

3.3.5 Inhibition of IRE1 activity attenuated hepatic DNL induced by one day feeding of HFru diet.

To investigate the relationship between the activation of the IRE1 branch upon HFru feeding and the concomitant increase in DNL and the impairment of insulin signaling transduction, we next examined whether dampening the activation of IRE1 with the chemical chaperone TUDCA [214] was able to reverse any of these events in the liver of HFru-fed mice. Administration of TUDCA to HFru-fed mice did not affect the levels of blood glucose, food intake or body weight, but normalized plasma levels of insulin (Table 10). As shown in Figure 3.6A, TUDCA administration abolished the increased phosphorylation of IRE1 and splicing of XBP1 induced by HFru feeding ($p<0.05$ vs. HFru). Along with the inhibition of IRE1 upon TUDCA treatment, the expressions of mSREBP-1c ACC, FAS, and SCD1 were also reduced to levels comparable to the CH-fed mice (Figure 3.6B), indicating that IRE1 activity is a major inducer for the enhanced hepatic DNL observed in the one day HFru-fed mice.

To exclude the possibility of metabolic effect of bile acids in the liver, we next administrated another compound, betulin to suppress ER stress. Betulin belongs to different class of compounds from TUDCA and it has been reported as a SREBP-1c inhibitor. In the current study, betulin showed similar effects on lipogenesis (Figure 3.8A) and ER stress (Figure 3.8B) as TUDCA. The suppression of DNL and ER stress abolished the impairment of hepatic insulin signaling transduction (Figure 3.8D-F) indicated by the suppression of p-IRS1^{ser307} and restored p-Akt with insulin stimulation. However, betulin failed to reduce the hepatic triglyceride in current study (Figure 3.8C).

Table 10 Basal metabolic parameters of TUDCA treated mice

	CH	HFru	HFru+TUDCA	HFru+Betulin
Body mass (g)	24.4 ±0.3	25.5 ±0.8	25.8 ±0.5	24.3 ±0.3
Caloric intake (kcal/g/day)	12.6 ±1.9	14.0 ±1.3	14.3 ±1.2	14.8 ±1.6
Blood glucose (mM)	9.1 ±1.0	9.0 ±0.5	9.1 ±0.3	9.5 ±0.4
Plasma insulin (pg/ml)	1267 ±131	1841 ±244*	1134 ±246	NA

Male C57BL/6J mice were fed either a chow (CH) or fructose-rich diet (HFru) for 1 day. The calculation of caloric intake was based on food intake (3.11 kcal/g for CH diet and 3.569 kcal/g for HFru diet). The animal was injected with TUDCA or vehicle four hours prior to feeding. Data are means ±SE of 5-10 mice per group. * $p < 0.05$ vs CH-fed mice.
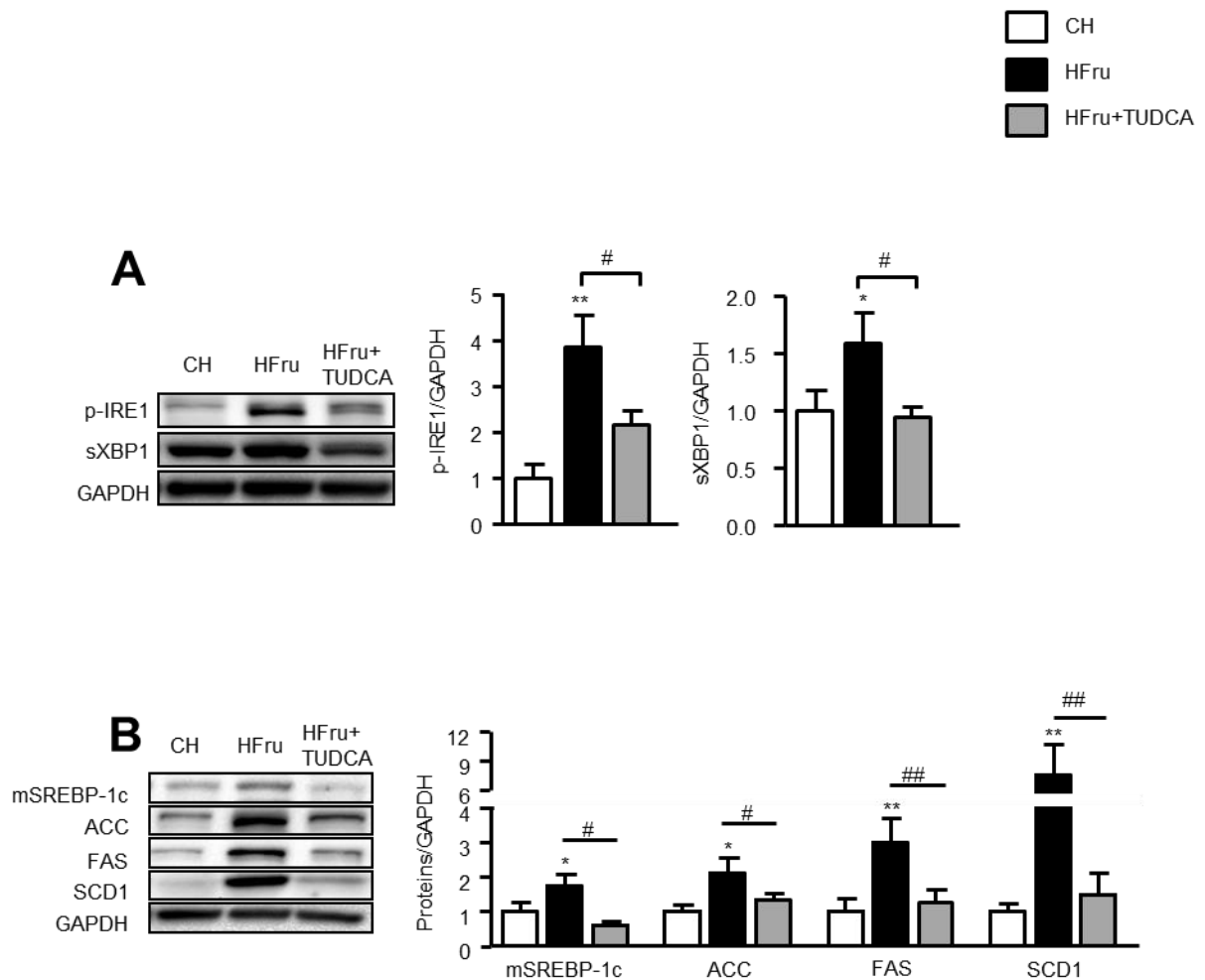
Figure 3.6 Inhibition of IRE1 activity attenuated hepatic DNL.

The chemical chaperone TUDCA was administered 4 hours prior to the commencement of one day feeding of HFru diet. The activity of IRE1 in the liver was determined by immunobloting of phosphorylated-IRE1 and spliced XBP1 in whole cell lysate **(A)**. Hepatic DNL was assessed by immunoblotting of: ACC, FAS, matured SREBP-1c and SCD1 **(B)**. SREBP-1c, ACC, FAS and SCD1 were determined by immunoblots from liver tissue. Representative blots are shown. Data are mean ± SE of 6-8 mice per group. * $p < 0.05$ compared with CH; # $p < 0.05$ compared with HFru.

3.3.6 Inhibition of IRE1 activity protected hepatic insulin signaling transduction by diminishing JNK activity.

Consistent with a reduction of the activity of IRE1, TUDCA administration also completely abolished the activation of JNK induced by one day feeding with HFru diet, as evidenced by the reduced phosphorylation of JNK and c-Jun (both $p<0.05$ vs. HFru, Figure 3.7A). This was associated with a concomitant reduction of IRS1 serine phosphorylation and restored insulin-stimulated phosphorylation of Akt in the liver. Intriguingly, the restored hepatic insulin signaling upon TUDCA treatment was found to be independent of any changes of TG content in the liver (Figure 3.7C). As membrane-associated PKCε has been demonstrated to be a key driver of impaired insulin signaling by lipid accumulation [139, 251], we hence measured the content of membrane-associated PKCε to further assess the role of lipid accumulation in the onset of impaired hepatic insulin signaling transduction induced by fructose. No significant differences were found in the membrane-associated PKCε following one day feeding of HFru diet compared to CH-fed mice (Figure 3.7D). TUDCA treatment also significantly reduced microsomal TG transfer protein (MTTP, Figure 3.7E), a protein required for the hepatic TG export. These results support the hypothesis that increased lipid content is unlikely to be a major contributing factor to the onset of hepatic insulin resistance induced by fructose.
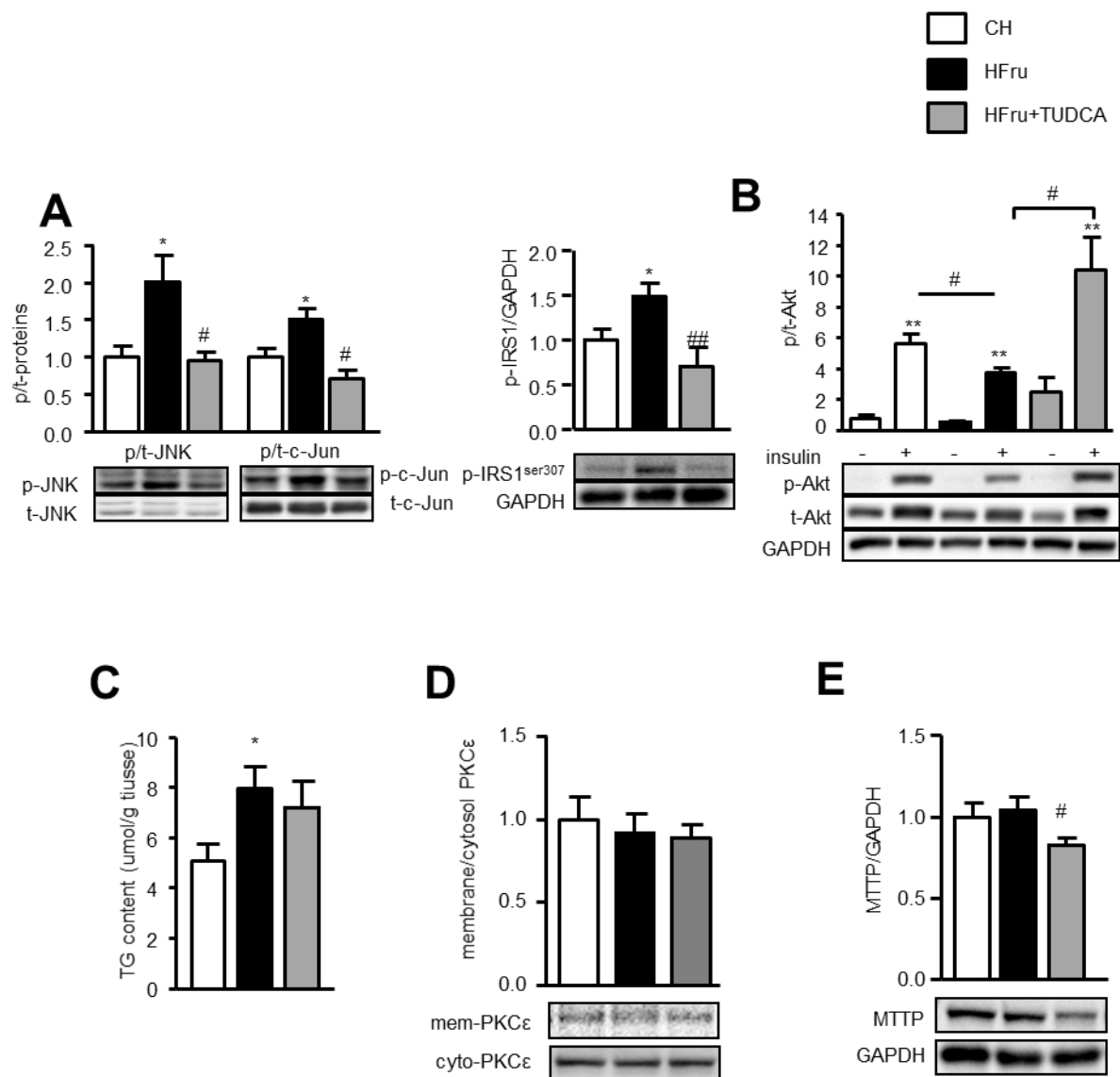
Figure 3.7 Inhibition of IRE1 activity down regulated JNK activity and protected hepatic insulin signal transduction.

The chemical chaperone TUDCA was administered 4 hours prior to the commencement of one day feeding of HFru diet. The activity of JNK and insulin signal transduction was examined by immunobloting of phosphorylated-JNK (Threonine 183/ Tyrosine 185), -c-Jun (serine 63), -IRS1 (serine 307) (A) and -Akt (serine 473) (B) in whole cell lysate of liver. Hepatic triglyceride (TG) content (C). Liver membrane and cytosolic fractions were immunoblotted for PKCε (D). Liver homogenate was immunoblotted for microsomal TG transfer protein (MTTP) (E). Data are mean $\pm$ SE of 6-8 mice per group. * $p<0.05$ compared with CH; # $p<0.05$ compared with HFru.
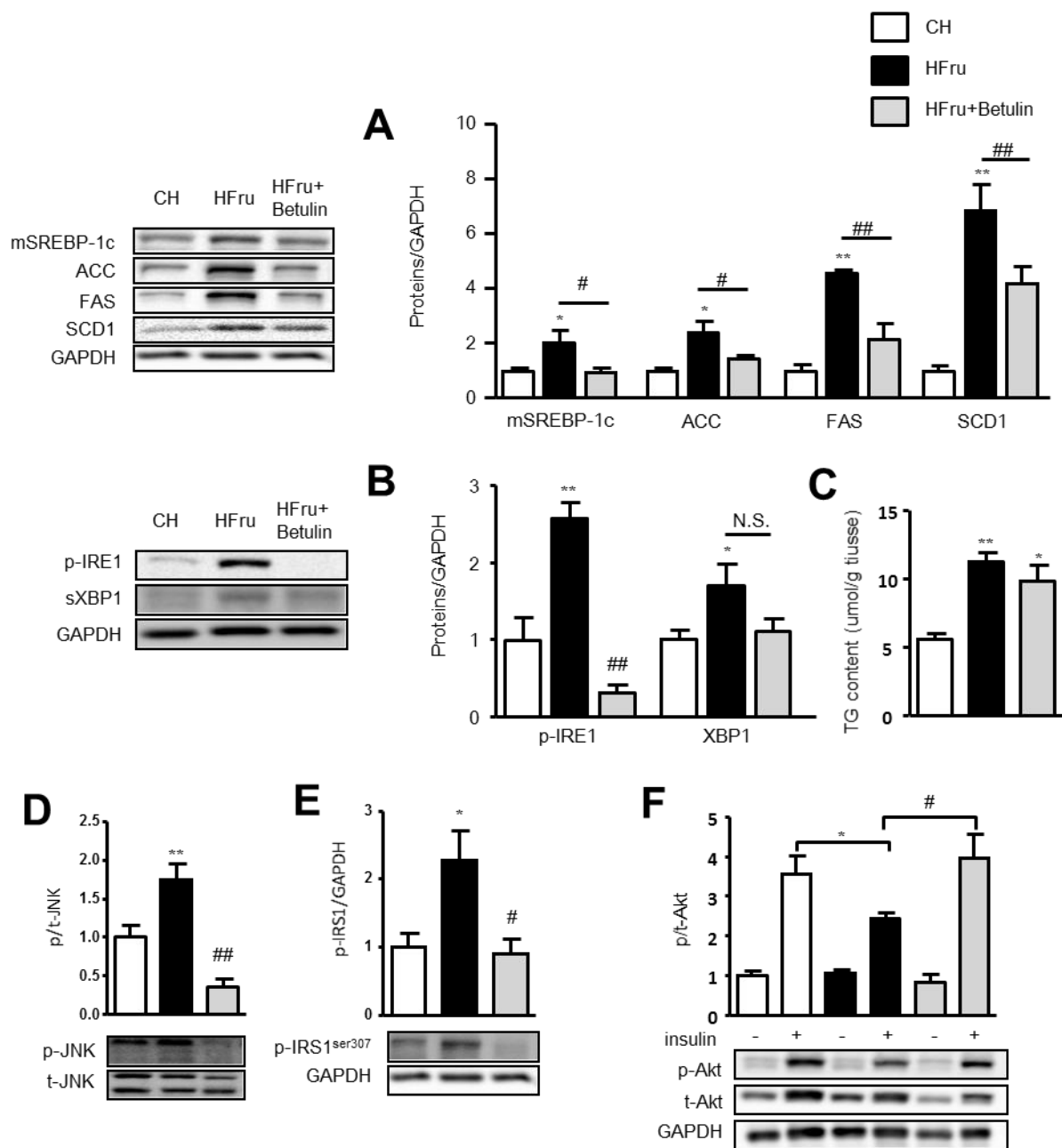
Figure 3.8 Inhibition of IRE1 and JNK activity protect hepatic insulin signaling transduction.

Betulin was administrated to the HFru-fed mice. Hepatic DNL was assessed by immunoblotting of: matured SBEBP-1c, ACC, FAS and SCD1 (A). The activity of IRE1 in the liver was determined by immunobloting of phosphorylated-IRE1 and spliced XBP1 in whole cell lysate (B). Hepatic triglyceride (TG) content (C). The activity of JNK and insulin signal transduction was examined by immunobloting of phosphorylated-JNK (Threonine 183/ Tyrosine 185 (D), -IRS1 (serine 307) (E) and -Akt (serine 473) (F) in whole cell lysate of liver. Representative blots are shown. Data are mean $\pm$ SE of 6-10 mice per group. * $p<0.05$ compared with CH; # $p<0.05$ compared with HFru.
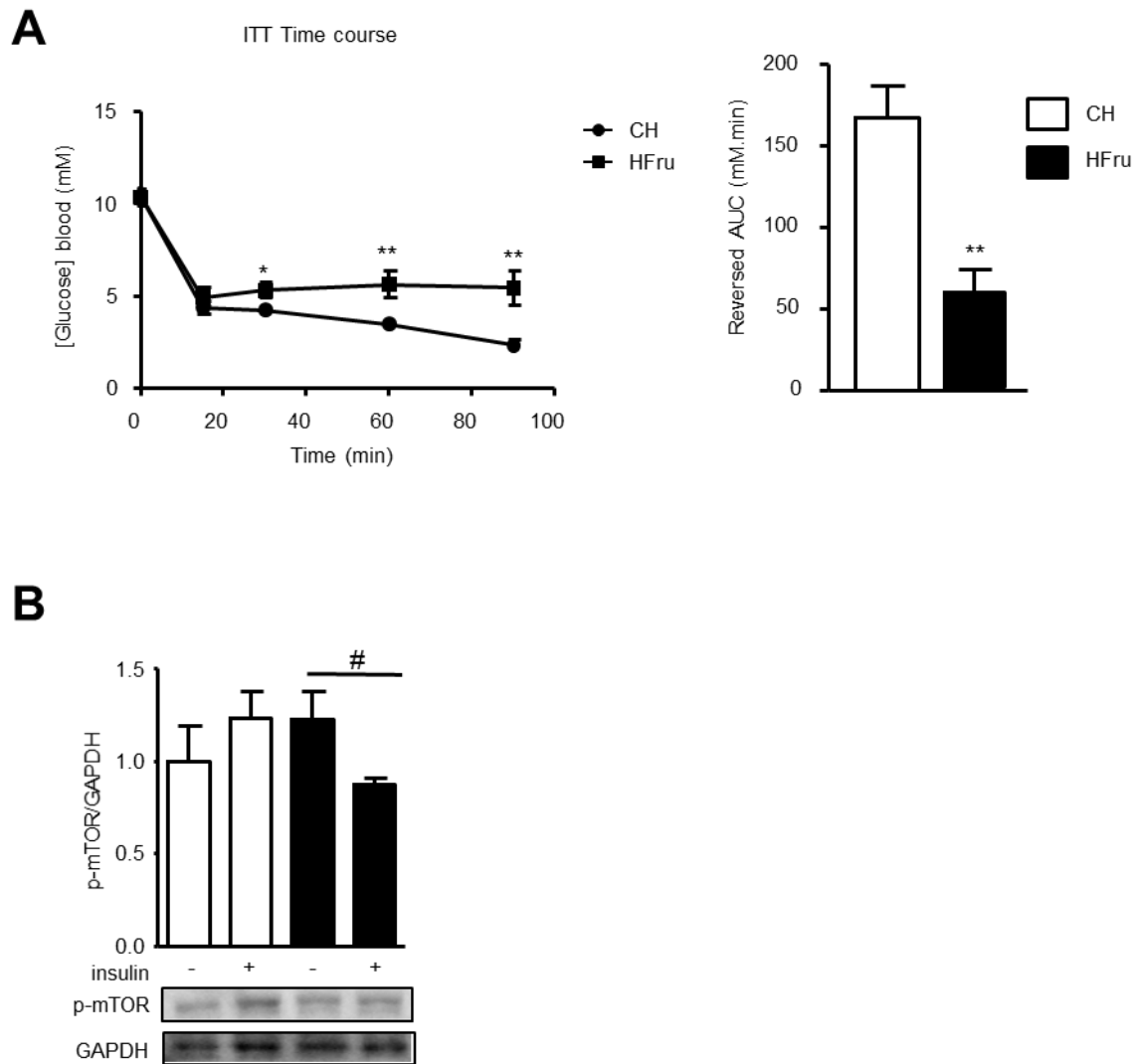
Figure 3.9 One day feeding of HFru diet impaired insulin action.

ITT was performed in one day feeding of HFru -or CH-fed mice and insulin tolerance was assessed by reversed AUC (A). The phosphorylation of mTOR was examined by immunobloting (B). Representative blots are shown. Data are mean $\pm$ SE of 6 mice per group. ** $p<0.01$ compared with CH; # $p<0.05$ compared with HFru.

3.4 Discussion

The chapter investigated the mechanisms of UPR signaling and hepatic DNL in relation to the onset of insulin resistance in the liver. Our data demonstrated that both UPR signaling and DNL are rapidly initiated and persisted in response to HFru feeding. Using a one day feeding model, we found the IRE1 branch to be the first UPR arm to be activated in response to fructose. The activation of IRE1 was associated with impaired hepatic insulin signaling as indicated by reduced Akt phosphorylation, likely via increased JNK activity and serine phosphorylation of IRS1. The key role of IRE1-JNK in triggering HFru-induced hepatic insulin resistance was evidenced by the fact that inhibition of IRE1 activation by the chemical chaperone TUDCA was able to block the activation of JNK, IRS1 serine phosphorylation and preserve the insulin-stimulated phosphorylation of Akt.

A growing body of evidence indicates that increased fructose intake is an important risk factor of metabolic syndrome including type 2 diabetes [215, 217, 221]. It has been shown in healthy subjects that ingestion of 20% fructose solution with meals can increase fasting blood glucose level and hepatic insulin resistance within 6 days [223]. Thus, the present study focused on the mechanisms of hepatic insulin resistance by feeding mice an HFru diet mimic the onset of fructose-induced insulin insensitivity in human. Dietary fructose is almost entirely metabolized in the liver [242] and converted into lipids via DNL unrestrained by cellular control, because it can bypass the feedback inhibition by ATP and citrate [218, 225]. If unutilized, the lipids synthesized from excess DNL will be channelled towards storage leading to hepatic steatosis which is considered to be closely related with insulin resistance. In addition to the potent stimulation of DNL, fructose is also able to induce UPR signaling in the liver [232].

UPR is demonstrated to contribute to insulin resistance [160, 193, 225] via IRE1/XBP1 [104, 252] or PERK/eIF2α [169] branch. Furthermore, it has been suggested that UPR activation *per se* promotes DNL which subsequently leads to hepatic steatosis and impairs insulin signaling transduction [131, 160, 253]. It has been reported that deletion of XBP1 in mice decreased DAG level, PKCε activity in the liver and protected against hepatic insulin resistance in response to one week of fructose feeding without suppressing JNK activation [161]. Our recent study also showed that DAG accumulation in chronic fructose feeding associated with ER stress and insulin resistance in the liver along with glucose intolerance [232]. As hepatic insulin resistance is suggested to initiate whole-body insulin resistance [254], we set to investigate the involvement of cellular events (UPR and DNL) in the development of hepatic insulin resistance induced by HFru feeding.

In order to establish a temporal relationship among these events, we compared the changes in PERK/eIF2α and IRE1/XBP1 branches at various durations of HFru feeding ranging from 3 days to 8 weeks. Consistent with our recent finding in mice fed with HFru diets for 1 week, we found that both PERK and IRE1 branches were activated at day 3 and maintained throughout the entire course of the experiment. This suggests that the activation of these two UPR branches was fully developed at this early stage and impaired insulin action was detected at 1 week. These effects sustained chronically to exert their long-term effects.

To further dissect the changes of UPR pathways at the onset of hepatic insulin resistance, we examined the effects of one day feeding of HFru diet on these pathways in relation to insulin signal transduction and whole body metabolism. Interestingly, we found that one day of HFru diet is sufficient to impair hepatic insulin signaling without detectable glucose intolerance. The lack of glucose intolerance is explainable by the fact that at this stage insulin action in

muscle and adipose tissue were still intact, as indicated by the maintained Akt phosphorylation in response to insulin stimulation. Our findings are also consistent with a study in humans showing that a short-term (6 days) ingestion of fructose results in insulin resistance in the liver without obvious impact on insulin sensitivity in skeletal muscle [223]. Similar findings of hepatic insulin resistance prior to detectable whole-body insulin resistance have been observed previously [45, 255].

Interestingly, the DNL pathway was significantly elevated by one day feeding of HFru diet in the liver and this was associated with the activation of only the IRE1 branch of the UPR signaling pathway, indicating that this arm rather than PERK branch may play a key role in the onset of hepatic insulin resistance in response to fructose feeding. Although IRE1/XBP1 is suggested to response to insulin [256], mice fed with HFru for 3 days and 8 weeks displayed ER stress accompanied by normal plasma insulin level (Table 1). This indicated that hyperinsulinemia was not the only trigger of IRE1 branch. IRE1 has been postulated to induce insulin resistance via two distinct mechanisms. Firstly, activated IRE1 results in the spicing of XBP1 leading to its maturation as an active transcription factor. The spliced XBP1 can upregulate key genes of fatty acid synthesis to increase *de novo* lipogenesis [158], leading to an accumulation of intermediate lipid metabolites including diacyglycerols (DAGs) [160, 232]. Increased DAGs in the liver can recruit protein kinase C epsilon (PKCε) to the plasma membrane where it can inhibit the insulin signaling pathways via serine phosphorylation of insulin mediators like IRS [139, 161]. This subsequently leads to decreased insulin-stimulated phosphorylation of downstream signaling effectors such as Akt resulting in insulin resistance [136]. In the present study, we found a marked increase in key proteins of DNL and lipid accumulation in the liver. However, our results did not show any enrichment in the membrane-associated PKCε following the one day feeding of HFru diet. Therefore, we

examined whether or not DNL, lipid accumulation and impaired insulin signaling transduction may be prevented by blocking the activation of the IRE1/XBP1 pathway. Our results showed that the inhibition of IRE1 and the subsequent splicing of XBP1 by TUDCA completely prevented fructose-induced DNL. This indicates the suppression of XBP1 splicing downregulated hepatic DNL. However, PKCε was not altered in response to decreased DNL, suggesting that the proposed DAG-PKCε mechanism is not an initiator of insulin resistance in the liver in this model.

The other postulated mechanism linking IRE1 to insulin resistance is via the activation of JNK [104, 125]. It has been proposed that upon activation IRE1 recruits the adaptor protein, TNF receptor-associated factor 2 (TRAF2) to the surface of the ER membrane. The IRE1-bound TRAF2 then activates the apoptosis-signaling kinase 1 (ASK1) leading to the phosphorylation and activation of JNK. JNK interferes with insulin signaling via serine/threonine phosphorylation of IRS proteins [257] and blunting its signal transduction to downstream molecules like Akt [258]. Consistent with these reports, there was a marked increase in JNK activity in the liver following one day feeding of HFru diet. As expected, the activated JNK was found to be associated with increased serine phosphorylation of IRS and impaired insulin signal transduction (decreased p-Akt in response to insulin stimulation). These data suggest that IRE1-mediated JNK activation initiate hepatic insulin resistance during acute HFru feeding. This mechanism is further supported by our subsequent study showing that inhibition of IRE1 with the chemical chaperone TUDCA was able to block the activation of JNK and serine phosphorylation of IRS1/2 and preserve insulin-stimulated phosphorylation of Akt in the liver during one day feeding of fructose.

Chronic administration of TUDCA has been reported to decrease hepatic triglyceride levels ob/ob mice [214]. It was puzzling to us in the first glance that hepatic TG content was not reduced by TUDCA. However, a recent report also showed the inability of TUDCA to reduce hepatic steatosis [259]. One possible reason for this might be that TUDCA was administered to mice in one dose only in our study. To further investigate this discrepancy, we examined whether the lack of reduction in hepatic TG export may also be due to a simultaneous decrease in TG export from the liver by measuring the level of MTTP, a lipid transfer protein required for the assembly and secretion of VLDL-triglyceride by the liver [260]. The decrease in liver MTTP may explain, at least in part, the lack of change in hepatic triglyceride content in TUDCA-treated HFru-fed mice. As the knockout of liver IRE1α has been shown to decrease MTTP activity [179], it is likely that the down regulation of MTTP may result from the IRE1 activation by TUDCA. The protected hepatic insulin signaling transduction by TUDCA without reducing liver TG is consistent our interpretation that activate IRE1 can trigger insulin resistance via the activation of JNK independently.

To further confirm the effect of IRE1/JNK on impaired insulin signaling transduction in the liver, we used betulin which was reported as a SREBP-1c inhibitor. Intriguingly, we found that despite the suppression of DNL, betulin could also reduce the p-IRE1 expression without affecting its downstream effector spliced-XBP1. However, another downstream target JNK which is catalyzed by the kinase activity of IRE1 showed a significant decrease. Simultaneously, impaired insulin signaling transduction was alleviated under betulin treatment. These results further support our hypothesis that JNK activation plays an important role in initiating hepatic insulin resistance.

In summary, the present study demonstrated that the IRE1-mediated JNK activation, rather than lipid accumulation, is a predominant trigger for the onset of hepatic insulin resistance induced by acute HFru feeding. However, this does not exclude the possibility that DNL-induced lipid accumulation may contribute to the development of hepatic insulin resistance in the long term. Our findings suggest that the IRE1/XBP1 pathway may be a potential target for pharmacological treatment of insulin resistance in the liver induced by high fructose consumptions.

Chapter 4

Induction of

Chronic Insulin Resistance

4.1 Introduction

Liver is one of the most metabolically active and insulin responsive organs, regulating glucose homeostasis, lipid metabolism and protein synthesize [244]. Under normal conditions, insulin suppresses hepatic glucose production via glycogenolysis and gluconeogenesis, while promoting glucose storage in the form of glycogen to help control postprandial glucose level. However, the ability of insulin to shut down glucose production from the liver is diminished under the state of hepatic insulin resistance which in turn leads to the manifestation of hyperglycemia [243]. Although the pathogenesis of hepatic insulin resistance is likely to be multi-factorial, increased endoplasmic reticulum stress and an accumulation of lipids within the liver have been demonstrated to be important mechanisms [249, 261].

Lipid accumulation in the liver or hepatic steatosis can lead to insulin resistance by interfering with the insulin signal transduction through lipid metabolites such as diacylglycerols and ceramide [261]. Hepatic steatosis can result from increased FA influx, elevated *de novo* lipogenesis and/or reduced fatty acid (FA) oxidation [244, 261]. In humans, elevated DNL from the increased consumption of sucrose is the predominant mechanism for the development of hepatic steatosis with fructose (breakdown product of sucrose) being the major culprit [225, 262].

Recent studies in animal models [160, 214] have identified a possible role of ER stress in the development of hepatic insulin resistance during elevated DNL. When ER stress occurs, the ER mounts the UPR which involves the activation of three major branches of signal transducers: IRE1, PERK and ATF6 [102]. Activation of these canonical mechanisms is crucial for cellular adaption and resolution of ER stress. However, chronic activation of UPR signaling has been demonstrated to activate c-jun N-terminal kinase and IκB kinase. The

IRE1 branch of the UPR can activate JNK [104] and IKK [124] by forming a complex with the tumor-necrosis factor-α-receptor-associated factor 2 (TRAF2). Meanwhile, the PERK/eIF2a branch has also been reported to be capable of activating JNK [263]. As activated JNK [125, 214] and/or IKK [264] can directly serine/threonine phosphorylate insulin-receptor-substrate (IRS) leading to the inhibition of insulin signaling transduction, it has been suggested that JNK and IKK are the key molecules linking activated UPR and hepatic insulin resistance [258].

A previous study from this laboratory reported that elevated DNL and insulin resistance in the liver of high fructose (HFru) fed mice is coupled to activation of the IRE1 and PERK branches of the UPR [193]. In the previous chapter, it was suggested that ER stress-related JNK activation plays predominant role in the development of hepatic insulin resistance. However, it is not clear whether ER stress remains as a key trigger of insulin resistance in the liver. Interestingly, hepatic DNL is increased by the activation of PPARα [265, 266] which has also been shown to reverse hepatic steatosis [267, 268]. Because ER stress is tightly associated with DNL, we hypothesized that treatment of HFru-fed mice with a PPARα agonist would activate both the IRE1 and PERK branches of the UPR while preventing hepatic steatosis. Under these conditions, we would then be able to interrogate the role of these two mechanisms (lipid accumulation or activated JNK/IKK) in hepatic insulin resistance in the face of increased ER stress. Our results revealed that accumulation of lipids namely DAGs, rather than the activation of JNK or IKK, is the key factor of hepatic insulin resistance during increased ER stress. Activation of PPARα with FENOFIBRATE is able to eliminate hepatic insulin resistance during HFru feeding by reducing DAG levels despite the presence of ER stress evidenced by the dual activation of the IRE1/XBP1 and PERK/eIF2α pathways.

4.2 Methods

4.2.1 Animal Study

The daily maintenance of animals was mentioned in details in the Chapter 2 (2.1). Fenofibrate (FB, Sigma-Aldrich, Australia) was supplemented to the animal by mixing into the diets at a concentration of 100 mg/kg/day. All experiments were approved by the Animal Ethics Committees of the RMIT University (#1012).

Body weight and food intake were measured daily. The whole body metabolic rate was measured at 22°C using an indirect calorimeter (Comprehensive Laboratory Animal Monitoring System, Columbus Instruments, OH, USA) as described in Chapter 2 between 5-8 days after the administration of fenofibrate. Mice were fasted for 5-7 hours before being killed. Tissues of interest were collected and freeze-clamped immediately. Epididymal fat mass was weighed using an analytical balance. Liver triglycerides and plasma insulin measurements and GTT were performed. The details were described in Chapter 2(2.1.2, 2.1.3 and 0). For the assessment of insulin signaling in the liver, the mice were injected with insulin (2U/kg BW, ip) 20 min before tissue collection.

4.2.2 Measurement of hepatic FA oxidation DNL

The details were described in 2.1.4.4 and 2.1.4.5.

4.2.3 Citrate synthase and β3-hydroxyacyl-CoA dehydrogenase activity

The details were described in 2.1.4.6.

4.2.4 Western blotting

The details were described in 2.3.

4.2.5 Analyses of hepatic lipids

The details were described in 2.1.4.3.

4.2.6 Statistical Analyses

Data are presented as means $\pm$ SE. One-way analysis of variance was used for comparison of relevant groups. When significant variations were found, the Turkey-Kramer multiple comparisons test was applied. Differences at *p*<0.05 were considered to be statistically significant.

4.3 Results

4.3.1 FB treatment normalised HFru feeding induced adiposity and improved glucose intolerance

HFru-feeding resulted in significant increases in calorie intake (~38%), the whole body oxygen consumption (VO_2, ~ 8%) and the respiratory exchange ratio (RER), body weight gain (1.2 g) and adiposity (67% in epididymal fat mass, p<0.05) compared to untreated CH-fed animal (CH-Veh) (Table 11). In CH-fed mice, fenofibrate treatment had no significant effects on body weight gain, adiposity, caloric intake or RER except for a 14% increase in VO_2 (p<0.05 vs CH-Veh). In HFru-FB-fed mice, fenofibrate significantly (all p<0.05) increased VO_2 (8%), reduced the RER and completely diminished HFru-induced body weight gain and adiposity. Fenofibrate lowered blood glucose and insulin levels in the HFru-fed mice (both p<0.01 HFru-FB), hence an improved HOMA-IR index. The untreated HFru-fed mice displayed glucose intolerance (Figure 4.1 A) compared to CH-Veh (Figure 4.1 A and B). Fenofibrate treatment completely normalized the glucose tolerance seen in the HFru-fed mice

to the levels of the CH-fed mice and reduced the requirement for plasma insulin level (Figure 4.1 C).

Table 11 Basal metabolic parameters of HFru-fed mice.

	CH-Veh	CH-FB	HFru-Veh	HFru-FB
Body mass (g)				
Day 0	27.0 ± 0.4	27.5 ± 0.4	28.0 ± 0.5	26.8 ± 0.4
Day 14	28.0 ± 0.4	27.9 ± 0.4	29.2 ± 0.4^{b}	$22.2 \pm 0.6^{b,d,e}$
EPI/BW	1.2 ± 0.1	1.0 ± 0.1	2.0 ± 0.3^{b}	$0.7 \pm 0.1^{a,d}$
Caloric intake (Kcal/kg.day)	411 ± 6.6	436 ± 12.3	$571 \pm 9.7^{b.f}$	$567 \pm 13.6^{b.f}$
VO_2 (l/kg.h)	3.23 ± 0.07	3.70 ± 0.14^{a}	3.50 ± 0.03^{b}	$3.78 \pm 0.13^{b,c,e}$
RER	0.93 ± 0.01	0.92 ± 0.01	0.97 ± 0.01^{b}	0.93 ± 0.02^{c}
Blood glucose (mM)	8.4 ± 0.3	10.5 ± 0.4^{b}	10.2 ± 0.5^{b}	$6.6 \pm 0.4^{b,d}$
Plasma insulin (pg/ml)	203 ± 23	91 ± 16^{b}	208 ± 26	82 ± 6^{d}
HOMA-IR	77.4 ± 9.0	40.9 ± 6.7^{a}	96.3 ± 16.8	$23.3 \pm 2.2^{b,d}$
Plasma triglyceride (μM)	354 ± 20	176 ± 10^{b}	264 ± 16^{b}	260 ± 32^{b}

Male C57BL/6J male mice were fed either a CH or fructose-rich diet (HFru) for 2 weeks with or without the supplementation of a PPARα agonist, fenofibrate (FB, 100 mg/kg/day). The data for whole body oxygen consumption (VO_2) and respiratory exchange ratio (RER) were the average values of 24 hours of measurement after 1 week of fenofibrate administration. HOMA-IR was calculated using the fasting blood glucose (mmol/L) multiplying by the fasting Insulin (mU/L) divided by 22.5. Data are means ± SE of 8–12 mice per group. a $p<0.05$, b $p<0.01$ vs untreated CH-fed mice (CH-Veh); c $p<0.05$, d $p<0.001$ vs untreated HFru-fed mice (HFru-Veh); e $p<0.001$ vs fenofibrate treated chow-fed mice (CH-FB).
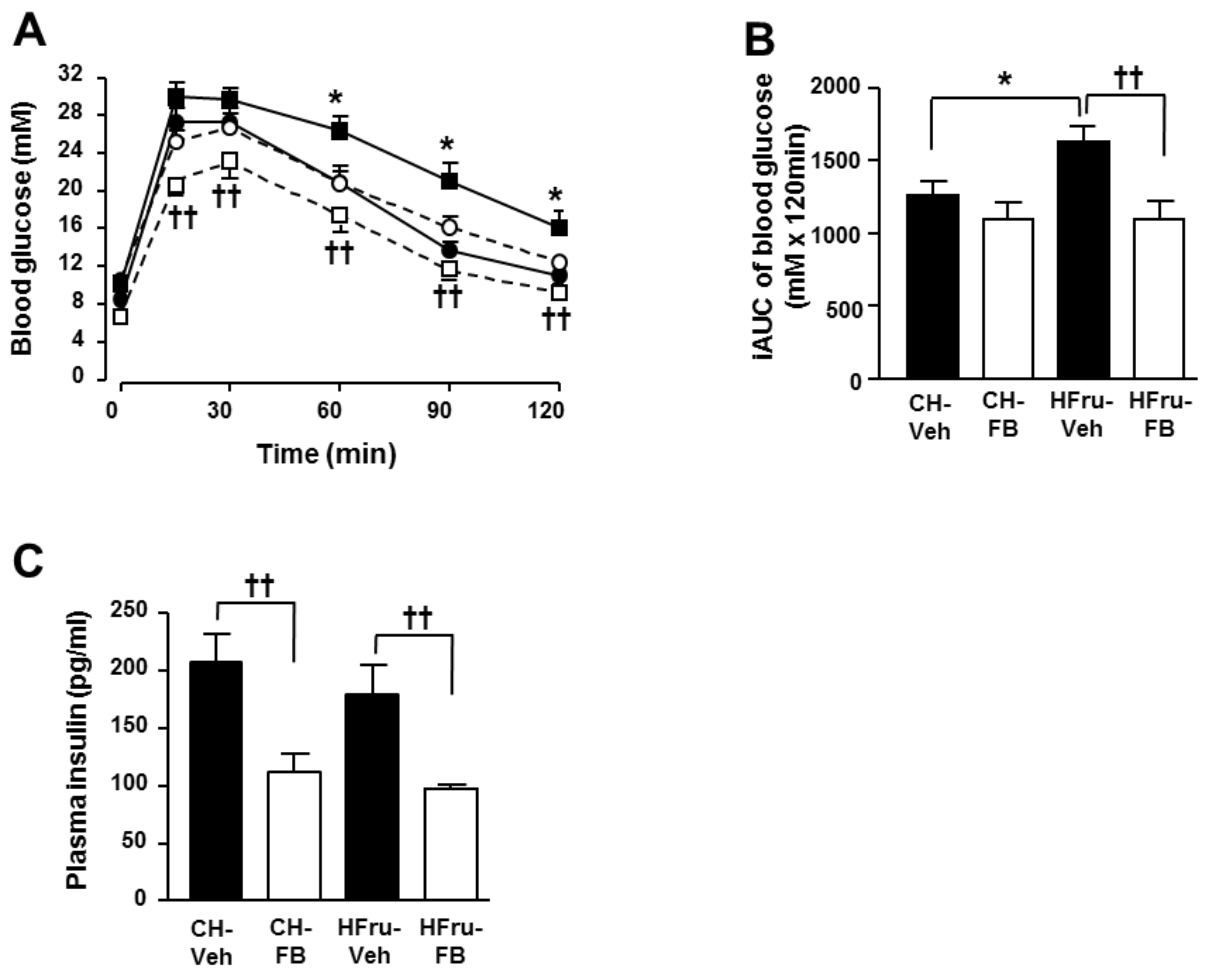
Figure 4.1 Effects of FB treatment on glucose tolerance.

Male C57BL/6J mice were fed a high fructose (HFru) diet with or without the supplementation of fenofibrate (FB, 100 mg/kg/day) as compared to a standard laboratory chow diet (CH). The experiments were performed after two weeks of chow (CH, ●), chow with fenofibrate (CH-FB, ○), high fructose (HFru, ■) or high fructose with fenofibrate (HFru-FB, □) feeding. (A) Glucose tolerance test (GTT) was performed with an injection of glucose (2.5 g/kg, *ip*) after 5-7 hours of fasting. (B) iAUC, incremental area under the curve for blood glucose level. (C) Plasma insulin level between 30-60 min of GTT. Data was means $\pm$ SE, 8-12 mice per group. * $p < 0.05$; †† $p < 0.01$ of the compared groups.

4.3.2 FB treatment restored hepatic insulin signal transduction in HFru-fed mice

In skeletal muscle, insulin stimulated phosphorylation of Akt (all *p*<0.001 vs corresponding basal) was unaltered by diet or fenofibrate treatment (Figure 4.2 C). In contrast, HFru feeding blunted insulin-stimulated phosphorylation of Akt (by 53%, *p*<0.01 vs CH) and its downstream target GSK3β (by 60%, *p*<0.001 vs CH) in the liver both of which were fully restored by treatment with fenofibrate (Figure 4.2 A and B). This indicated HFru feeding resulted in impairment of hepatic insulin signaling and that treatment of fenofibrate was effective in restoring hepatic insulin sensitivity.
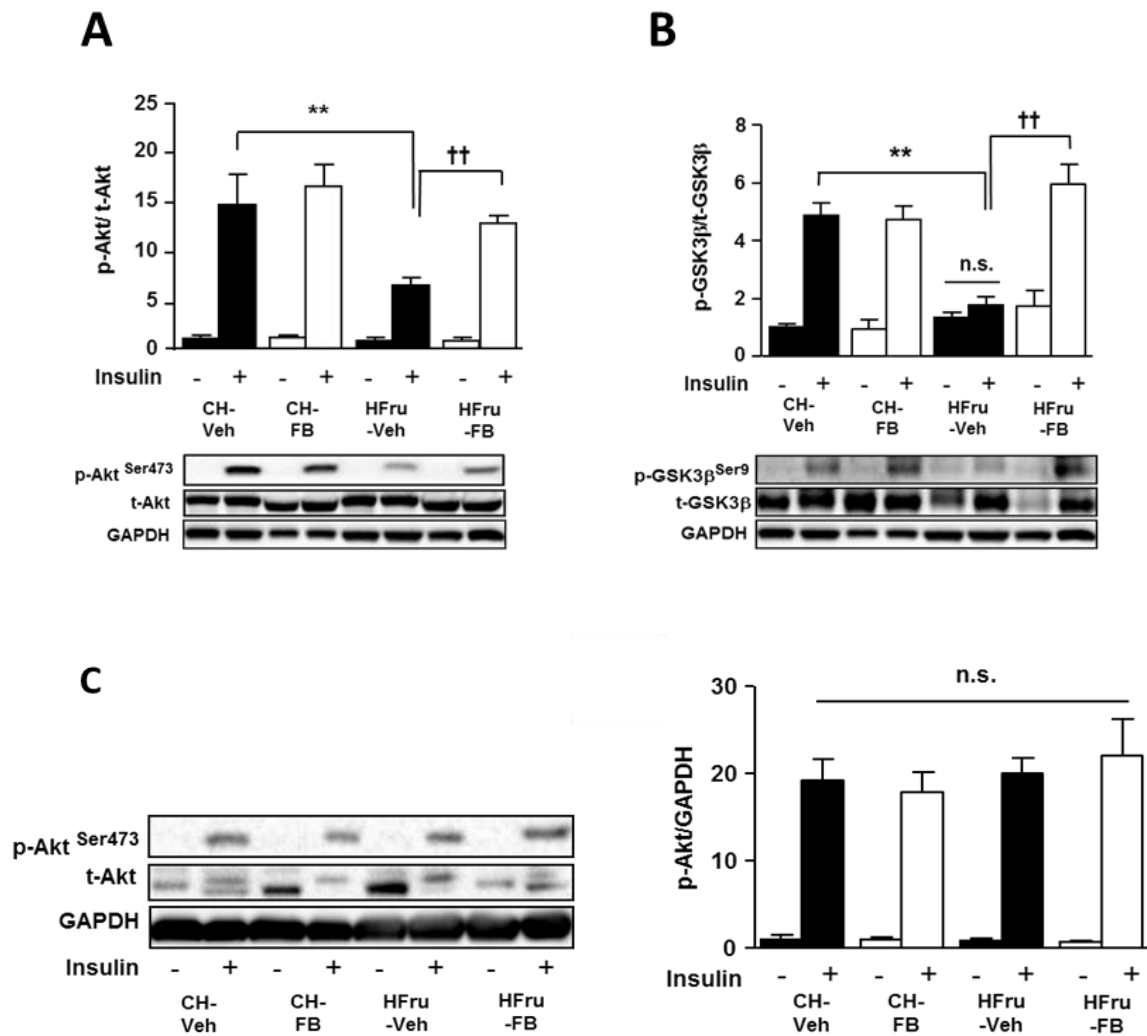
Figure 4.2 Effects of fenofibrate treatment on hepatic insulin signal transduction.

After two weeks of feeding, animals were fasted for 5-7 hours before tissue collection. Liver homogenate were prepared for immunoblotting: (A) representative blots of phosphorylated- and total-Akt (Ser473) with densitometry in the liver, (B) representative blots of phosphorylated- and total- GSK3β (Ser219) with densitometry in the liver in response to a bolus of insulin stimulation (2U/kg, ip). (C) Muscle homogenate were prepared for immunoblotting. The representative blots for phosphorylated- and total- Akt (Ser473) and GSK3β (Ser219) with densitometry in the muscle in response to a bolus of insulin stimulation (2U/kg, ip). Each lane represents a single mouse. Data are mean $\pm$ SE of 8 mice per group. All insulin stimulated groups reached statistical significance of $p < 0.01$ compared to their corresponding basal groups unless otherwise indicated. ** $p < 0.01$; †† $p < 0.001$ of the compared groups.

4.3.3   FB treatment normalised hepatic lipid accumulation

Lipid accumulation in the liver (i.e. hepatic steatosis) is believed to be closely linked to insulin resistance [244]; we hence examined the effects of fenofibrate treatment on hepatic lipid content. As expected, chronic HFru feeding induced a marked increase in hepatic triglyceride (TG) levels (2.7-fold, $p<0.01$ vs CH) which was ameliorated by the treatment of fenofibrate (Figure 4.3 A), while the fasting plasma TG levels were similar between the HFru-Veh and HFru-FB group (Table 11). In agreement with an increased TG levels, hepatic DAG content in HFru-fed mice was also elevated by 53% ($p<0.05$ vs CH) which was normalised by the treatment with fenofibrate (Figure 4.3 B). Total content of hepatic ceramide was attenuated by 57% ($p<0.001$ vs CH) by HFru-feeding, but was restored (ns. vs CH and CH-FB) by the treatment of fenofibrate (Figure 4.3 C). These data suggest a role of DAG in the hepatic insulin resistance resulting from prolonged HFru feeding.

Figure 4.3 Effects of FB treatment on hepatic lipid content.

After two weeks of feeding, animals were fasted for 5-7 hours before tissue collection. Liver homogenate were extracted for the assessment of total TG (A), DAG (B) and ceramide (C) content. Data are mean $\pm$ SE of 8 mice per group. ** $p < 0.01$; †† $p < 0.001$ of the compared groups.

4.3.4 FB treatment increased hepatic fat oxidation under HFru-feeding

As enhanced FA oxidation is one of the key events resulting from the activation of PPARα by FB in the liver [198, 202, 269], we measured molecular markers of oxidative capacity in the livers of mice. The expression of peroxisomal acyl-Coenzyme A oxidase-1 (ACOX1), a direct downstream effector of PPARα activation, which catalyzes the first step of peroxisomal -oxidation of FAs [203], was markedly up-regulated in response to the treatment with fenofibrate (Figure 4.4 A). Moreover, the phosphorylation of ACC which regulates the mitochondrial β-oxidation of FAs was markedly elevated (8-fold, $p<0.001$ vs CH-Veh and HFru-Veh) in response to fenofibrate treatment in the liver of the HFru-fed mice (Figure 4.4 B). In line with an increased oxidative capacity, the activity of β-HAD, which catalyzes the third step of mitochondrial β-oxidation, was augmented by 2.4-fold ($p<0.01$ vs CH-Veh and HFru-Veh) with fenofibrate treatment in the HFru-fed mice (Figure 4.4 C). The activity of citrate synthase was significantly enhanced (by 19%, $p<0.01$ vs CH) under HFru feeding independent of PPARα activation (Figure 4.4 D), indicating PPARα activation specifically enhances the oxidative capacity of the liver without affecting mitochondrial content under HFru feeding. Hepatic FA oxidation was increased (~60%) by the treatment of fenofibrate in the HFru-fed mice and this was due to an increase in the component resistant to the inhibition by etomoxir (Figure 4.4 E).

Figure 4.4 Effects of FB treatment on key enzymes of FA oxidation.

After two weeks of feeding, animals were fasted for 5-7 hours before tissue collection and liver homogenates were immunoblotted for key enzymes related to oxidative capacity: representative blots of ACOX1 (A), phosphorylated-ACC (Ser79) (B), the specific activities of β-HAD (C), and citrate synthase (D). Each lane represents a single mouse. Data are mean ± SE of 10 mice per group. (E) Hepatic fatty acid (FA) oxidation was measured in separate liver homogenates using ^{14}C-palmitate as a substrate in the presence or absence of 0.02 mM etomoxir (detail methods can be found in the supplementary information). Data are mean ± SE of 6-8 mice per group. * $p < 0.05$; ** $p < 0.01$ vs CH; † $p < 0.05$, †† $p < 0.001$ of the compared groups.

4.3.5   FB treatment triggered the activation of UPR pathways in the liver

Having established that treatment of fenofibrate was effective in eliminating hepatic lipid accumulation and restoring insulin signaling, we next sought to examine its effects on the three major UPR pathways. The phosphorylation of IRE1 (Figure 4.5 A), spliced form of XBP1 (sXBP1; Figure 4.5 B), phosphorylation of PERK and eIF2α (Figure 4.5 C and D), as well as the expression CHOP (Figure 4.5 E) were markedly enhanced by PPARα activation regardless of the feeding conditions. In addition, the expression of GADD34, a well-characterized phosphatase of eIF2α [102] was concomitantly down-regulated in response to PPARα activation (Figure 4.5 F). As expected, HFru feeding significantly increased the phosphorylated form of IRE1 (Figure 5 A, $p<0.05$ vs CH) and eIF2α (Figure 4.5 D, $p<0.01$ vs CH). No changes were detected in the maturation of activating transcription factor 6 (ATF6) as a result of HFru-feeding or fenofibrate treatment (Figure 4.5 G).

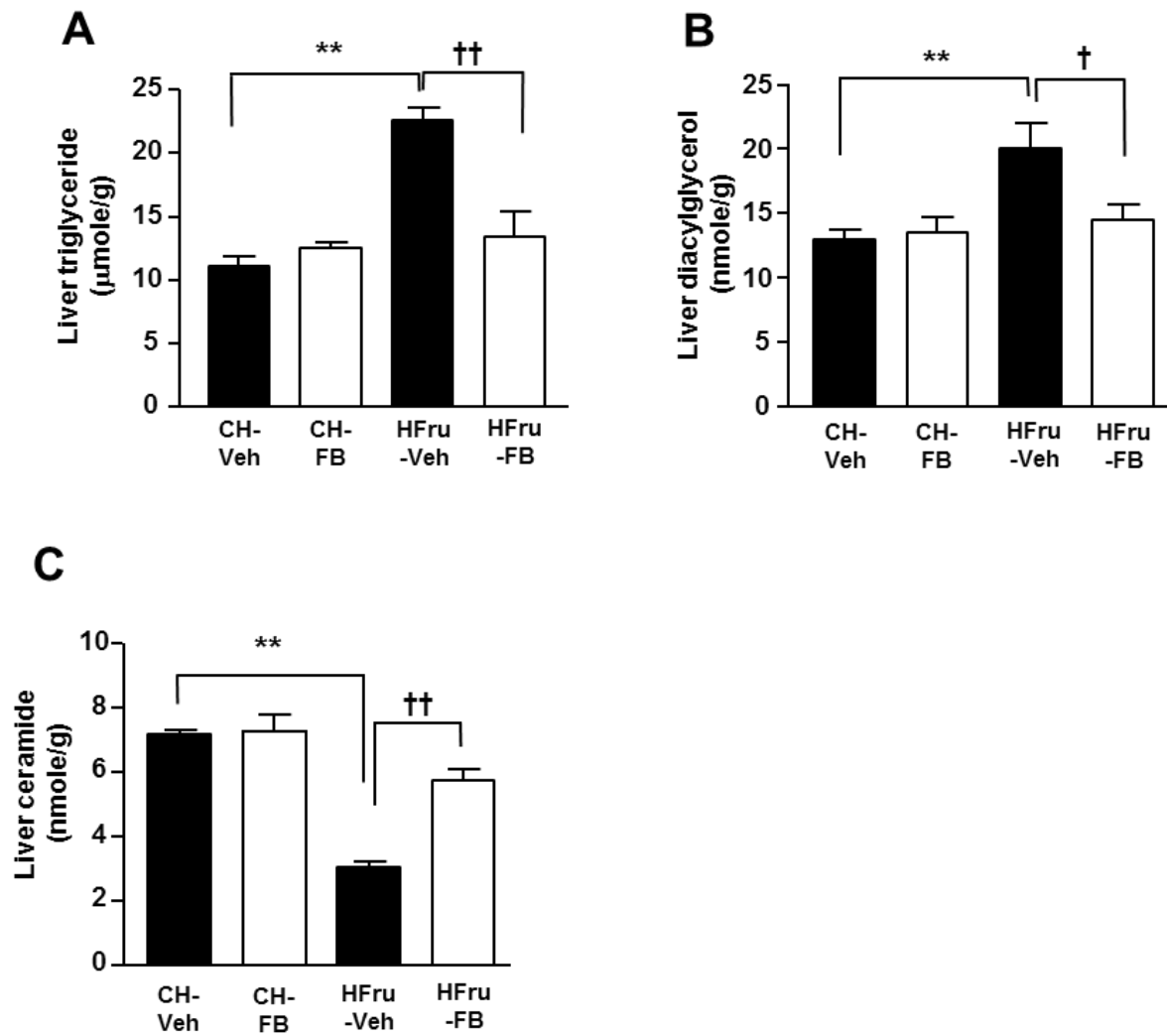Figure 4.5 Effects of FB treatment on hepatic UPR signaling.

After two weeks of feeding, animals were fasted for 5-7 hours before tissue collection and liver homogenates were immunoblotted for markers of ER stress: representative blots of phosphorylated-IRE1 (Ser724) (A), spliced form of XBP1 (B), phosphorylated-PERK (Thr980) (C), phosphorylated-eIF2α (Ser51) (D), CHOP (E), GADD34 (F) and ATF6 (G) with densitometry. Each lane represents a single mouse. Data are mean $\pm$ SE from 8 to 10 mice per group. * $p < 0.01$ vs CH, †† $p < 0.01$ of the compared groups.

4.3.6 FB-induced UPR signaling was accompanied by an enhanced DNL

As both activation of PPARα [198] and UPR signaling [160] can promote DNL in the liver via the action of sterol regulatory element-binding protein-1c (SREBP1c) [157], we hence examined the expression of SREBP1c and key enzymes involve in this process. Our western blotting analysis revealed up-regulations of the mature form of SREBP1c (mSREBP1c, 3-fold, $p<0.05$ vs CH-Veh), ACC (3.5-fold, $p<0.01$ vs CH-Veh), FAS (2.5-fold, $p<0.001$ vs CH) and SCD1 (14.5-fold, $p<0.01$ vs CH-Veh) in the liver of the HFru-fed mice (Figure 4.6A-D). PPARα activation in the CH-fed mice stimulated the expression of mSREBP1c, ACC, FAS and SCD1 to levels comparable to that of the HFru-fed mice. PPARα activation in conjunction with HFru-feeding elicited a further increase in the expression of mSREBP1c (6-fold) and SCD1 (38-fold, both $p<0.001$ vs HFru-Veh), but not ACC (2.8-fold, $p<0.01$ vs CH) nor FAS (2.9-fold, $p<0.001$ vs CH, both not different vs HFru-Veh). Consitent with the up-regulated lipogenic enzymes, hepatic DNL was significantly increased (~38 %) by PPARα activation in CH-fed mice and this increase was maintained in fenofibrate treated HFru-fed mice (Figure 4.6 E). These data suggested the fenofibrate-induced modulation of UPR signaling may enhance the lipogenic capacity of liver independent of the effects of dietary fructose.
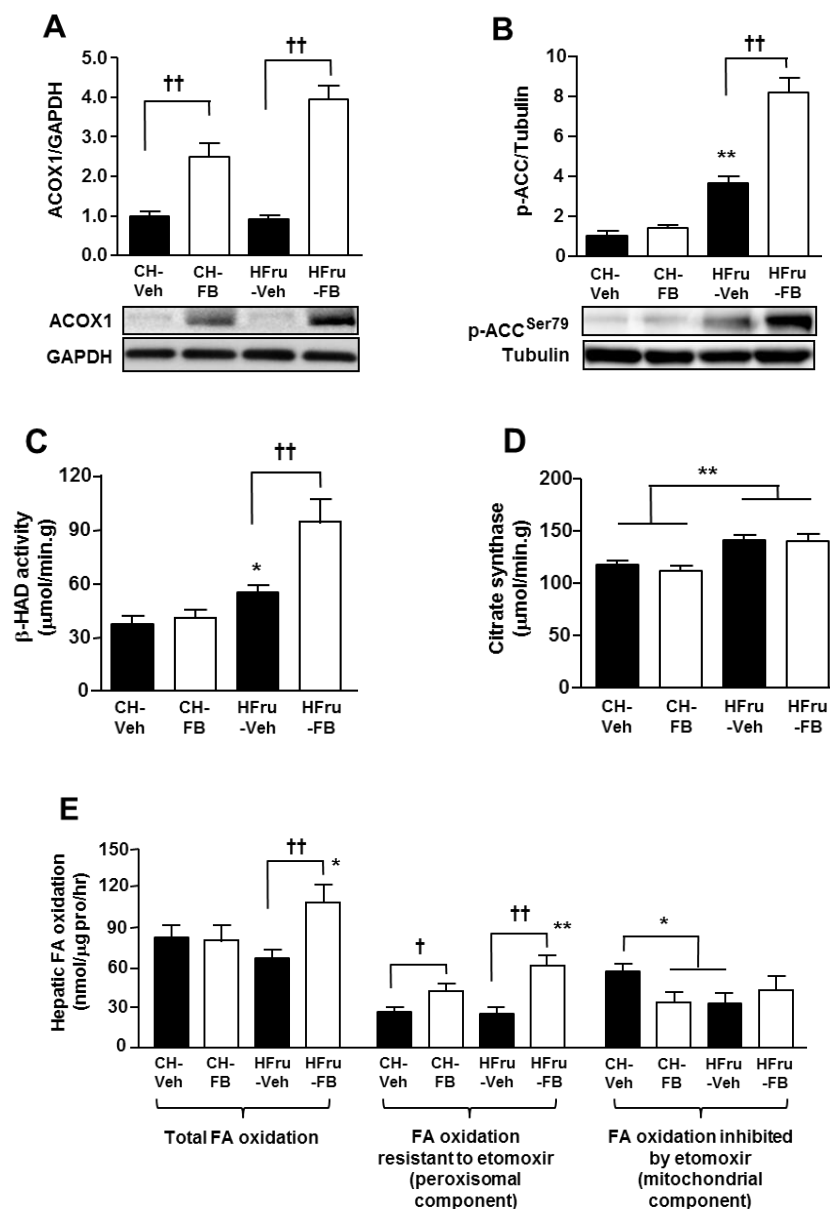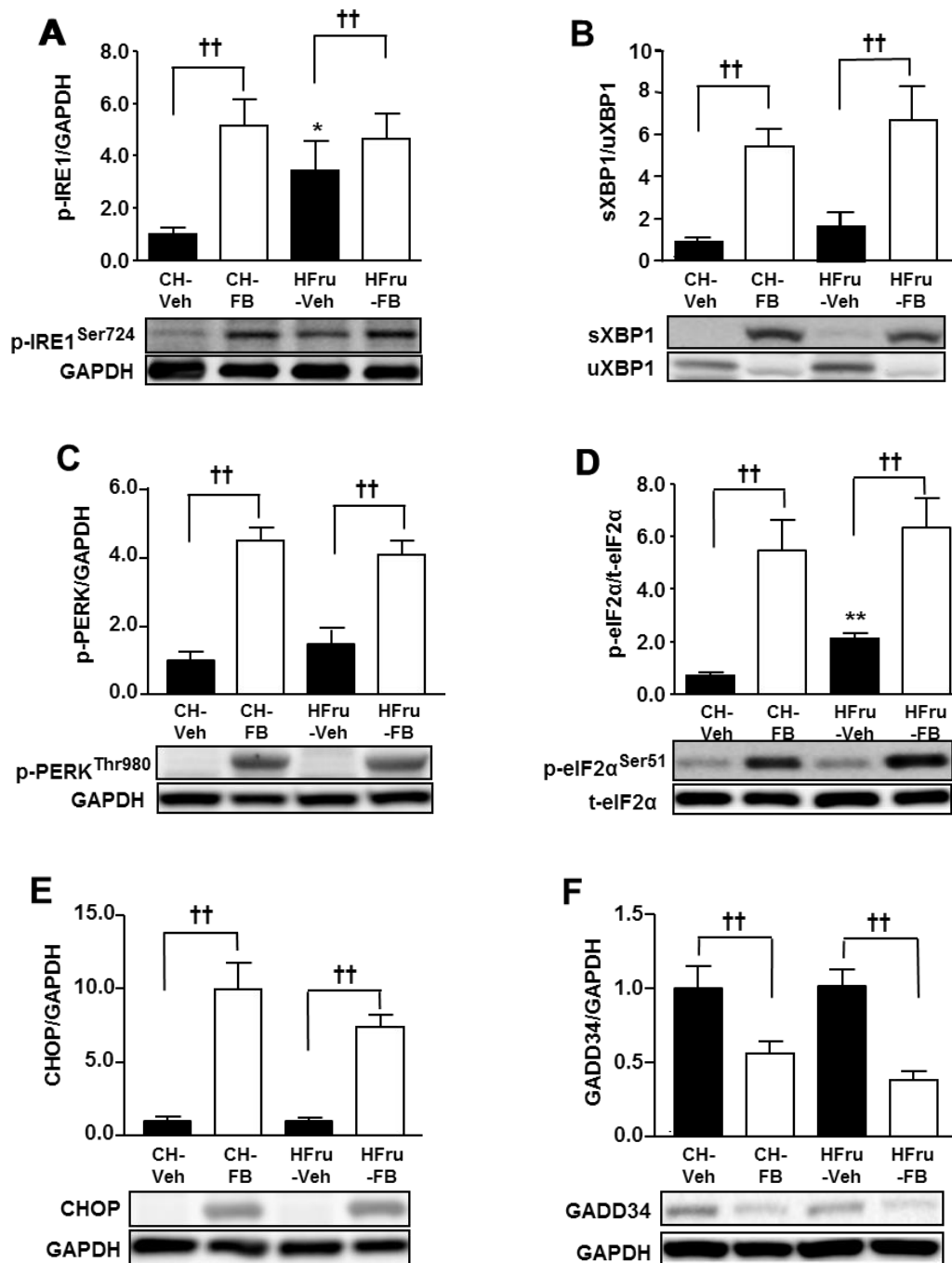
Figure 4.6 Effects of FB treatment on hepatic DNL.

After two weeks of feeding, animals were fasted for 5-7 hours before tissue collection and liver homogenates were immunoblotted for key enzymes related to lipogenic capacity: representative blots of the matured form of SREBP1c (mSREBP1c) (A), ACC (B), FAS (C) and SCD1 (D) with densitometry. Data are mean ± SE of 10 mice per group. (E) Hepatic DNL was measured by the incorporation of [3H]-H2O into hepatic triglyceride (detail methods can be found in the supplementary information). Data are mean ± SE of 6 to 8 mice per group. * p < 0.05 vs CH; ** p < 0.01; †† p < 0.001 of the compared groups.

4.3.7   The downstream effects of the FB -induced UPR signaling

Production of deleterious lipids (lipotoxicity) via DNL and activation of serine/threonine kinases are key consequences of UPR signaling which interferes with insulin signal transduction at various points [258]. As shown in Figure 3B, treatment of fenofibrate was able to correct the elevated DAG content induced by HFru-feeding. Meanwhile, activation of JNK and IKK are well-demonstrated consequences of UPR signaling resulting in the impairment of insulin signal transduction [249]. HFru feeding did not result in a significant induction of JNK (Figure 4.7 A) or IKK (Figure 4.7 B), and the expression of IκBα (Figure 4.7 C), the downstream target of IKK [270], remained unaffected which is consistent with our previous observation [193]. Despite the significant induction of the two specific arms of UPR pathways, the phosphorylation status of these kinases remained unaffected in response to fenofibrate treatment (Figure 4.7 A to C). These data suggested PPARα activation is effective in eliminating lipotoxicity and that the fenofibrate-induced UPR signaling did not result in the activation of these stress kinases.
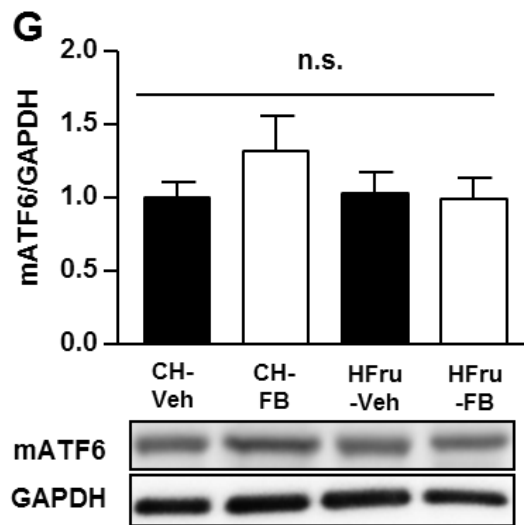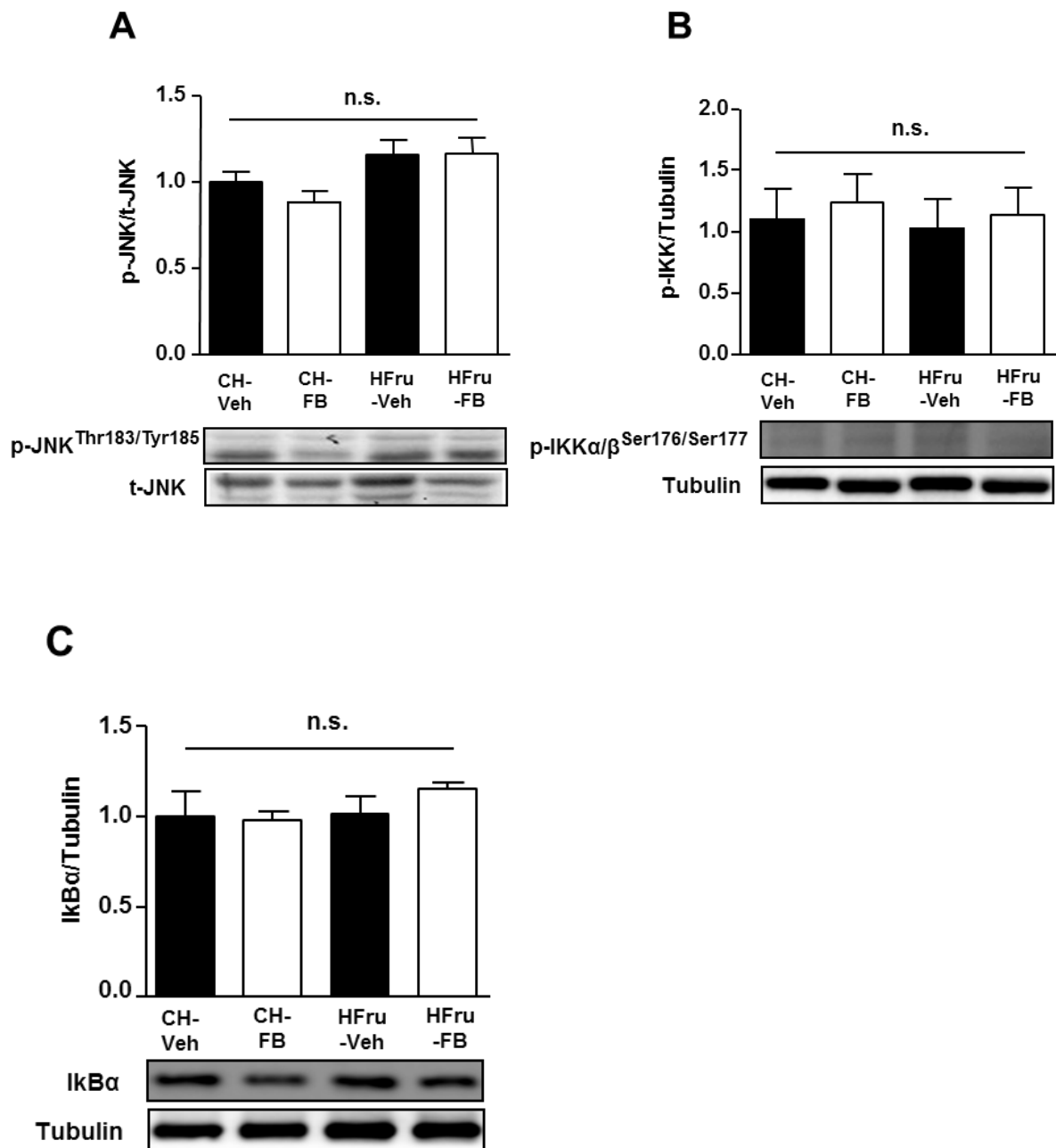
Figure 4.7 Effects of FB treatment on JNK and IKK activation.

After two weeks of feeding, animals were fasted for 5-7 hours before tissue collection and liver homogenates were immunoblotted for evidence of JNK and IKK activation: representative blots of phosphorylated-JNK (A), phosphorylated-IKK (B), IκBα (C). Data are mean ± SE of 8 mice per group. n.s. denotes no statistical differences.

Supplementary data:
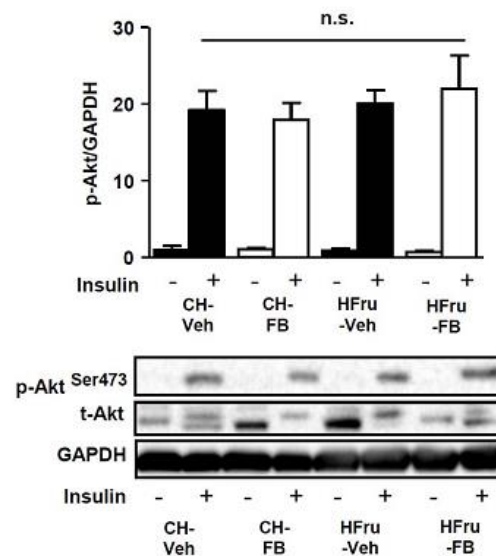
Supplementary Figure 1.Densitometry of insulin-stimulated Akt phosphorylation in muscle. After two weeks of feeding, animals were fasted for 5-7 hours before tissue collection and red quadriceps muscle homogenates were immunoblotted for phosphorylated-Akt (Ser473) in response to a bolus of insulin stimulation (2U/kg, ip). Data are mean $\pm$ SE from 8 to 10 mice per group. All insulin stimulated samples reached statistical significance of p < 0.01 comparedto that of the non-stimulated. No significant difference was observed among the stimulated groups.
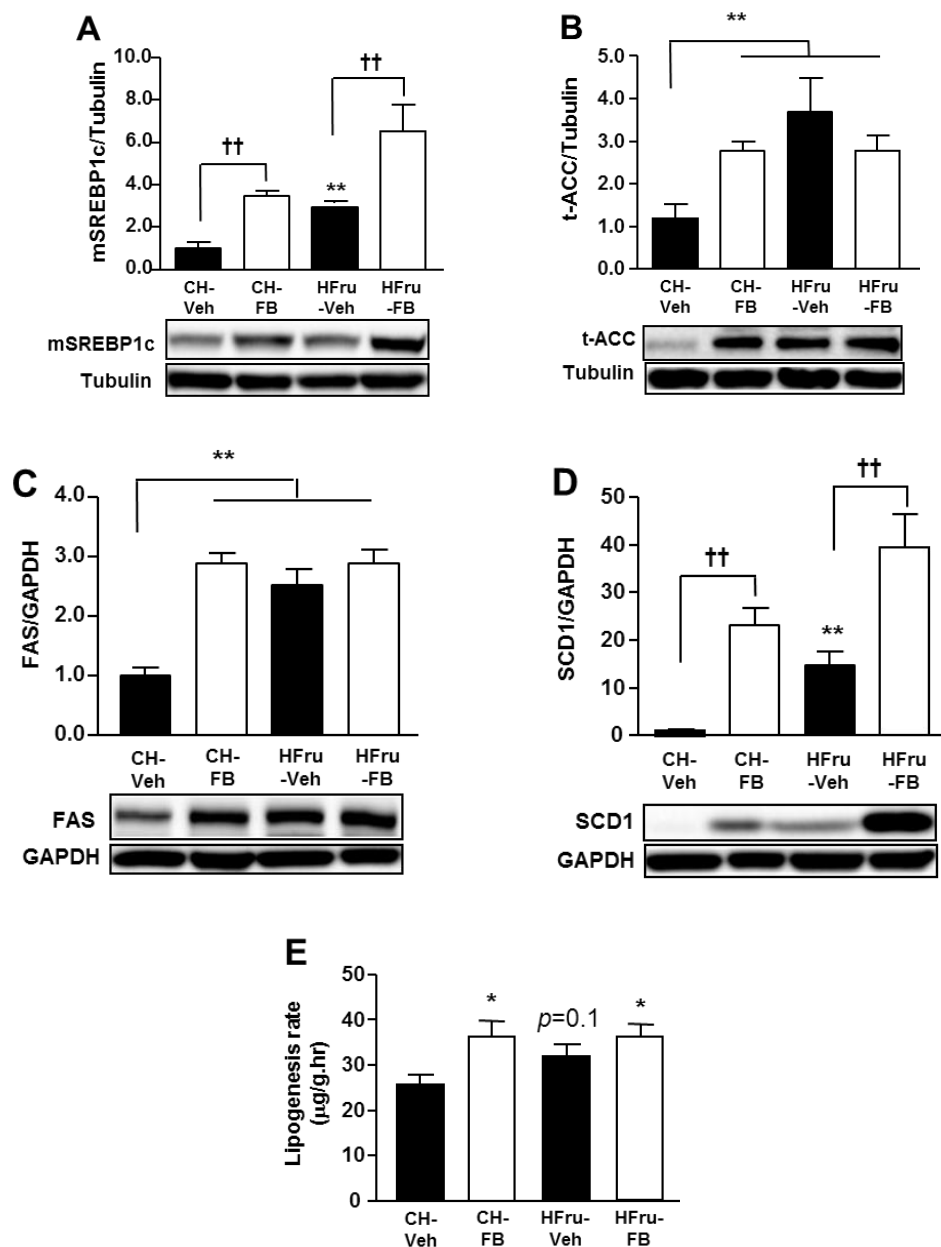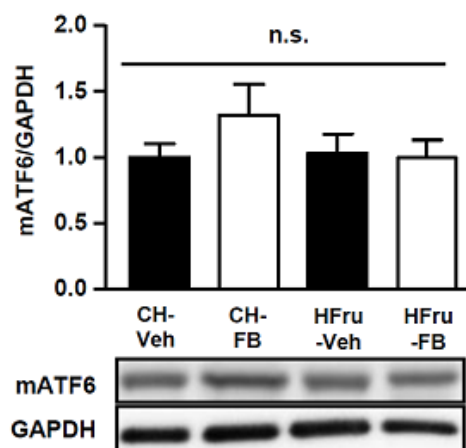

Supplementary Figure 2. Effects of FB treatment on ATF6. After two weeks of feeding, animals were fasted for 5-7 hours before tissue collection and liver homogenates were immunoblotted for ATF6. Representative blot is shown with densitometry. Eachlane represents a single mouse. Data are mean $\pm$ SE from 8 to 10 mice per group. n.s. denotes no statistical differences.

4.4 Discussion

In this chapter, we established a hepatic ER stress model independent of lipid accumulation in the liver with the administration of PPARα activator, fenofibrate (FB), in HFru-fed mice. This model enabled us to examine the effects of ER stress on hepatic insulin sensitivity devoid of the influence of hepatic steatosis. The results revealed that PPARα activation completely eliminates HFru-induced hepatic steatosis and insulin resistance without altering JNK and IKK in the face of marked dual activation of the IRE1/XBP1 and PERK/eIF2α branches of the UPR pathways. These findings indicate that hepatic steatosis, but not JNK, is required for ER stress to cause insulin resistance. To the best of our knowledge, this is the first report to demonstrate that PPARα activation induces UPR signaling while ameliorating hepatic insulin resistance.

PPARα is a key transcriptional regulator for lipid metabolism and it can be endogenously activated by FAs, as well as pharmacologically by agonists like fenofibrate [265]. Fenofibrate is a specific agonist of PPARα commonly used to treat dyslipidaemia and hypercholesterolemia in humans [200]. These beneficial effects are attributed to the PPARα-driven peroxisomal and mitochondrial β-oxidation and microsomal ω-oxidation of FA with the liver being a major site of action [271]. The results showed that fenofibrate treatment was effective in activating PPARα *in vivo* as evidenced by the increased expression of ACOX1 (also known as palmitoyl-CoA oxidase) [272] which is a direct target of PPARα. The concomitant increase in VO_2 and the induction of the phosphorylated form of ACC and β-HAD activity along with the augmented FA oxidation in the liver are indicative of an enhanced oxidative capacity and energy expenditure which are consistent with the reported effects of PPARα activation [271, 273]. In line with the upregulation of ACOX1 expression, fenofibrate-induced increase in hepatic FA oxidation can be attributed to the enhanced

peroxisomal oxidation that is not inhabitable by etomoxir which blocks the entry of long-chain FAs into mitochondria for oxidation. It has been reported that peroxisomal oxidation break down (very) long-chain FAs into medium and short chain FAs further oxidation in mitochondria [273]. Unlike long chain FAs, the short- and medium-chain FAs do not rely on CPT1 to enter the mitochondria [273] which may explain, at least in part, the increased oxygen consumption as observed at the whole body level. It is likely that the reduced body weight and adiposity observed only in fenofibrate treated HFru-fed mice is due to the enhanced peroxisomal oxidation which was not evident in treated CH-fed mice.

The restored HOMA-IR resulting from the lowered fasting blood glucose and insulin levels, together with the restored hepatic insulin signal transduction in the HFru-fed mice by fenofibrate are suggestive of improved insulin sensitivity in these mice. This interpretation is also supported by the striking reduction in insulin secretion in fenofibrate treated chow fed mice while maintaining unaltered glucose clearance. The insulin-sensitising effect of fenofibrate observed in the present study is consistent with our previous report of the insulin sensitizing effect of PPARα activation in high fat fed insulin resistant rats as determined by the hyperinsulinemic-euglycemic clamp [274].

The ER plays a pivotal role in protein processing to maintain cellular homeostasis under physiological conditions through the three canonical branches of UPR signaling pathways: PERK/elF2α, IRE1/XBP1 and ATF6. The initiating proteins PERK, IRE and ATF6 all have sensors facing the ER lumen and they can be activated under ER stress such as the accumulation of misfolded proteins [102, 258]. Activated IRE1/XBP1 pathway has been suggested to promote DNL in the liver leading to the production of lipids [160, 261]. In addition, both IRE1 [104] and PERK [163] have been suggested to activate JNK and IKK.

These mechanisms, acting in concert or alone, are sufficient to impair insulin signaling in the liver. However, it has been difficult to separate the effect of activated UPR pathways on hepatic insulin signaling *in vivo* from the influence of lipid accumulation. Moreover, fenofibrate is a lipid-lowering drug commonly used in humans and fructose consumption is closely related to the epidemic of obesity and fatty liver [262, 275]. Thus, the approach of fenofibrate administration to insulin resistant mice induced by HFru feeding not only allowed us to dissect this integral relationship, but also provided new insight into the mechanisms relevant to the conditions in humans.

Both DAG and ceramide are key lipid intermediates linking hepatic steatosis to insulin resistance [261]. Our results showed that liver DAG content was higher in HFru-fed mice (as a result of increased DNL) and this is consistent with a previous report in HFru-fed mice [161]. DAG can activate protein kinases C ε (PKCε) which in turn phosphorylates the insulin receptor substrate 1 (IRS1) at serine 307 to disrupt tyrosine phosphorylation of IRS1 [276]. This could blunt IRS-mediated phosphorylation of its downstream signaling target such as Akt [140]. While maintaining elevated DNL (as indicated by mSREBP1c, ACC, FAS, SCD1, and the incorporation of $[^3H]$-H_2O into triglyceride) induced by HFru diet, fenofibrate was able to outpace DNL by a much greater effect to accelerate FA oxidation (as indicated by the 14-16% increase in VO_2, 3.9-fold, 8-fold and 2.1-fold increases in ACOX1, pACC and β-HAD, respectively), hence eliminating the accumulation of TG and DAG. This may offer an explanation towards the improved insulin signaling by fenofibrate. In HFru-fed rat, hepatic ceramide has been reported to be increased [239] and this lipid metabolite can suppress the phosphorylation of Akt via protein phosphatase 2A [135, 146]. In the present study ceramide is unlikely to be a contributor for the blunted insulin signaling because its level in HFru-FB mice was similar to the level in chow-fed mice. However, the precise role of ceramide

requires further investigation as the cellular location may be a key determinant of its effect on insulin sensitivity [277].

The other key mechanism for ER stress induced insulin resistance is the activation of JNK and associated stress kinases. Sustained ER stress has been shown to cause hepatic insulin resistance via the induction of JNK and IKK [125, 214] and all three canonical arms of the UPR pathways are capable of activating JNK and IKK signaling under conditions of severe ER stress [249]. Consistent with our previous finding [193] HFru feeding was accompanied by the presence of ER stress. Despite further activation of the IRE1/XBP1 and PERK/eIF2α signaling by the activation of PPARα with fenofibrate, the unaltered phosphorylation of JNK and IKK or Iκ-B content argues against their role in the improved insulin signaling properties in the liver. In addition, cellular ceramide is also known to be implicated in the up-regulation of IKK and JNK [146]. The fact that neither ceramide nor these stress-related kinases were up-regulated by fenofibrate is also consistent with the interpretation of the reduction in DAGs as a more likely mechanism for the alleviation of hepatic insulin resistance by the activation of PPARα. Of interest, Jurczak et al. [161] has recently demonstrated alleviation of hepatic DAG accumulation in mice with conditional knockout of XBP1. The absence of XBP1 can reverse fructose-induced insulin resistance despite the presence of ER stress and JNK activation which supports the notion of DAGs being the major culprit for hepatic insulin resistance induced by HFru feeding.

It has been suggested that mild ER stress may enhance hepatic insulin signaling and protect against lipotoxicity via the induction of an adaptive UPR [278]. Mice carrying liver specific deletion of IRE1 displayed overt steatosis when challenged with ER stress inducers [99], while genetic ablation of either ER stress-sensing or ER quality control molecules also

resulted in the development of hepatic steatosis [173]. Furthermore, IRE1 has been reported capable of repressing the expression of key metabolic transcriptional regulators, including CCAAT/enhancer-binding protein (C/EBP) β, C/EBPδ, PPARγ, and enzymes involved in triglyceride biosynthesize [173], which suggests that UPR might be an important mechanism for mitigating steatosis. The results in the this chapter highlight the need for further investigation to examine whether specific UPR signaling may in fact contribute to the PPARα-mediated effects on insulin sensitivity.

Although attenuated body weight gain in the HFru-fed mice induced by fenofibrate may confound our interpretation at the first glance, the pivotal role of lipids (but not the activated UPR *per se*) in ER stress associated insulin resistance is also demonstrated in CH-FB fed mice without body weight change (compared to CH-fed mice). Despite similar dual activation of both IRE1/XBP1 and PERK/eIF2α pathways in the fenofibrate-treated CH-fed mice, insulin-mediated phosphorylation of Akt and GSK3β remained intact in the absence of lipid accumulation. This interpretation is consistent with a previous study showing reduced liver lipids as the underlying mechanism of improved hepatic insulin sensitivity during body weight loss in patients with type 2 diabetes [279].

In summary, these results indicated that lipid (particularly DAG) accumulation, but not the activation of JNK or IKK, is required for ER stress to cause hepatic insulin resistance and glucose intolerance during HFru consumption. Increased peroxisomal oxidation of FAs and energy expenditure are likely to underpin the observed reduction in hepatosteatosis and insulin resistance in fenofibrate-treated HFru-fed mice despite marked increases in UPR signaling and *de novo* lipogenesis. Therefore, activation of PPARα with fenofibrate ameliorates HFru-induced hepatic insulin resistance by eliminating lipid deposition by

blocking its link with ER (Figure 4.8). This chapter also suggests a need for further investigation as to whether activation of specific UPR pathways may in fact contribute to the therapeutic effects of fibrate drugs which are commonly used in humans.
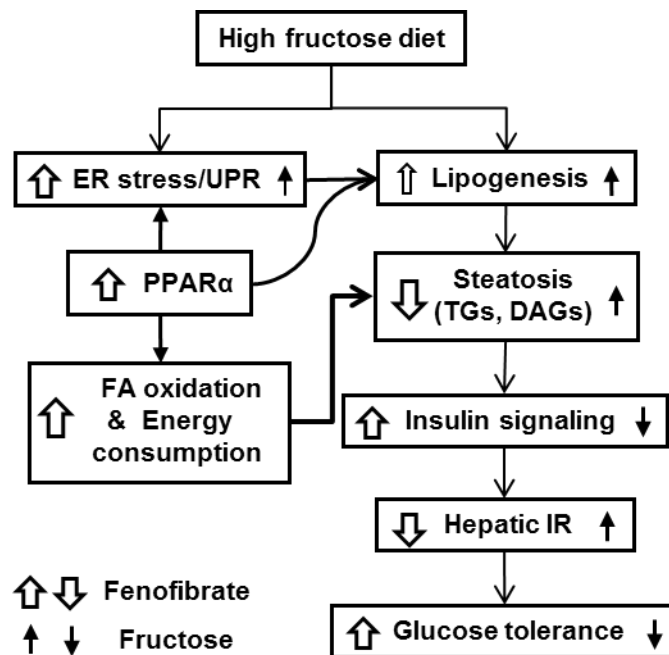
Figure 4.8 Illustration of PPARα -mediated effects on ER stress, lipid metabolism, and insulin sensitivity in the liver.

HFru feeding accentuates the accumulation of TG and DAG in the liver through the induction of DNL. The accumulation of these lipid metabolites attenuates normal insulin signal transduction leading to hepatic insulin resistance, resulting in the reduction of glucose tolerance. PPARα activation by fenofibrate may also directly stimulate lipogenesis, which may involve the signaling of specific arms of the UPR pathways. However, the predominant effect of potentiated oxidative capacity (primarily peroxisomal oxidation) driven by PPARα is capable of eliminating lipid accumulation, thus overcoming fructose-induced hepatic insulin resistance (IR) and glucose intolerance.

Chapter 5

Interaction between

DNL and ER stress

5.1   Introduction

The role of either ER stress and lipid accumulation in the initial insulin resistance in the liver has been discussed in Chapter Chapter 3 and Chapter Chapter 4. The mechanisms of ER stress and lipid accumulation leading to hepatic insulin resistance were different at different stage of insulin resistance. According to previous study, lipid accumulation *per se* appeared to be insufficient to induce insulin resistance in the liver at early stage. However, it becomes a predominant factor to exacerbate insulin resistance in long term HFru-fed mice. Relatively, the effect of JNK activation on hepatic insulin resistance reduced. This result is consistent with current literature report [162]. These changes led us to explore the relationship between ER stress and lipid accumulation. Although most current reports suggested that lipid accumulation induce ER stress (details in 1.6.2), ER is a critical organelle for lipid processing where many enzymes involved in intermediary and complex lipid metabolism reside [258]. Thus, UPR is considered to be able to regulate the lipid processing. Indeed, some studies indicated that enhanced ER stress could also upregulate lipid accumulation (details in 1.6.1). However, the relationship between ER stress and lipid metabolism remains unclear in fructose over consumption model.

The study in this chapter utilized fructose to induce ER stress in cultured cells, aimed to mimic the high fructose feeding model in animals. According to the results from previous studies, the suppression of ER stress by TUDCA led to decrease of lipogenesis and lipid accumulation in the liver. On the other hand, the downregulation of lipogenesis by betulin administration resulted in a significant reduction of IRE1. To further confirm the sequence of the occurrence of ER stress and DNL, we treat cells with betulin which has been used in previous study.

Our data showed that fructose treatment enhanced lipogenic proteins (tACC, FAS and SCD1). The triglyceride level also increased in fructose-treated cells. Both IRE1 and eIF2α were stimulated significantly by fructose administration. Betulin administration suppressed tACC and FAS but not SCD1. Consistent with what we observed in the animal, betulin treatment did not reduce the TG level. Interestingly, betulin failed to inhibit p-IRE1 as well as p-eIF2α. All these results suggested that lipid may not be a critical cause of ER stress in fructose-overconsumption model.

5.2   Methods

5.2.1   Cell culture

The details were described in 2.2.1.

5.2.2   Cell treatment

FAO (differentiated rat liver cell) and HepG2 (human liver carcinoma cell) cells were seeded into 12- well plates when the confluence reached 75% in the flask. The cells were incubated in the DMEM medium (Cat. 11885) with 1% Penicillin-Streptomycin-Glutamine (PSG) for 24 hours. Medium was then changed into the "cultured mediums" with 1% PSG. Cells were cultured with these mediums for 24 hours and were harvested for following analysis.

Table 12 Cultured mediums.

	Glucose	FBS	Fructose
Serum-control	10 mM	10%	-
Control	10 mM	-	-
Serum-Fructose	10 mM	10%	25 mM
Fructose	10 mM	-	25 mM
Serum-High glucose	50 mM	10%	-
High glucose	50 mM	-	-

5.2.3 Protein extraction from cells

Medium was removed from the wells and cells were rinsed with PBS for twice and scraped immediately following the addition of HES buffer. The cell lysate was transferred into a 1.5 ml microcentrifuge tube. Syringe needles were used to break down cells. The lysate was centrifuged at 3000 rpm for 10 min. The supernatant was removed and the pellet was suspended with 100 μl HES buffer. The lysate was then applied for protein assay or stored at -80 ºC.

Table 13 HES buffer.

Stock		Fresh	
HEPES	5 mM	NaF	10 mM
EDTA	0.5 mM	PMSF	1 mM

	Stock	Fresh	
sucrose	250 mM	protease/phosphatase inhibitors	10 ul/ml

5.2.4 Western blotting

The details were described in 2.3.

5.2.5 Statistical Analyses

Data are presented as means $\pm$ SE. One-way analysis of variance was used for comparison of relevant groups. When significant variations were found, the Tukey-Kramer multiple comparisons test was applied. Differences at $p<0.05$ were considered to be statistically significant.

5.3 Results

5.3.1 Establishment of cell model

FAO cells are a differentiated rat liver cell line derived from rat H4IIIE hepatoma cells. HepG2 is a human liver carcinoma cell line. To identify which cell line fitted with our model and what kind of cultured medium was suitable for the hypothesis, both cell lines were cultured with several different mediums. The result showed that with respect to lipogenesis, FAO cells exhibited a high level of lipogenesis in response to the fructose media indicated by significant increase in ACC and FAS (Figure 5.1 A, B). In contrast, FAO cells which were treated with serum-control, serum-fructose, serum-high glucose and high glucose medium did

not show an increase in lipogenesis as shown by no difference in either ACC or FAS. HepG2 showed significant upregulation of ACC when treated with either serum-control or fructose medium (Figure 5.1 A). Relatively, the level of FAS did not exhibit any significant changes between groups (Figure 5.1 B). However, when treated with 10 mM glucose and 25 mM fructose, FAS tended to be upregulated, but was not significant (p=0.068 vs control, t-test).

Regarding ER stress response, FAO cells failed to show any enhancement of phosphorylation of IRE1 regardless of media condition used (Figure 5.1 C). However, p-eIF2α modestly increased when cells were treated with 50mM glucose in the presence or absence of FBS (Figure 5.1 D). HepG2 cells, alternatively, exhibited activation of both p-IRE1 and p-eIF2α in response to most media conditions (Figure 5.1 C, D).

According to the previous data and the hypothesis, HepG2 appeared to be an appropriate candidate to achieve the requirement of induction of both ER stress and *de novo* lipogenesis. Meanwhile, though HepG2 cells were able to response to several alternative mediums, fructose became the priority as it has been used in our previous study *in vivo*. In the medium with additional fructose, the presence of FBS appeared to have negative effects on lipogenesis proved by non-significant augments in both ACC and FAS expression. Hence we select HepG2 as the cell line and the medium which contains 10mM glucose and 25mM fructose without FBS (fructose media) as the cultured medium for the following studies.
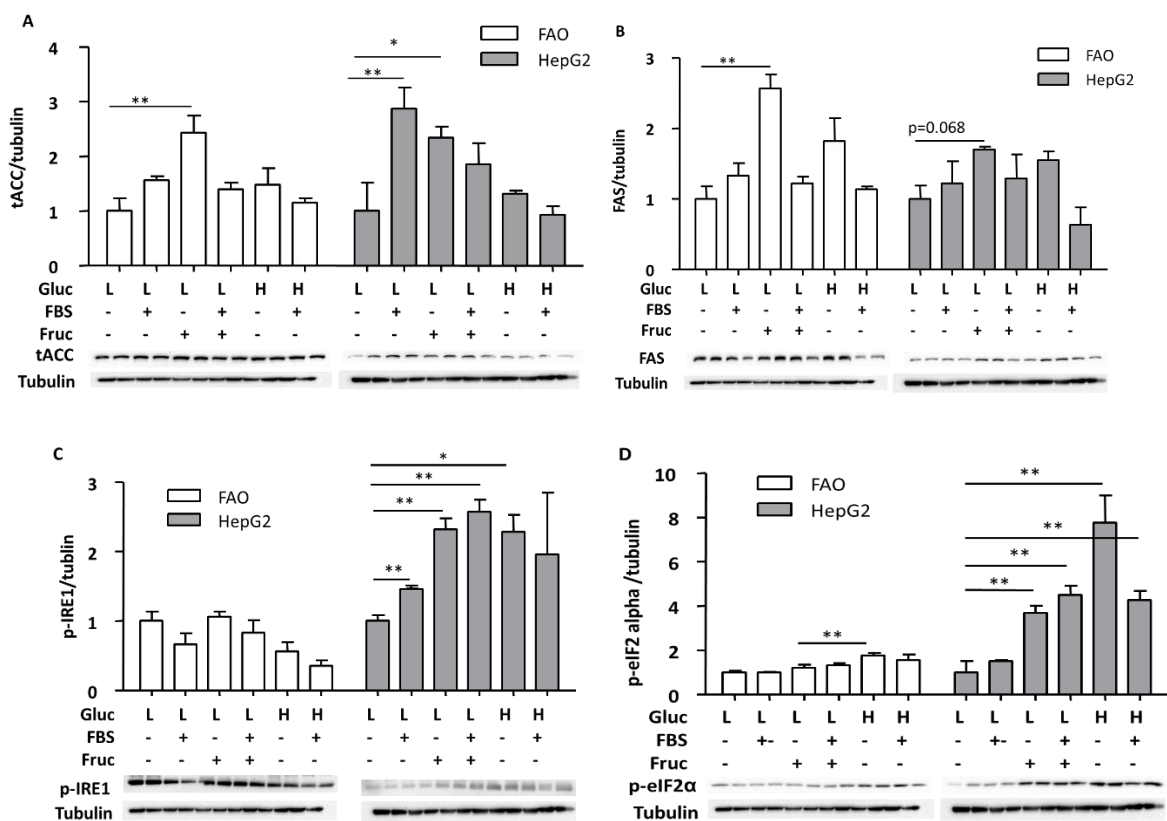
Figure 5.1 Lipogenesis and ER stress in FAO or HepG2 in different mediums.

FAO or HepG2 cells were incubated as described in the methods. Cell homogenates were immunoblotted for evidence of ACC (A), FAS (B), p-IRE1 (C) and p-eIF2α (D). Data are mean $\pm$ SE of 3-4 replicates. * $p <0.05$, ** $p <0.01$ for compared group. L, concentration was 25mM. H, concentration was 50mM.

5.3.2   Betulin treatment suppressed lipogenesis

The results suggest that the lipogenesis was augmented in response to 25 mM fructose treatment. The expression of ACC was upregulated (p=0.063) (Figure 5.2 A). FAS and SCD1 (Figure 5.2 B, C) which were other two critical lipogenic enzymes were significantly increased. However, the extent of stimulation of ACC (20%) and FAS (21%) (Figure 5.2 A, B) with fructose induced lipogenesis in cells was not as strong as in animals. SCD1 was upregulated for more than 3-fold change in fructose treated cells (Figure 5.2 C). Betulin treatment in fructose media reduced the levels of both ACC and FAS while the level of SCD1 remained as high as in fructose treatment (Figure 5.2 A, B). The expressions of both enzymes were reduced to the level that was approximately 50% of the control group. However, the intracellular TG content was not reduced by betulin administration (Figure 5.2 D). These data suggest that fructose-induced lipogenesis in HepG2 cells was reduced at least partially by betulin.
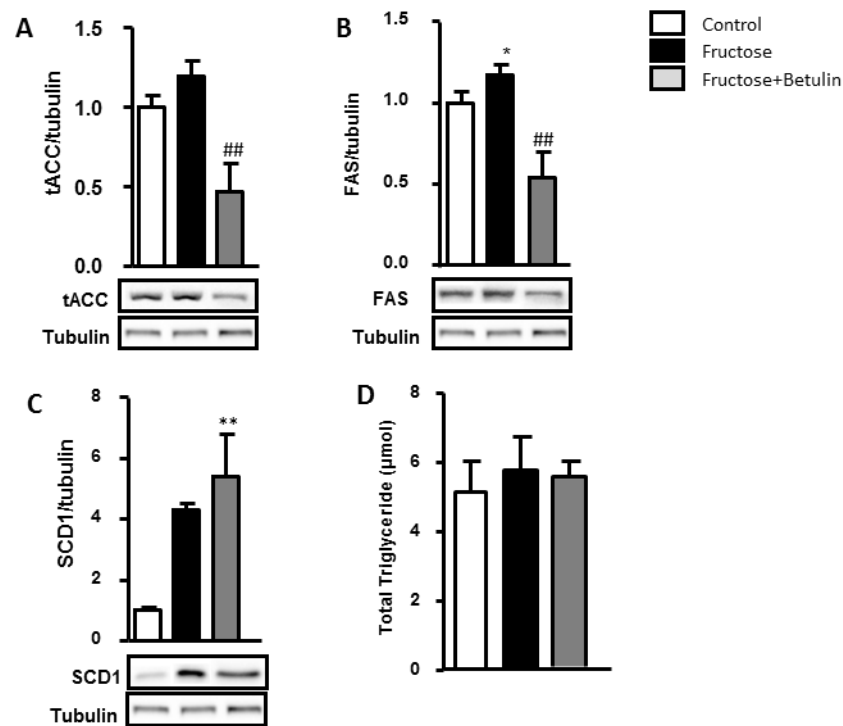
Figure 5.2 Suppression of ACC and FAS but not SCD1 by betulin.

HepG2 cells were incubated in fructose media in the presence or absence of betulin (10µM) for 24 hours. Cell homogenates were immunoblotted for evidence of ACC (A), FAS (B) and SCD1 (C). Cell triglyceride (TG) content (D) was determined following 24 hours incubation. Data are mean ± SE of 3-4 replicates. * $p <0.05$, ** $p <0.01$ for control group, ## $p<0.01$ for fructose group.

5.3.3 Betulin treatment did not moderate ER stress

Protein overloaded or excess lipid accumulation has been suggested to trigger ER stress in some cultured cell types [189]. High fructose promoted lipogenesis, leading to an augment of expression of lipogenic enzymes. Meanwhile, exacerbated ER stress was detected as shown by the significant elevation of p-IRE1 (1.8-fold increasing) and p-eIF2α (2-fold) (Figure 5.3 A, B). In the presence of betulin, in contrast, neither p-IRE1 nor p-eIF2α was affected (Figure 5.3 A, B).
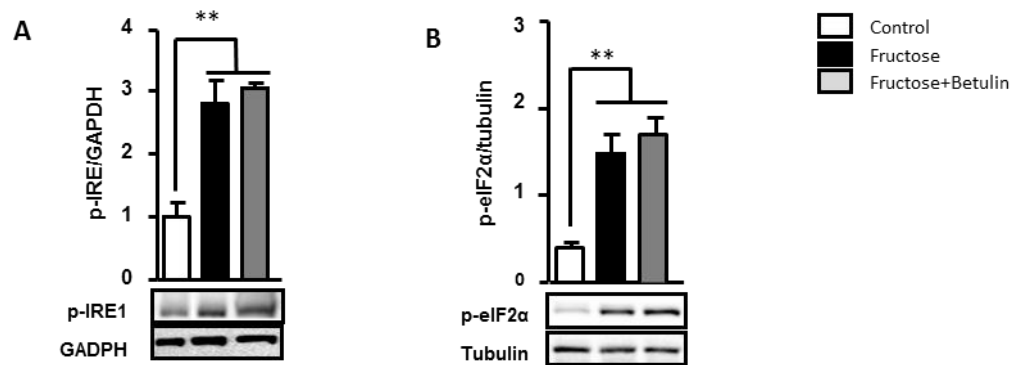
Figure 5.3 Betulin did not have negative effects on p-IRE1 or p-eIF2α.

HepG2 cells were incubated in 25mM glucose DEME with 25mM fructose in the presence or absence of betulin (10μM) for 24 hours. Cell homogenates were immunoblotted for evidence of p-IRE1 (A) and p-eIF2α (B). Data are mean $\pm$ SE of 3-4 replicates. * p <0.05, ** p <0.01; of compared group.

5.4 Discussion

The relationship between ER stress/UPR and lipid accumulation has previously been considered as bidirectional in different models [160, 172, 173] [186, 187]. In the current study, ER stress was induced by fructose rather than fatty acid (palmitate), or other pharmacological inducers such as tunicamycin or thapsigargin [170]. This study investigated the interaction between ER stress and DNL under the challenge of high fructose. Our data demonstrated that both ER stress-initiated UPR signaling and DNL were magnified in response to fructose treatment. Different to results that presented in the animal model, both IRE1 and PERK branches were enhanced. The activation of both the signaling arms was accompanied by augment of lipogenesis which was consistent with the result that we found in the animal model. The relationship between activated UPR and lipogenesis was investigated using betulin administration, in an attempt to block lipogenesis. With the presence of betulin, lipogenic enzymes were significantly diminished. However, the magnified phosphorylation of IRE1 and eIF2α induced by high fructose were not altered by betulin, suggesting that increasing lipogenesis did not contribute to the activation of the IRE1 and PERK branches of the UPR under the condition of fructose oversupply.

ER stress can be induced by endogenous factors or pharmacological chemicals. Lipid, especially saturated fatty acid, is considered to be an effective trigger of endogenous factor of chronic ER stress. The link between aberrant lipid metabolism and disturbance of ER function in the liver might be a disruption of calcium homeostasis. Suneng and his colleagues investigated the alterations of both protein and lipid during ER stress in ob/ob mice. SERCA is a group of calcium ATPase which transfers Ca^{2+} from the cell cytosol to the lumen. Their results demonstrated that increased SERCA expression restored calcium homeostasis and caused significant reductions in p-IRE1 and CHOP and a slight suppression of p-eIFf2α in the

obese liver [194]. Romain and his colleagues demonstrated that the acyl chain saturation could stabilize the dimer of IRE1 and PERK which indicated an activated UPR signaling. The change of lipid composition was also able to activate IRE1α and PERK [280].

In this Chapter, the upregulation by fructose of both ACC and FAS was quite modest compared with the results from *in vivo* study. Consistently, the TG level did not increase significantly by fructose treatment. Nevertheless, the impact of betulin on ACC and FAS was significant compared with fructose treatment and the levels of ACC and FAS under betulin treatment were even lower than the control. These results suggested that betulin administration downregulate the DNL in HepG2 cells and this negative effect may not be specific to fructose administration. The fold change of p-IRE1 was comparable to that seen with HFru feeding in mice (3.3.3). In addition, we observed that p-eIF2α which belongs to PERK branch of the UPR was also enhanced by fructose. Different to previous literature reports, ER stress was not improved when the lipid synthesize was suppressed by betulin in context of high fructose treatment. These results are different from the previous animal study (Chapter Chapter 3). This could because the period of betulin treatment was not long enough or the dosage was not high enough as there is little literature about betulin on ER stress. Further optimization is required. However, these data showed that ER stress would not be affected by the change of DNL under certain condition. Moreover, ER stress can be induced by fructose in 24 hours while DNL was unaltered in HepG2 cells. This result is supported by our current report [250] which showed the ER stress and DNL in the liver occurred sequentially in HFru-fed mice. To summary, hepatic ER stress could occur prior to DNL under HFru administration although it might be regulated by DNL afterwards.

Chapter 6

High Fat Diet-induced

Insulin Resistance

6.1 Introduction

High fat (HFat)-feeding animal is a classic model in the research of insulin resistance and type 2 diabetes. It was originally introduced by Surwit et al. in 1988 [281]. HFat-fed mice showed insulin resistance and glucose intolerance with the presence of hyperglycemia and hyperinsulinemia [282, 283] which are typical characters of type 2 diabetes in human. Besides of the induction of insulin resistance and diabetes, HFat diet also promotes lipid accumulation that related to obesity and fatty liver disease. Different from the dietary fructose, dietary fat contributes to the triglyceride directly. However, the mechanism is different (Figure 6.1). The pathway of dietary fat to triglyceride bypasses the synthesis of saturated of FA which is a process defined as *de novo* lipogenesis (DNL). Critical proteins in DNL such as ACC, FAS and SCD1 [284-286] could not be stimulated in high fat (HFat)-fed mice as in HFru-fed mice [193].

Despite excess lipid accumulation, ER stress has been suggested to be another critical factor to induce insulin resistance [155]. The impact of ER stress on hepatic insulin resistance has been discussed has been discussed in Chapter Chapter 3 and Chapter Chapter 4. Nevertheless, it is not clear whether the effect of ER stress on blunted insulin signaling transduction is specifically related to HFru diet. To address this question, HFat-fed mice are used as a comparison of HFru-fed mice. We hypothesized that ER stress-related impairment of insulin signaling transduction in the liver is specific to the HFru diet.

The HFat diet is known to cause hepatic steatosis by increased extrahepatic lipid supply as well as insulin resistance [235, 287]. In current study, HFat-fed mice for either one day or 2 weeks displayed hepatic steatosis and blunted insulin resistance as HFru-fed mice. However,

ER stress was not detected in the HFat-fed mice. These results indicated that ER stress-induced hepatic insulin resistance is closely related to fructose overconsumption at early stage.
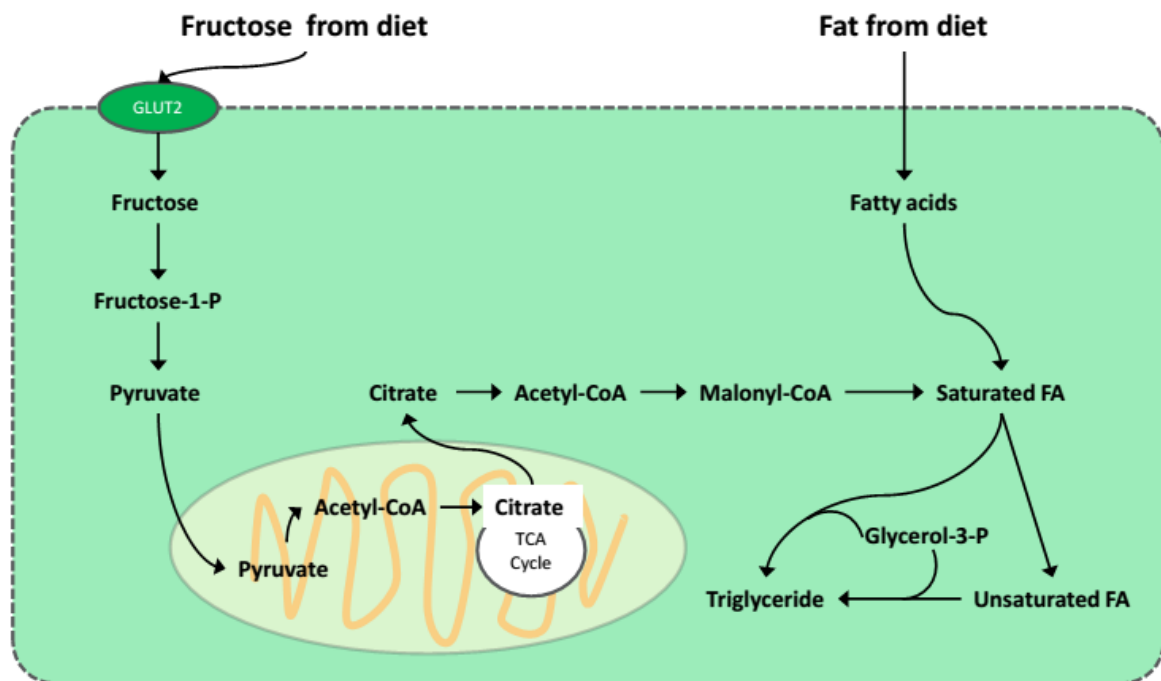
Figure 6.1 Triglyceride synthesis from different nutrition.

Fructose enters cells through GLUT2 and is further phosphorylated to Fructose-1-P. Fructose-1-P is converted to pyruvate which then enters mitochondria and is catalyzed to citrate in TCA cycle. Once citrate is exported into the cytoplasma, it is converted to saturated fatty acid (FA) by stages. The saturated FA with glycerol-3-P can be synthesized to triglyceride. Saturated FA could be catalyzed to unsaturated FA which can be also synthesized to triglyceride with the presence of glycerol-3-P. Fat from the diet enters the cells as fatty acids. The fatty acids are processed into saturated FA to form triglyceride.

6.2 Methods

6.2.1 Animal study

Male C57BL/6J mice (12 weeks old) from the Animal Resources Centre (Perth, Australia) were kept at 22 ± 1 °C on a 12h light/dark cycle. After 2 weeks of acclimatization, mice were fed for either one day or 2 weeks with either normal chow diet (70% calories from starch, ~10% calories from fat, and ~20% calories from protein; Gordon's Specialty Stock Feeds, Yanderra, Australia) or high fat (HFat) diet as described in our previous studies [193]. HFat diet was provided to the mice from 6pm to 2pm (20 hrs) on the following day when they were sacrificed. All experiments were approved by the Animal Ethics Committee of RMIT University.

Body weight and food intake were measured before and after experiments. After one day of feeding, the mice were fasted for four hours before the collection of plasma samples for the measurement of insulin levels by radioimmunoassay (Linco/Milipore, Billerica, MA) [232, 238, 248] and glucose levels using a glucometer (AccuCheck II; Roche, Australia). Tissues of interest were collected and freeze-clamp immediately for subsequent analyses. Glucose tolerance test (GTT; 2g kg^{-1} BW, *i.p.*) was conducted in a separate group of mice following a four hours fasting and blood glucose levels were measured at 0, 15, 30, 60 and 90 minutes using a glucometer (AccuCheck II; Roche, Australia). The area under curve (AUC) was calculated to estimate glucose intolerance. For the assessment of insulin signaling in the liver, 5-7 hour-fasted mice were injected with insulin (2U kg^{-1} BW, *i.p.*) 20 min prior to tissue collection [193, 232].

6.2.2 Measurement of triglyceride levels

The details were described in 2.1.4.2.

6.2.3 Western blotting

The details were described in 2.3.

6.2.4 Gene expression

Isolation of RNA from animal tissues

Mice liver tissues (20~30mg) were homogenized in 1 ml TRIZOL® reagent (Invitrogen, Catalog No.15596026) with a power homogenizer. 200 μl of Chloroform (VWR, Catalog No.22711324) was added to each homogenate and the mixture was capped securely and vigorously hand inverted for 15 seconds followed by incubation at room temperature for 5 mins. The homogenates were subsequently centrifuged at 13,000x rpm for 15 mins at 4℃. The mixture was separated into a lower red, phenol chloroform phase containing protein, an interphase containing DNA, and a colourless upper aqueous phase containing RNA. Only the RNA-containing upper aqueous phase was transferred to a set of fresh micro-centrifuge tubes, and mixed with 500 μl of isopropanol (Sigma-Aldrich, Catalog No.I9516) before another centrifuge at 13,000x rpm for 20 mins at 4℃. The RNA precipitate formed a gel-like pellet on the bottom side of the tube after centrifugation. The supernatant was removed and the pellet was washed twice with 500 μl 75% ethanol (Merck, Catalog No.1.07017.2511). The sample was then mixed by vortexing and centrifuged at 13,000x rpm for 5 mins at 4℃. The supernatant (ethanol) was removed and the RNA pellet was air dried. At the end of the

procedure, the pellet was dissolved in 100 μl Ambion® DEPC-treated water (Invitrogen, Catalog No.AM9916) for RNA concentration determination.

Measurement of RNA concentration

RNA concentration was quantified by using a NanoDrop Spectrophotometer (Eppendorf Thermo Scientific, Australia) at an absorbance of 260/280 nm (A260/280). The NanoDrop Spectrophotometer was initialized by 1.0 μl of DEPC water, which was also used as a blank. Each RNA sample (1.0 μl) was loaded onto the sampling platform for the measurement of RNA concentration.

Complimentary DNA synthesis by reverse transcription

Purified RNA with known concentrations was used to generate the complementary DNA (cDNA) using a Reverse Transcription System (Bio-Rad Laboratories Inc., USA) with random primers according to manufacturer's instructions. RNA in each of samples was diluted to the same final concentration (1 μg/8 μl) by using DEPC water in a sterile 1.5 ml eppendorf tube on ice. To remove the original DNA in each sample, RNA and primer master mix was prepared (1 μg of RNA templates, 1 μl Dnase I reaction buffer and 1 μl Dnase I amplification grade) (Invitrogen, Catalog No.11904-018) in a sterile 1.5 ml eppendorf tube and incubated at room temperature for 15 mins. 1 μl of 25 mM EDTA was then added and incubated for 10 mins at 65℃. RNA (2 μl from the above sample mix) and a reverse transcription master mix (1x reverse transcription buffer, 2x dNTP mix, 1x random primers, 1 μl reverse transcriptase (Invitrogen, Catalog No.18064-014), DEPC water to a final volume of 18 μl and they were added to each reaction tube to give a final reaction volume of 20 μl. The tubes were then placed in a controlled-temperature heat block and first equilibrated at 25℃

for 10 mins, then 37 ℃ for 2 hours, then 85 ℃ for 5 seconds and finally maintained at 4 ℃. The cDNA products from reverse transcription reactions were stored at 4 ℃ to use for real time-PCR analysis.

Real-time polymerase chain reaction

The cDNA samples were analysed for genes of interest by real-time polymerase chain reaction (rt-PCR) using the SYBR Green real-time PCR system (Bio-Rad Laboratories Inc., USA). A reaction master mixture (1x IQ SYBR Green Supermix (Bio-Rad Laboratories Inc., USA; Catalog No.170-8882), 500 nM primers forward and 500 nM reverse primers, DEPC water to a final volume of 24 µl) for each gene of interest was prepared and added to each 1 µl cDNA samples in a sterile 96-well plate. The plate was placed in a controlled-temperature heat block equilibrated at 50 ℃ for 2 mins, 95 ℃ for 3 mins and 40~50 cycles of 95 ℃ for 15 seconds, 72 ℃ for 30 seconds. The gene expression from each sample was analysed in duplicates and normalised against the ribosomal housekeeper gene 18S (GeneWorks, Australia). All reactions were performed on the iQ^{TM} 5 Real-time PCR Detection System (Bio-Rad Laboratories Inc., USA). The results are expressed as relative gene expression using the ΔCt method. Primers used for specific genes are listed in **Table 14**.

Table 14 Primer sequences for measurements of gene expressions in mice

Gene		Primer sequences
18S	Forwrad:	5'-CGCCGCTAGAGGTGAAATTCT
	Reversed:	5'-CGAACCTCCGACTTTCGTTCT
SREBP1c	Forwrad:	5'-AACGTCACTTCCAGCTAGAC
	Reversed:	5'-CCACTAAGGTGCCTACAGAGC
ACC	Forwrad:	5'-AGGAGATCCGCAGCTTG
	Reversed:	5'-ACCTCTGCTCGCTGAGTGC

Gene	Primer sequences	
FAS	Forwrad:	5'- TGCTCCCGACTGCAGGC
	Reversed:	5'- GCCCGGTAGCTCTGGGTGTA
SCD1	Forwrad:	5'-CCTCCGGAAATCAACGAGAG
	Reversed:	5'-CAGGACGGATGTCTTCTTCCA

6.2.5   Statistical Analyses

Data are presented as means $\pm$ SE. One-way analysis of variance was used for comparison of relevant groups. When significant variations were found, the Turkey-Kramer multiple comparisons test was applied. Differences at $p<0.05$ were considered to be statistically significant.

6.3   Results

6.3.1   HFat diet did not induce DNL in the liver

Mice were fed a HFat diet for one day or 2 weeks. Bodyweight did not result in any significant differences between HFat-fed and CH-fed mice after one day. The HFat-fed mice gained significant bodyweight compared with CH-fed mice after 2 weeks (Table 15). However, there was no significant different in of caloric intake between groups (Table 15). The mature form of the transcription factor SREBP1c was significantly elevated (Figure 6.2 A). However, the downstream targets of SREBP1c, known as tACC, FAS and SCD1 (Figure 6.2 B-D, K) were not upregulated compared to control except SCD1. Triglyceride (TG) levels in the liver were also examined. As expected, hepatic TG was significantly increased after a one day HFat feeding (Figure 6.2 I). To further investigate the effect of HFat diet on hepatic DNL, mice were fed with HFat diet for 2 weeks. The mature form of SREBP1c presented an

increasing trend in HFat-fed mice but it was not significant (Figure 6.2 E). The expression of tACC (Figure 6.2 F) and FAS (Figure 6.2 G) did not show an upregulation in HFat-fed mice. In addition, SCD1 (Figure 6.2 H) displayed a significant reduction compared with CH-fed mice. These results suggested that HFat diet was incapable to stimulate the DNL in the liver by. However, the TG content in the liver was elevated significantly (Figure 6.2 J). This could because of the fatty acid influx from the diet.

Table 15 Basal metabolic parameters of HFat-fed mice.

	CH	HFat (1 day)	HFat (2 weeks)
Body mass (g)			
Day 0	27.0±0.3	26.9 ±0.4	27.1±0.3
Day 1	27.1 ±0.4	27.1 ±0.4	ND
Day 14	28.0±0.4	ND	30.0±0.5*
Caloric intake	12.6 ±1.9	18.0 ± 1.4*	17.1±0.5*
EPI fat mass (% BW)	1.3±0.1	ND	3.3±0.3*
Blood glucose (mM)	8.8±0.4	9.2 ±0.5*	11.8±0.5**#
Plasma insulin (pg/ml)	203±23	313±64*	371±76**#

Male C57BL/6J male mice were fed either a CH or fat-rich diet (HFru) for either one day or 2 weeks. Data are means ±SE of 8-10 mice per group. * $p<0.05$, ** $p<0.01$ vs CH-fed mice; # $p<0.05$, ## $p<0.001$ vs HFat (one day feeding).
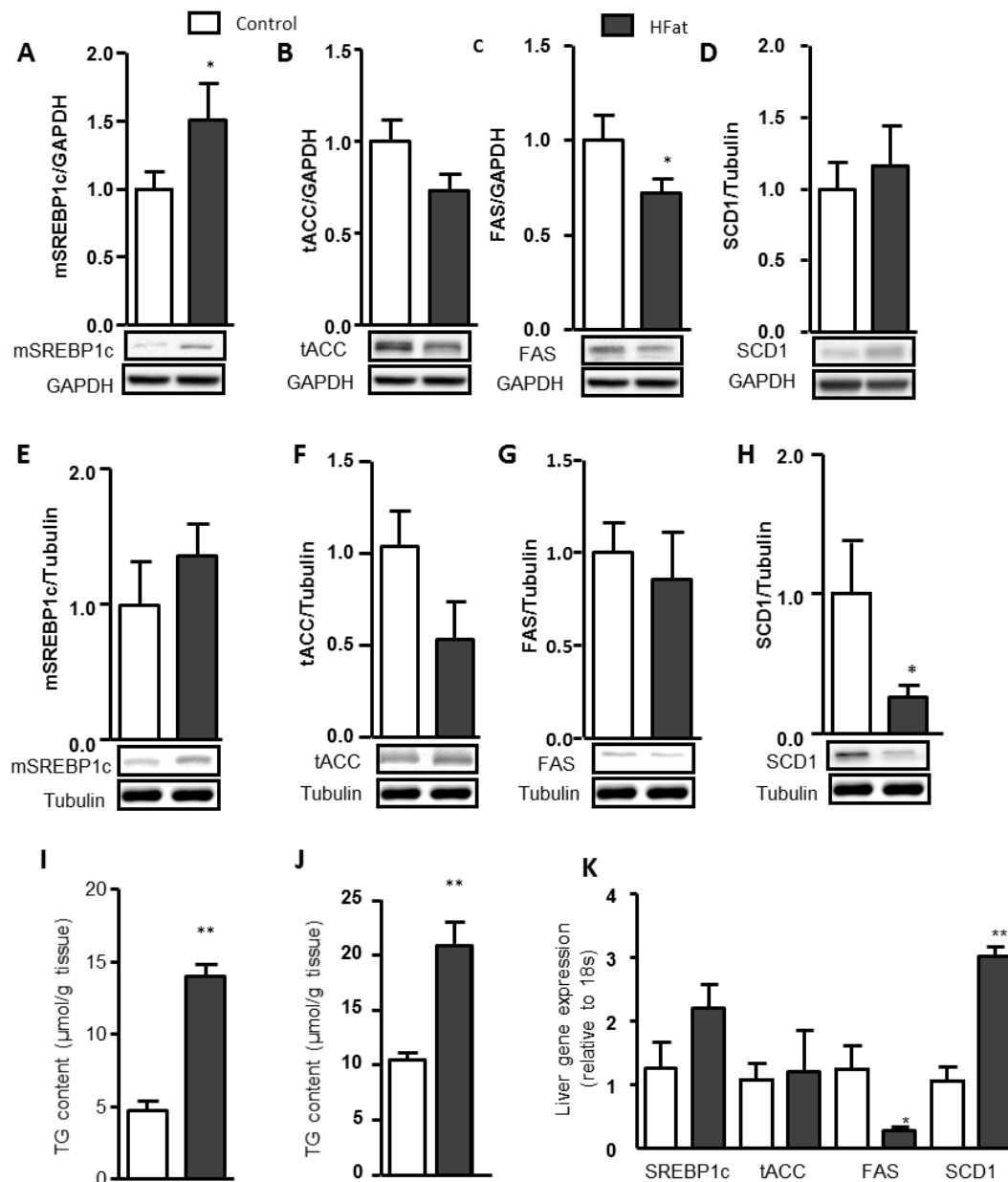
Figure 6.2 HFat diet did not induce DNL in the liver.

Liver homogenate were extracted for the assessment of the DNL: mSREBP1c (A), tACC (B), FAS(C) and SCD1 (D) were determined by immunoblotting was determined and lipogenic gene expression following 4 hours of fasting from animals fed with HFat diet for one day. mSREBP1c (E), tACC (F), FAS(G) and SCD1(H) were determined by immunoblotting was determined following 4 hours of fasting from animals fed with HFat diet for 2 weeks. Tissue TG content (I) from animals fed with HFat diet for one day and (J) from animals fed with HFat diet for 2 weeks was determined. Data are mean $\pm$ SE of 8 mice per group. * $p < 0.05$, ** $p < 0.01$; compared with control.

6.3.2 HFat diet was not able to induce ER stress in the liver

Lipid overload is thought to stimulate ER stress [186, 187]. Hence, we examined whether ER stress was activated in HFat-fed mice. Mice were first fed HFat for one day. In contrast to feeding a HFru diet, HFat diet did not upregulate the IRE branch of the ER stress as suggested by the unaltered levels of p-IRE1 and XBP1 (Figure 6.3 A). Similarly, JNK was not activated as revealed by the unaltered p-JNK and t-JNK (Figure 6.3 C). Interestingly, the phosphorylation of eIF2α which belongs to the PERK arm of the ER stress response, showed a significant increase in HFat-fed mice (~0.5 fold change, $p<0.05$) (Figure 6.3 B). However CHOP, also involved in the PERK pathway, did not increase significantly (Figure 6.3 B). When the feeding duration of HFat diet was extended to 2 weeks, a significant increase in spliced XBP1 was detected without changin p-IRE1 (Figure 6.3 D). However, JNK was again not activated (Figure 6.3 F). In addition, PERK branch of ER stress was not activated, as indicated by the lack of change in both p-PERK and p-eIF2α (Figure 6.3 E).
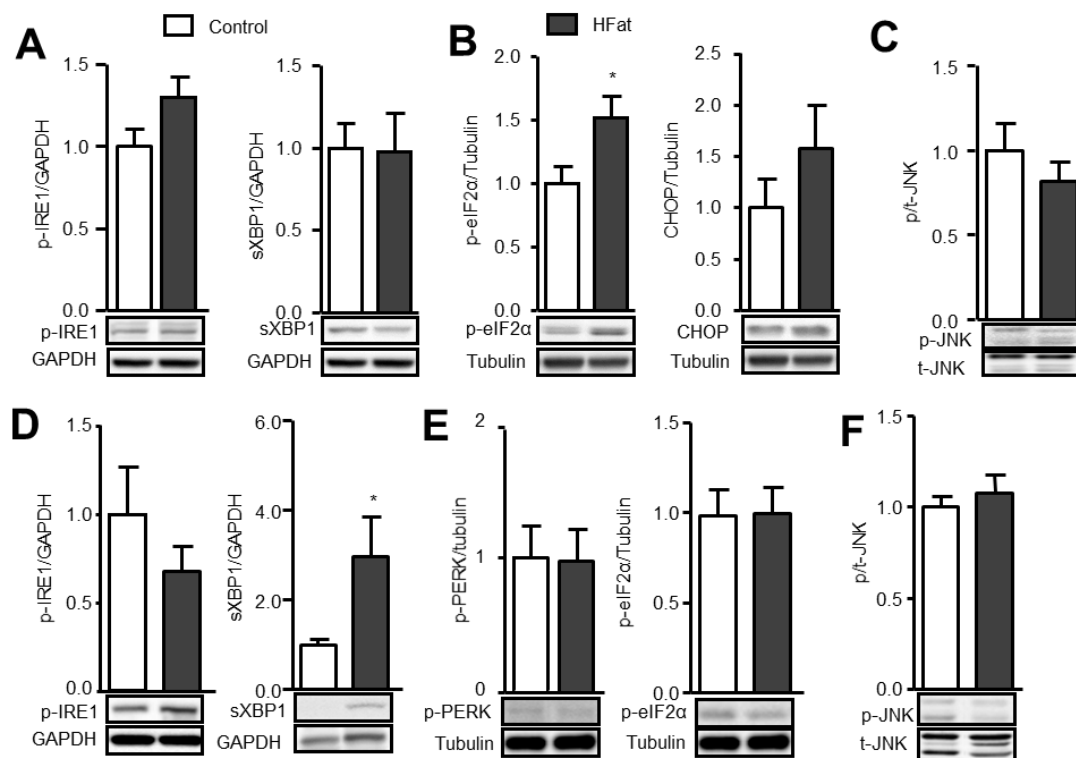
Figure 6.3 HFat diet did not activate UPR in the liver.

Liver homogenate were extracted for the assessment of the activation of UPR signaling pathways. Phosphorylated-IRE1, spliced XBP1 (A), p-eIF2α, CHOP (B) and p-/t-JNK (C) were determined by immunoblotting from animals fed with HFat diet for one day. Phosphorylated-IRE1, spliced XBP1 (D), p-eIF2α, CHOP (E) and p-/t-JNK (F) were determined by immunoblotting from animals fed with HFat diet for 2 weeks. Data are mean ± SE of 8 mice per group. * $p < 0.05$, ** $p < 0.01$; compared with control.

6.3.3 HFat diet blunted insulin signaling transduction in the liver.

Excess lipid accumulation is well known to induce insulin resistance [83, 135, 136]. In HFat-fed animals, blood glucose levels were elevated even after one day feeding and it was further upregulated after 2 weeks of high fat (Table 15). HFat-fed mice also exhibited hyperinsulinemia from one day to 2 weeks feeding (Table 15). In accordance with this, impaired insulin actions, as indicated by the reduced p-Akt response to acute insulin stimulation, was detected in the liver. After one day feeding of HFat, p-Akt in response to insulin stimulation was significantly downregulated (by 50%) compared to the appropriate control (Figure 6.4 A). In addition to the blunted hepatic insulin signaling transduction, mice were glucose intolerant, as indicated by the significant increasing incremental area under curve (iAUC) from the GTT (Figure 6.4 C). The levels of p-Akt in HFat-fed mice for 2 weeks showed further reduction (by 67%). The iAUC from GTT (Figure 6.4 C) consistently showed greater change. These data indicating more severe impaired insulin action in the liver (Figure 6.4 B). As expected, mice developed glucose intolerance as demonstrated by the augmented iAUC (Figure 6.4 D).
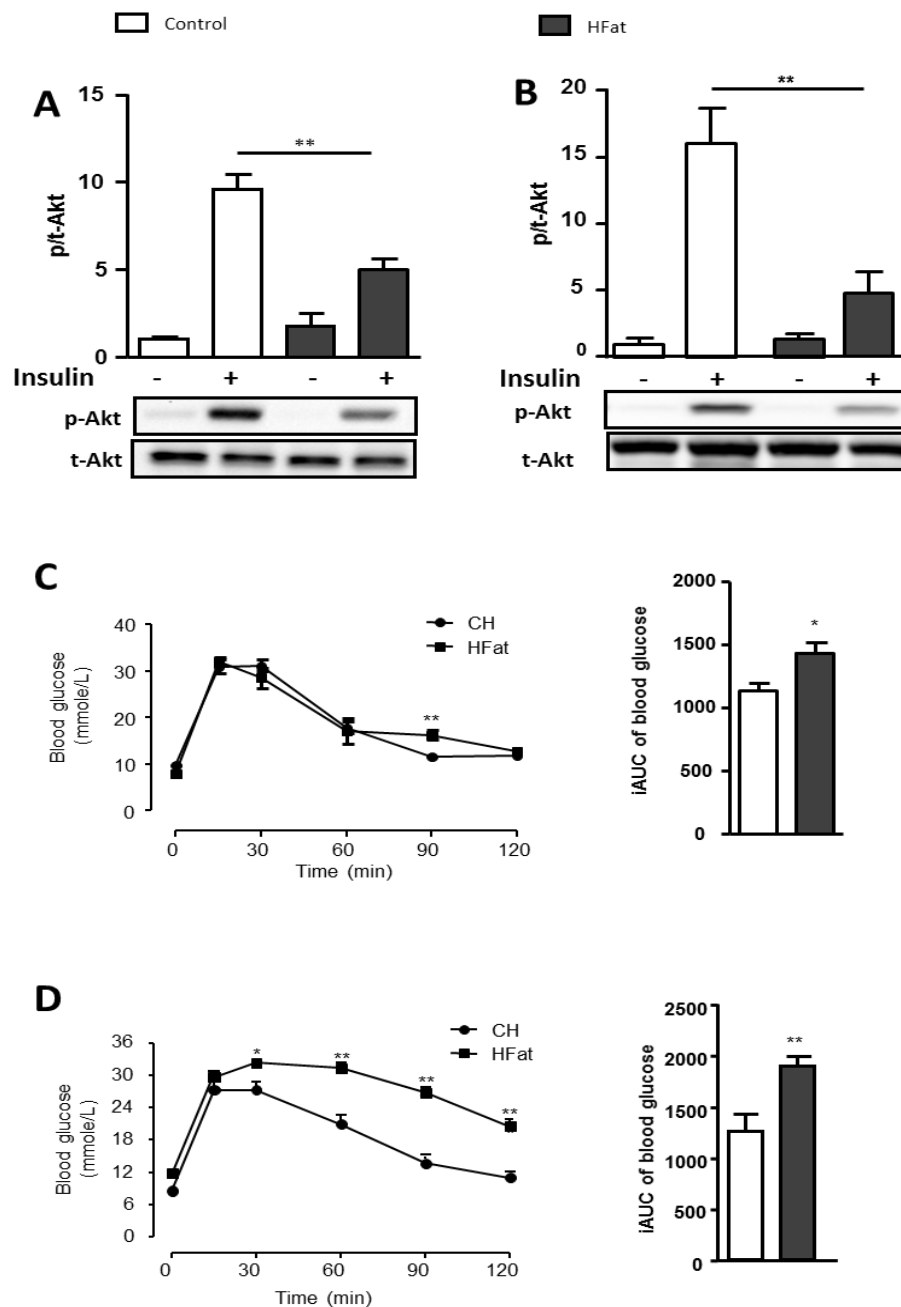
Figure 6.4 Impaired hepatic insulin action in response to HFat feeding.

Insulin signal transduction was assessed by immunoblotting of key transducer: phosphorylated-Akt (serine 473) and total-Akt in whole cell lysate of liver in HFat-fed mice for one day (A) and 2 weeks (B). Representative western blots are shown. Glucose tolerance test (GTT) was performed with an injection of glucose (2.5 g/kg, *ip*) after 5-7 hours of fasting. GTT curve and iAUC, incremental area under the curve for blood glucose level from HFat-fed mice for either one day (C) or 2 weeks (D). Data are mean $\pm$ SE of 8 mice per group. * *p* <0.05, ** *p* <0.01; compared with control.

6.4   Discussion

Hepatic insulin resistance can be triggered via different mechanisms [130] [131, 132] [157-160]. HFru-related ER stress has been demonstrated to contribute to this disorder in previous chapters. However, mice fed with a HFat diet displayed insulin resistance and glucose intolerance after one day without the activation of ER stress. This observation suggests that there may be other factors to trigger hepatic insulin resistance in HFat-fed mice at early stage.

In this chapter, mice were fed a HFat diet for either one day or 2 weeks. As expected, hepatic triglyceride content showed significantly elevated on both one day and 2 weeks feeding. However, DNL was not upregulated, in contrast to the response to a HFru diet. After one day feeding with HFat diet, both tACC (p=0.06) and FAS (p<0.05) tend to be reduced without a significant change in SCD1. When the feeding duration lasted for 2 weeks, SCD1 was significantly suppressed by HFru, while tACC and FAS showed a decreasing trend. These results are consistent with our previous studies [193] and further confirms that exogenous supply of FAs in the HFat diet impair DNL [288]. Intriguingly, the mature form of SREBP1c was not downregulated, unlike its downstream targets (e.g. ACC and FAS). This may be due to the activation of SREBP1c being dependent on proteolytic cleavage [289] and, that this process is affected by fatty acids [290]. In addition, SREBP1c is suggested to respond to insulin [60], and may thus enhanced by the high plasma insulin levels associated with HFat-fed mice.

Lipid-related ER stress has been discussed in previous chapters (1.6.2). The HFat-fed mice exhibited significant increase of triglyceride in the liver. However, the IRE1 branch of the UPR did not show any activation, as indicated by unaltered p-IRE1 and sXBP1. Moreover, p-JNK did not exhibit activation. Phosphorylated-eIF2α, a downstream protein of PERK, was

significantly increased in HFat-fed mice, but by only about 50%. In addition, CHOP, another downstream protein in the PERK branch did not exhibit a significant difference between chow and HFat fed mice. Despite a remarkable increase in sXBP1, p-IRE1, p-eIF2α or CHOP was not upregulated in response to a HFat-fed mice. These data suggested that HFat diet was unable to completely induce ER stress in the liver after 2 weeks. However, some studies have previously demonstrated that HFat-induced obesity induced by long-term HFat feeding is closely related to ER stress. ER stress is detected in the liver of obese humans and is reduced after weight loss [291]. Similarly, mice that fed a HFat diet for 16 weeks developed hepatic ER stress, indicated by increased p-PERK and p-eIF2α [125]. This maybe because the lipid accumulation in our model was not enough to trigger ER stress. However, it has been reported that animals fed for HFat diet for 3 days can develop insulin resistance in the liver [45, 254]. These results indicated that there are other factors rather than ER stress to initiate insulin resistance in HFat-fed mice model.

This study also excluded the possibility that the activation of IRE1 branch in HFru-fed mice was due to the hyperinsulinemia. IRE1 and XBP1 are suggested to be able to upregulate by insulin [158]. However, both HFat- and HFru-fed mice displayed hyperinsulinemia while only HFru-fed mice showed upregulated ER stress.

Chapter 7

General Discussion

and Future Directions

This chapter will summarise the major findings of the studies that have been performed in this thesis, and reach the overall conclusions from these findings. I will also discuss the limitations of the studies in this thesis and propose future studies to address remaining issues.

7.1   Major findings

Type 2 diabetes is one of the most prevalent chronic diseases worldwide, of which insulin resistance is a key metabolic defect [2, 38, 39]. Many studies have suggested the link of excess lipid accumulation, stress and insulin resistance, and have investigated the potential mechanisms responsible for lipid or stress contributing to insulin resistance [244]. However, the exact pathways of the development of insulin resistance are not fully understood. Understanding the molecular mechanisms leading to insulin resistance is required, for the improved development of therapeutic treatments for type 2 diabetes. This thesis focused on the suggested role of ER stress and lipid accumulation on hepatic insulin resistance.

As described in 1.5 and 1.6, the relationship between ER stress, lipid accumulation and insulin resistance are complicated because the effects that these factors have on each other. In this thesis, acute and 2 weeks HFru-feeding models were developed to explore the mechanisms underlying the pathogenesis of this disorder. As well as the capability of high fat diet to induce insulin resistance [282], fructose over-consumption has been proposed to be another potential trigger of impaired insulin action [225]. Therefore, both HFru and HFat diets were applied to mice in this project.

In acute feeding with either HFru or HFat diet, mice showed impaired insulin signaling transduction in the liver. In addition, HFat-fed mice were glucose intolerant, while HFru-fed mice showed normal glucose tolerance, indicating different metabolic mechanisms between

mice fed the different diets. HFru-, but not HFat-fed, mice displayed ER stress. The subsequent studies focused on the HFru diet, which could upregulate ER stress and insulin resistance simultaneously. When I investigated the insulin activated signaling pathways, namely phosphorylated IRS1 and Akt, the results showed blunted signaling only in the liver, but not in peripheral skeletal muscle or adipose tissue, indicating that liver is the first site to develop insulin resistance during HFru feeding. These results are consistent with studies in rodents in which HFat-induced whole-body insulin resistance is initiated by impaired hepatic insulin action, and aggravated by skeletal muscle insulin resistance [45, 254]. All these studies indicated that the liver plays a critical role in the initial development of insulin resistance and thus we focused on studying hepatic metabolism.

In addition to the activation of ER stress/UPR, hepatic DNL, which may then lead to lipid accumulation from carbohydrate, was rapidly initiated. I hypothesised that the activation of IRE1 was associated with both upregulated DNL and impaired insulin action. ER stress is suggested to induce hepatic insulin resistance by increasing DNL [180] and directly interfering with insulin signaling via the activation of JNK [158]. The key role for IRE1/JNK in triggering hepatic insulin resistance induced by HFru feeding was supported by the finding that inhibition of IRE1 activation by the chemical chaperone TUDCA was able to block activation of JNK, IRS1 serine phosphorylation and preserve the insulin-stimulated phosphorylation of Akt. The unaltered PKCε activity in HFru-fed mice indicated that the initial hepatic insulin resistance may be independent of DAG accumulation.

In summary, Chapter Chapter 3 showed for the first time that HFru diet is able to induce ER stress in the acute phase, and that the activated ER stress (mainly in the IRE1 branch of this phenomenon) is closely related to the development of insulin resistance in the liver. Prior to

this study, ER stress was suggested not to be a direct causal factor in hepatic insulin resistance [162]. In this study, we observed that suppression of ER stress pathways by TUDCA, a chemical chaperone, could improve impaired insulin action in the liver, while there was no change on other insulin resistance associated pathways, such as PKCε activation and lipid accumulation. Interestingly, we demonstrated that IRE1/XBP1 was the first UPR pathways activated arm n response to HFru diet, while the PERK arm was significantly induced only after 3 days HFru-feeding. These results indicated that IRE1 branch is more closely associated with initial hepatic insulin resistance rather than PERK branch.

The mechanism by which fructose induces ER stress is not yet clear. The possibility that the hyperinsulinemia induced by HFru diet could upregulates IRE1 and XBP1 is unlikely, as HFat-fed mice did not have ER stress, but remained hyperinsulinemic. The possible pathways involved in HFru-induced insulin resistance may be related to the mTOR [292] signaling and activation of autophagy [293, 294].

This thesis also used a longer term feeding model of HFru-diet induced insulin resistance to mimic the pathological condition in humans. In addition to the suppression of insulin signaling pathways in the liver, glucose intolerance indicated by significantly reduced iAUC was also detected. Moreover, HFru-fed mice displayed significantly higher fasting blood glucose levels. All the data indicated that mice that were fed with HFru for an extended period developed a more severely impaired insulin action. As expected, hepatic ER stress and DNL were both enhanced by HFru-feeding. JNK phosphorylation was unaltered in response to IRE1 activation challenging the role of JNK in mediating insulin resistance. This led us to explore other possibilities. I examined hepatic DAG and ceramide levels which are known

triggers of insulin resistance. The data showed that DAG levels significantly increased, while ceramide displayed the opposite trend in HFru-fed mice.

These results indicated that DAG may play a pivotal role for insulin resistance, rather than ER stress, in this HFru-feeding model. To further confirm this hypothesis, fenofibrate (FB) was administrated to downregulate lipid synthesize and determine its impact on insulin action. As expected, we found a significant reduction in DAG levels as well as TG content in the liver. Blunted insulin signaling was restored, and glucose tolerance was improved with FB treatment. Interestingly, ER stress was remarkably elevated in response to FB. Both IRE1/XBP1 and PERK/eIF2α arms signaling activated. These findings suggest that lipid accumulation (mainly DAGs), rather than the activation of JNK or IKK, is pivotal for ER stress to trigger hepatic chronic insulin resistance. Therefore, by reducing the accumulation of deleterious lipids, hepatic insulin resistance can be ameliorated against increased ER stress.

JNK and IKK, which are able to interfere with IRS can be activated by different pathways in the context of insulin resistance, not limited to ER stress [155, 295]. In the acute model, JNK activation was diminished when IRE1 phosphorylation was reduced in HFru-fed mice with TUDCA treatment, suggesting that activated JNK was associated with the upregulation of IRE1. However, the mechanism of the loss of JNK activation in HFru-fed mice in this model is not yet clear. In addition, JNK remained unaltered when IRE1 was markedly increased by FB treatment. This latter response might be due to FB itself suppressing JNK phosphorylation [296].

In the HFru study, DAG levels exhibited trend to increase following longer period of feeding. This change of DAG became a major contributor of hepatic insulin resistance, surpassing the negative regulation of IRE1-JNK pathways. This explanation is supported by a study in which

mice lacking XBP1 (IRE1 substrate) fed a fructose diet for 1 week exhibited increased hepatic insulin sensitivity during clamp despite the activation of hepatic ER stress markers and of JNK [162].

Since ER stress and DNL both play an important role in the development of insulin resistance in the liver, I investigated the relationship between ER stress and DNL in a cultured cell model. Fructose, rather than common inducers of ER stress (tunicamycin or thapsigargin), was used to induce ER stress to maintain a consistency with HFru feeding showed *in vivo*. Similar to what found *in vivo*, both ER stress and DNL were induced in response to fructose administration *in vitro*. Betulin was added to suppress DNL by inhibiting the cleavage of the lipogenic transcription factor SREBP1c. These results showed that the suppression of lipogenesis did not affect the activation of ER stress by fructose, indicating that the induction of ER stress could be independent of excess lipid content.

SUMMARY & CONCLUSIONS

Based on the results obtained from this thesis, a number of conclusions can be drawn as follows:

In the context of HFru-feeding, hepatic insulin resistance could result from ER stress and/or excess lipid accumulation in the liver. The underlying mechanisms are different over time. In acute conditions (one day), HFru diet stimulated ER stress and upregulated DNL in the liver. Increased ER stress was suggested from IRE1/XBP1 activity. Consequently, JNK was induced, which then interfered with IRS function, to block insulin signaling pathways. However, the IRE1-mediated activation of JNK, rather than lipid accumulation, appears to

play a more critical role at the onset of hepatic insulin resistance induced by HFru feeding (as indicated by results obtained from the very short term study).

HFru diet induced XBP1 activation promoted DNL, which then led to hepatic lipid accumulation and impaired insulin action. As the feeding period extended from one day to 2 weeks, the negative effect of lipid accumulation in the liver through the induction of DNL became more severe. The accumulation of lipid metabolites (such as DAGs) attenuated normal insulin signal transduction leading to hepatic insulin resistance, resulting in a reduction in glucose tolerance. Meanwhile, the lack of activation of JNK suggested that JNK function was not required for ER stress-related hepatic insulin resistance in long term HFru-feeding. Intriguingly, PPARα activation induced by FB administration may also directly stimulate DNL, perhaps dependent on signaling from IRE1 and PERK branches. Despite this, the predominant effect triggered by PPARα was to potentiate oxidative capacity and to eliminate lipid accumulation, thus overcoming fructose-induced hepatic insulin resistance (IR) and glucose intolerance.

In summary, the predominantly negative effect of JNK activation induced by IRE1 might be overcome by the persistently increasing lipid accumulation, possibly becomes a secondary inducer of insulin resistance in the long term. The findings from this study here suggest that IRE1 may be a potential target for pharmacological treatment of insulin resistance in the liver induced by high fructose consumption.

7.2   Future directions

PPARα activation is closely related to lipid metabolism which has been suggested to be linked to ER stress. The study in Chapter 4 demonstrated an association between PPARα activation

and ER stress in the liver. The upregulation of ER stress with FB administration was accompanied by elevation in both lipid synthesize and oxidation. However, the role of PPARα in these changes needs more investigation. The preliminary data from this lab suggest that PPARα activation plays an essential role in the FB-induced ER stress and lipogenesis. Further studies will need to examine how PPARα activation induces ER stress in a PPARα knockout mice model.

Studies undertaken in this thesis demonstrate that the ER stress rather than excess lipid plays a dominant role in blunting hepatic insulin signaling pathway in response to HFru consumption. However, excess lipid accumulation following longer period of feeding became more critical to develop hepatic insulin resistance in HFru-fed mice. ER stress appears to be able to drive DNL rather than being induced by excess lipid. In addition, I found that HFat diet with the same feeding period as HFru diet was not able to induce ER stress. All the results indicated that the contribution of ER stress on the initiation of insulin resistance in the liver is nutrition-specific in a given period. Therefore, further studies are warranted to understand the mechanism of how fructose triggers ER stress. Over the past decade, increasing evidence shows that autophagy is closely associated with ER stress in the liver [297, 298]. Genetic ablation of autophagy proteins leads to hepatic ER stress and insulin resistance [299]. More recently, the crosstalk between ER stress and mTOR signaling pathway has been of a great interest in the field [292]. It has been suggested that mTOR interferes with ER stress by regulating protein synthesize in the short term [292, 300]. As mTOR has been shown to be induced by HFru feeding [301] and has been shown to correlate with autophagy, it is reasonable to expect that mTOR and autophagy pathways may be involved in the link between fructose consumption and ER stress. According to the preliminary data from our laboratory, mice could be fed with HFru diet to activate mTOR or autophagy pathways.

Inhibitors of either mTOR or autophagy could be administrated to mice to interfere with these pathways. Their simultaneous impact on of ER stress could aslo be investigated. The outcome of such studies might then provide further insight into mechanisms of dietary fructose in insulin resistance and the metabolic syndrome. The significance of this work not only lies in bridging gaps in our current understanding but also provides a scientific basis for drug design and discovery for the prevention and treatment of type 2 diabetes.

REFERENCES

[1] American Diabetes A. Diagnosis and classification of diabetes mellitus. Diabetes care. 2014;37 Suppl 1:S81-90.

[2] WHO. Diabetes fact sheet. 2013.

[3] (UK) RCoP. Type 2 Diabetes: National Clinical Guideline for Management in Primary and Secondary Care (Update). London2008.

[4] Atkinson MA, Bluestone JA, Eisenbarth GS, Hebrok M, Herold KC, Accili D, et al. How does type 1 diabetes develop?: the notion of homicide or beta-cell suicide revisited. Diabetes. 2011;60:1370-9.

[5] American Diabetes A. Gestational diabetes mellitus. Diabetes care. 2004;27 Suppl 1:S88-90.

[6] Rathmann W, Giani G. Global prevalence of diabetes: estimates for the year 2000 and projections for 2030. Diabetes care. 2004;27:2568-9; author reply 9.

[7] Palermo A, Maggi D, Maurizi AR, Pozzilli P, Buzzetti R. Prevention of type 2 diabetes mellitus: is it feasible? Diabetes/metabolism research and reviews. 2014;30 Suppl 1:4-12.

[8] Adeniyi AF, Adeleye JO, Adeniyi CY. Diabetes, sexual dysfunction and therapeutic exercise: a 20 year review. Current diabetes reviews. 2010;6:201-6.

[9] Cukierman T, Gerstein HC, Williamson JD. Cognitive decline and dementia in diabetes--systematic overview of prospective observational studies. Diabetologia. 2005;48:2460-9.

[10] Nouwen A, Nefs G, Caramlau I, Connock M, Winkley K, Lloyd CE, et al. Prevalence of depression in individuals with impaired glucose metabolism or undiagnosed diabetes: a systematic review and meta-analysis of the European Depression in Diabetes (EDID) Research Consortium. Diabetes care. 2011;34:752-62.

[11] Thorve VS, Kshirsagar AD, Vyawahare NS, Joshi VS, Ingale KG, Mohite RJ. Diabetes-induced erectile dysfunction: epidemiology, pathophysiology and management. Journal of diabetes and its complications. 2011;25:129-36.

[12] Forbes JM, Cooper ME. Mechanisms of diabetic complications. Physiological reviews. 2013;93:137-88.

[13] Crawford TN, Alfaro DV, 3rd, Kerrison JB, Jablon EP. Diabetic retinopathy and angiogenesis. Current diabetes reviews. 2009;5:8-13.

[14] Kdoqi. KDOQI Clinical Practice Guidelines and Clinical Practice Recommendations for Diabetes and Chronic Kidney Disease. American journal of kidney diseases : the official journal of the National Kidney Foundation. 2007;49:S12-154.

[15] Jung CH, Baek AR, Kim KJ, Kim BY, Kim CH, Kang SK, et al. Association between Cardiac Autonomic Neuropathy, Diabetic Retinopathy and Carotid Atherosclerosis in Patients with Type 2 Diabetes. Endocrinology and metabolism. 2013;28:309-19.

[16] Saltiel AR, Kahn CR. Insulin signalling and the regulation of glucose and lipid metabolism. Nature. 2001;414:799-806.

[17] Dimitriadis G, Mitrou P, Lambadiari V, Maratou E, Raptis SA. Insulin effects in muscle and adipose tissue. Diabetes research and clinical practice. 2011;93 Suppl 1:S52-9.

[18] Watson RT, Kanzaki M, Pessin JE. Regulated membrane trafficking of the insulin-responsive glucose transporter 4 in adipocytes. Endocrine reviews. 2004;25:177-204.

[19] Saltiel AR, Pessin JE. Insulin signaling in microdomains of the plasma membrane. Traffic. 2003;4:711-6.

[20] Abu-Amero KK, Kondkar AA, Oystreck DT, Khan AO, Bosley TM. Microdeletions involving Chromosomes 12 and 22 Associated with Syndromic Duane Retraction Syndrome. Ophthalmic genetics. 2014:1-8.

[21] Shepherd PR. Mechanisms regulating phosphoinositide 3-kinase signalling in insulin-sensitive tissues. Acta physiologica Scandinavica. 2005;183:3-12.

[22] Corvera S, Czech MP. Direct targets of phosphoinositide 3-kinase products in membrane traffic and signal transduction. Trends in cell biology. 1998;8:442-6.

[23] Partovian C, Simons M. Regulation of protein kinase B/Akt activity and Ser473 phosphorylation by protein kinase Calpha in endothelial cells. Cellular signalling. 2004;16:951-7.

[24] Bayascas JR, Alessi DR. Regulation of Akt/PKB Ser473 phosphorylation. Molecular cell. 2005;18:143-5.

[25] Lizcano JM, Alessi DR. The insulin signalling pathway. Current biology : CB. 2002;12:R236-8.

[26] Brazil DP, Hemmings BA. Ten years of protein kinase B signalling: a hard Akt to follow. Trends in biochemical sciences. 2001;26:657-64.

[27] Deprez J, Vertommen D, Alessi DR, Hue L, Rider MH. Phosphorylation and activation of heart 6-phosphofructo-2-kinase by protein kinase B and other protein kinases of the insulin signaling cascades. The Journal of biological chemistry. 1997;272:17269-75.

[28] Hajduch E, Litherland GJ, Hundal HS. Protein kinase B (PKB/Akt)--a key regulator of glucose transport? FEBS Lett. 2001;492:199-203.

[29] Bengoechea-Alonso MT, Ericsson J. A phosphorylation cascade controls the degradation of active SREBP1. The Journal of biological chemistry. 2009;284:5885-95.

[30] Laplante M, Sabatini DM. mTOR signaling at a glance. Journal of cell science. 2009;122:3589-94.

[31] Gual P, Le Marchand-Brustel Y, Tanti J. Positive and negative regulation of glucose uptake by hyperosmotic stress. Diabetes & metabolism. 2003;29:566-75.

[32] Morino K, Petersen KF, Shulman GI. Molecular mechanisms of insulin resistance in humans and their potential links with mitochondrial dysfunction. Diabetes. 2006;55 Suppl 2:S9-S15.

[33] Zick Y. Molecular basis of insulin action. Novartis Foundation symposium. 2004;262:36-50; disucssion -5, 265-8.

[34] Zick Y. Ser/Thr phosphorylation of IRS proteins: a molecular basis for insulin resistance. Science's STKE : signal transduction knowledge environment. 2005;2005:pe4.

[35] Paz K, Hemi R, LeRoith D, Karasik A, Elhanany E, Kanety H, et al. A molecular basis for insulin resistance. Elevated serine/threonine phosphorylation of IRS-1 and IRS-2 inhibits their binding to the juxtamembrane region of the insulin receptor and impairs their ability to

undergo insulin-induced tyrosine phosphorylation. The Journal of biological chemistry. 1997;272:29911-8.

[36] Mothe I, Van Obberghen E. Phosphorylation of insulin receptor substrate-1 on multiple serine residues, 612, 632, 662, and 731, modulates insulin action. The Journal of biological chemistry. 1996;271:11222-7.

[37] Moeschel K, Beck A, Weigert C, Lammers R, Kalbacher H, Voelter W, et al. Protein kinase C-zeta-induced phosphorylation of Ser318 in insulin receptor substrate-1 (IRS-1) attenuates the interaction with the insulin receptor and the tyrosine phosphorylation of IRS-1. The Journal of biological chemistry. 2004;279:25157-63.

[38] Eckel RH, Grundy SM, Zimmet PZ. The metabolic syndrome. Lancet. 2005;365:1415-28.

[39] Alberti KG, Zimmet P, Shaw J, Group IDFETFC. The metabolic syndrome--a new worldwide definition. Lancet. 2005;366:1059-62.

[40] Courtney HC OJ-. Insulin Resistance. In: Madame Curie Bioscience Database [Internet]. Austin (TX): Landes Bioscience;; 2000-.

[41] Meigs JB, Rutter MK, Sullivan LM, Fox CS, D'Agostino RB, Sr., Wilson PW. Impact of insulin resistance on risk of type 2 diabetes and cardiovascular disease in people with metabolic syndrome. Diabetes care. 2007;30:1219-25.

[42] Bays H, Mandarino L, DeFronzo RA. Role of the adipocyte, free fatty acids, and ectopic fat in pathogenesis of type 2 diabetes mellitus: peroxisomal proliferator-activated receptor agonists provide a rational therapeutic approach. The Journal of clinical endocrinology and metabolism. 2004;89:463-78.

[43] Erion DM, Shulman GI. Diacylglycerol-mediated insulin resistance. Nature medicine. 2010;16:400-2.

[44] Magnusson I, Rothman DL, Katz LD, Shulman RG, Shulman GI. Increased rate of gluconeogenesis in type II diabetes mellitus. A 13C nuclear magnetic resonance study. The Journal of clinical investigation. 1992;90:1323-7.

[45] Kraegen EW, Clark PW, Jenkins AB, Daley EA, Chisholm DJ, Storlien LH. Development of muscle insulin resistance after liver insulin resistance in high-fat-fed rats. Diabetes. 1991;40:1397-403.

[46] Rask-Madsen C, Kahn CR. Tissue-specific insulin signaling, metabolic syndrome, and cardiovascular disease. Arteriosclerosis, thrombosis, and vascular biology. 2012;32:2052-9.

[47] Sethi JK, Vidal-Puig AJ. Thematic review series: adipocyte biology. Adipose tissue function and plasticity orchestrate nutritional adaptation. Journal of lipid research. 2007;48:1253-62.

[48] Langin D. Adipose tissue lipolysis as a metabolic pathway to define pharmacological strategies against obesity and the metabolic syndrome. Pharmacological research : the official journal of the Italian Pharmacological Society. 2006;53:482-91.

[49] Cohen JC, Horton JD, Hobbs HH. Human fatty liver disease: old questions and new insights. Science. 2011;332:1519-23.

[50] Nagle CA, Klett EL, Coleman RA. Hepatic triacylglycerol accumulation and insulin resistance. Journal of lipid research. 2009;50 Suppl:S74-9.

[51] Collins JM, Neville MJ, Hoppa MB, Frayn KN. De novo lipogenesis and stearoyl-CoA desaturase are coordinately regulated in the human adipocyte and protect against palmitate-induced cell injury. The Journal of biological chemistry. 2010;285:6044-52.

[52] Schutz Y. Concept of fat balance in human obesity revisited with particular reference to de novo lipogenesis. International journal of obesity and related metabolic disorders : journal of the International Association for the Study of Obesity. 2004;28 Suppl 4:S3-S11.

[53] Mashek DG. Hepatic Fatty Acid Trafficking: Multiple Forks in the Road. Advances in nutrition. 2013;4:697-710.

[54] J.E. Vance DEV. Biochemistry of lipids, lipoproteins, and membranes. 4 ed: Elsevier Science; 2002.

[55] Green CD, Ozguden-Akkoc CG, Wang Y, Jump DB, Olson LK. Role of fatty acid elongases in determination of de novo synthesized monounsaturated fatty acid species. Journal of lipid research. 2010;51:1871-7.

[56] Gonzalez-Baro MR, Lewin TM, Coleman RA. Regulation of Triglyceride Metabolism. II. Function of mitochondrial GPAT1 in the regulation of triacylglycerol biosynthesis and insulin action. American journal of physiology Gastrointestinal and liver physiology. 2007;292:G1195-9.

[57] Jeon TI, Osborne TF. SREBPs: metabolic integrators in physiology and metabolism. Trends in endocrinology and metabolism: TEM. 2012;23:65-72.

[58] Dentin R, Pegorier JP, Benhamed F, Foufelle F, Ferre P, Fauveau V, et al. Hepatic glucokinase is required for the synergistic action of ChREBP and SREBP-1c on glycolytic and lipogenic gene expression. The Journal of biological chemistry. 2004;279:20314-26.

[59] Shimomura I, Shimano H, Horton JD, Goldstein JL, Brown MS. Differential expression of exons 1a and 1c in mRNAs for sterol regulatory element binding protein-1 in human and mouse organs and cultured cells. The Journal of clinical investigation. 1997;99:838-45.

[60] Osborne TF. Sterol regulatory element-binding proteins (SREBPs): key regulators of nutritional homeostasis and insulin action. The Journal of biological chemistry. 2000;275:32379-82.

[61] Raghow R, Yellaturu C, Deng X, Park EA, Elam MB. SREBPs: the crossroads of physiological and pathological lipid homeostasis. Trends in endocrinology and metabolism: TEM. 2008;19:65-73.

[62] Chen G, Liang G, Ou J, Goldstein JL, Brown MS. Central role for liver X receptor in insulin-mediated activation of Srebp-1c transcription and stimulation of fatty acid synthesis in liver. Proceedings of the National Academy of Sciences of the United States of America. 2004;101:11245-50.

[63] Ferre P, Foufelle F. Hepatic steatosis: a role for de novo lipogenesis and the transcription factor SREBP-1c. Diabetes Obes Metab. 2010;12 Suppl 2:83-92.

[64] Shimomura I, Bashmakov Y, Ikemoto S, Horton JD, Brown MS, Goldstein JL. Insulin selectively increases SREBP-1c mRNA in the livers of rats with streptozotocin-induced diabetes. Proceedings of the National Academy of Sciences of the United States of America. 1999;96:13656-61.

[65] Fleischmann M, Iynedjian PB. Regulation of sterol regulatory-element binding protein 1 gene expression in liver: role of insulin and protein kinase B/cAkt. The Biochemical journal. 2000;349:13-7.

[66] Repa JJ, Liang G, Ou J, Bashmakov Y, Lobaccaro JM, Shimomura I, et al. Regulation of mouse sterol regulatory element-binding protein-1c gene (SREBP-1c) by oxysterol receptors, LXRalpha and LXRbeta. Genes & development. 2000;14:2819-30.

[67] Schultz JR, Tu H, Luk A, Repa JJ, Medina JC, Li L, et al. Role of LXRs in control of lipogenesis. Genes & development. 2000;14:2831-8.

[68] Liu X, Qiao A, Ke Y, Kong X, Liang J, Wang R, et al. FoxO1 represses LXRalpha-mediated transcriptional activity of SREBP-1c promoter in HepG2 cells. FEBS Lett. 2010;584:4330-4.

[69] Matsuzaka T, Shimano H, Yahagi N, Amemiya-Kudo M, Okazaki H, Tamura Y, et al. Insulin-independent induction of sterol regulatory element-binding protein-1c expression in the livers of streptozotocin-treated mice. Diabetes. 2004;53:560-9.

[70] Frederico MJ, Vitto MF, Cesconetto PA, Engelmann J, De Souza DR, Luz G, et al. Short-term inhibition of SREBP-1c expression reverses diet-induced non-alcoholic fatty liver disease in mice. Scand J Gastroenterol. 2011;46:1381-8.

[71] Amatruda JM, Livingston JN, Lockwood DH. Cellular mechanisms in selected states of insulin resistance: human obesity, glucocorticoid excess, and chronic renal failure. Diabetes/metabolism reviews. 1985;1:293-317.

[72] Kawaguchi T, Takenoshita M, Kabashima T, Uyeda K. Glucose and cAMP regulate the L-type pyruvate kinase gene by phosphorylation/dephosphorylation of the carbohydrate response element binding protein. Proceedings of the National Academy of Sciences of the United States of America. 2001;98:13710-5.

[73] Ishii S, Iizuka K, Miller BC, Uyeda K. Carbohydrate response element binding protein directly promotes lipogenic enzyme gene transcription. Proceedings of the National Academy of Sciences of the United States of America. 2004;101:15597-602.

[74] Li MV, Chang B, Imamura M, Poungvarin N, Chan L. Glucose-dependent transcriptional regulation by an evolutionarily conserved glucose-sensing module. Diabetes. 2006;55:1179-89.

[75] Flowers MT, Miyazaki M, Liu X, Ntambi JM. Probing the role of stearoyl-CoA desaturase-1 in hepatic insulin resistance. The Journal of clinical investigation. 2006;116:1478-81.

[76] Postic C, Dentin R, Denechaud PD, Girard J. ChREBP, a transcriptional regulator of glucose and lipid metabolism. Annual review of nutrition. 2007;27:179-92.

[77] Benhamed F, Denechaud PD, Lemoine M, Robichon C, Moldes M, Bertrand-Michel J, et al. The lipogenic transcription factor ChREBP dissociates hepatic steatosis from insulin resistance in mice and humans. The Journal of clinical investigation. 2012;122:2176-94.

[78] Lloyd MD, Darley DJ, Wierzbicki AS, Threadgill MD. Alpha-methylacyl-CoA racemase--an 'obscure' metabolic enzyme takes centre stage. The FEBS journal. 2008;275:1089-102.

[79] Berg JM TJ, Stryer L. Biochemistry. 5th edition: New York: W H Freeman;; 2002.

[80] Berg JM TJ, Stryer L. Biochemistry. 5th edition: New York: W H Freeman;; 2002.

[81] Alberts B JA, Lewis J, et al. . Molecular Biology of the Cell. 4th edition. New York: Garland Science; 2002.

[82] Marin JL-MaC. Fat Detection: Taste, Texture, and Post Ingestive Effects. Boca Raton (FL): CRC Press; 2010.

[83] Holland WL, Knotts TA, Chavez JA, Wang LP, Hoehn KL, Summers SA. Lipid mediators of insulin resistance. Nutrition reviews. 2007;65:S39-46.

[84] Rutkowski DT, Hegde RS. Regulation of basal cellular physiology by the homeostatic unfolded protein response. J Cell Biol. 2010;189:783-94.

[85] Lee JS, Mendez R, Heng HH, Yang ZQ, Zhang K. Pharmacological ER stress promotes hepatic lipogenesis and lipid droplet formation. Am J Transl Res. 2012;4:102-13.

[86] Schonthal AH. Endoplasmic Reticulum Stress: Its Role in Disease and Novel Prospects for Therapy. Scientifica. 2012;2012:857516.

[87] Booth C, Koch GL. Perturbation of cellular calcium induces secretion of luminal ER proteins. Cell. 1989;59:729-37.

[88] Lodish HF, Kong N. Perturbation of cellular calcium blocks exit of secretory proteins from the rough endoplasmic reticulum. The Journal of biological chemistry. 1990;265:10893-9.

[89] Suzuki CK, Bonifacino JS, Lin AY, Davis MM, Klausner RD. Regulating the retention of T-cell receptor alpha chain variants within the endoplasmic reticulum: Ca(2+)-dependent association with BiP. J Cell Biol. 1991;114:189-205.

[90] Schroder M. Endoplasmic reticulum stress responses. Cellular and molecular life sciences : CMLS. 2008;65:862-94.

[91] Ozcan L, Tabas I. Role of endoplasmic reticulum stress in metabolic disease and other disorders. Annual review of medicine. 2012;63:317-28.

[92] Luo B, Lee AS. The critical roles of endoplasmic reticulum chaperones and unfolded protein response in tumorigenesis and anticancer therapies. Oncogene. 2013;32:805-18.

[93] Lai E, Teodoro T, Volchuk A. Endoplasmic reticulum stress: signaling the unfolded protein response. Physiology. 2007;22:193-201.

[94] Ni M, Lee AS. ER chaperones in mammalian development and human diseases. FEBS Lett. 2007;581:3641-51.

[95] Szegezdi E, Logue SE, Gorman AM, Samali A. Mediators of endoplasmic reticulum stress-induced apoptosis. EMBO Rep. 2006;7:880-5.

[96] Calfon M, Zeng H, Urano F, Till JH, Hubbard SR, Harding HP, et al. IRE1 couples endoplasmic reticulum load to secretory capacity by processing the XBP-1 mRNA. Nature. 2002;415:92-6.

[97] Patil C, Walter P. Intracellular signaling from the endoplasmic reticulum to the nucleus: the unfolded protein response in yeast and mammals. Current opinion in cell biology. 2001;13:349-55.

[98] Travers KJ, Patil CK, Wodicka L, Lockhart DJ, Weissman JS, Walter P. Functional and genomic analyses reveal an essential coordination between the unfolded protein response and ER-associated degradation. Cell. 2000;101:249-58.

[99] Zhang K, Wang S, Malhotra J, Hassler JR, Back SH, Wang G, et al. The unfolded protein response transducer IRE1alpha prevents ER stress-induced hepatic steatosis. The EMBO journal. 2011;30:1357-75.

[100] Iqbal J, Dai K, Seimon T, Jungreis R, Oyadomari M, Kuriakose G, et al. IRE1beta inhibits chylomicron production by selectively degrading MTP mRNA. Cell metabolism. 2008;7:445-55.

[101] Ali MM, Bagratuni T, Davenport EL, Nowak PR, Silva-Santisteban MC, Hardcastle A, et al. Structure of the Ire1 autophosphorylation complex and implications for the unfolded protein response. The EMBO journal. 2011;30:894-905.

[102] Ron D, Walter P. Signal integration in the endoplasmic reticulum unfolded protein response. Nature reviews Molecular cell biology. 2007;8:519-29.

[103] Zhang K, Kaufman RJ. From endoplasmic-reticulum stress to the inflammatory response. Nature. 2008;454:455-62.

[104] Urano F, Wang X, Bertolotti A, Zhang Y, Chung P, Harding HP, et al. Coupling of stress in the ER to activation of JNK protein kinases by transmembrane protein kinase IRE1. Science. 2000;287:664-6.

[105] Lee AH, Iwakoshi NN, Glimcher LH. XBP-1 regulates a subset of endoplasmic reticulum resident chaperone genes in the unfolded protein response. Molecular and cellular biology. 2003;23:7448-59.

[106] Lee K, Tirasophon W, Shen X, Michalak M, Prywes R, Okada T, et al. IRE1-mediated unconventional mRNA splicing and S2P-mediated ATF6 cleavage merge to regulate XBP1 in signaling the unfolded protein response. Genes & development. 2002;16:452-66.

[107] Hetz C, Chevet E, Harding HP. Targeting the unfolded protein response in disease. Nature reviews Drug discovery. 2013;12:703-19.

[108] Upton JP, Wang L, Han D, Wang ES, Huskey NE, Lim L, et al. IRE1alpha cleaves select microRNAs during ER stress to derepress translation of proapoptotic Caspase-2. Science. 2012;338:818-22.

[109] Oikawa D, Kitamura A, Kinjo M, Iwawaki T. Direct association of unfolded proteins with mammalian ER stress sensor, IRE1beta. PloS one. 2012;7:e51290.

[110] Kimata Y, Kohno K. Endoplasmic reticulum stress-sensing mechanisms in yeast and mammalian cells. Current opinion in cell biology. 2011;23:135-42.

[111] Harding HP, Novoa I, Zhang Y, Zeng H, Wek R, Schapira M, et al. Regulated translation initiation controls stress-induced gene expression in mammalian cells. Molecular cell. 2000;6:1099-108.

[112] Harding HP, Zhang Y, Zeng H, Novoa I, Lu PD, Calfon M, et al. An integrated stress response regulates amino acid metabolism and resistance to oxidative stress. Molecular cell. 2003;11:619-33.

[113] Haze K, Yoshida H, Yanagi H, Yura T, Mori K. Mammalian transcription factor ATF6 is synthesized as a transmembrane protein and activated by proteolysis in response to endoplasmic reticulum stress. Molecular biology of the cell. 1999;10:3787-99.

[114] Novoa I, Zeng H, Harding HP, Ron D. Feedback inhibition of the unfolded protein response by GADD34-mediated dephosphorylation of eIF2alpha. J Cell Biol. 2001;153:1011-22.

[115] Hiscutt EL, Hill DS, Martin S, Kerr R, Harbottle A, Birch-Machin M, et al. Targeting X-linked inhibitor of apoptosis protein to increase the efficacy of endoplasmic reticulum stress-induced apoptosis for melanoma therapy. The Journal of investigative dermatology. 2010;130:2250-8.

[116] Yamamoto K, Sato T, Matsui T, Sato M, Okada T, Yoshida H, et al. Transcriptional induction of mammalian ER quality control proteins is mediated by single or combined action of ATF6alpha and XBP1. Developmental cell. 2007;13:365-76.

[117] Flower RJ. Prostaglandins, bioassay and inflammation. British journal of pharmacology. 2006;147 Suppl 1:S182-92.

[118] Shoelson SE, Lee J, Yuan M. Inflammation and the IKK beta/I kappa B/NF-kappa B axis in obesity- and diet-induced insulin resistance. International journal of obesity and related metabolic disorders : journal of the International Association for the Study of Obesity. 2003;27 Suppl 3:S49-52.

[119] Yuan M, Konstantopoulos N, Lee J, Hansen L, Li ZW, Karin M, et al. Reversal of obesity- and diet-induced insulin resistance with salicylates or targeted disruption of Ikkbeta. Science. 2001;293:1673-7.

[120] Steppan CM, Bailey ST, Bhat S, Brown EJ, Banerjee RR, Wright CM, et al. The hormone resistin links obesity to diabetes. Nature. 2001;409:307-12.

[121] Cai D, Yuan M, Frantz DF, Melendez PA, Hansen L, Lee J, et al. Local and systemic insulin resistance resulting from hepatic activation of IKK-beta and NF-kappaB. Nature medicine. 2005;11:183-90.

[122] Shoelson SE, Lee J, Goldfine AB. Inflammation and insulin resistance. The Journal of clinical investigation. 2006;116:1793-801.

[123] Garg AD, Kaczmarek A, Krysko O, Vandenabeele P, Krysko DV, Agostinis P. ER stress-induced inflammation: does it aid or impede disease progression? Trends in molecular medicine. 2012;18:589-98.

[124] Hu P, Han Z, Couvillon AD, Kaufman RJ, Exton JH. Autocrine tumor necrosis factor alpha links endoplasmic reticulum stress to the membrane death receptor pathway through IRE1alpha-mediated NF-kappaB activation and down-regulation of TRAF2 expression. Molecular and cellular biology. 2006;26:3071-84.

[125] Ozcan U, Cao Q, Yilmaz E, Lee AH, Iwakoshi NN, Ozdelen E, et al. Endoplasmic reticulum stress links obesity, insulin action, and type 2 diabetes. Science. 2004;306:457-61.

[126] Davis RJ. Signal transduction by the JNK group of MAP kinases. Cell. 2000;103:239-52.

[127] Deng J, Lu PD, Zhang Y, Scheuner D, Kaufman RJ, Sonenberg N, et al. Translational repression mediates activation of nuclear factor kappa B by phosphorylated translation initiation factor 2. Molecular and cellular biology. 2004;24:10161-8.

[128] Goodall JC, Wu C, Zhang Y, McNeill L, Ellis L, Saudek V, et al. Endoplasmic reticulum stress-induced transcription factor, CHOP, is crucial for dendritic cell IL-23 expression. Proceedings of the National Academy of Sciences of the United States of America. 2010;107:17698-703.

[129] Zhang K, Shen X, Wu J, Sakaki K, Saunders T, Rutkowski DT, et al. Endoplasmic reticulum stress activates cleavage of CREBH to induce a systemic inflammatory response. Cell. 2006;124:587-99.

[130] Samuel VT, Liu ZX, Qu X, Elder BD, Bilz S, Befroy D, et al. Mechanism of hepatic insulin resistance in non-alcoholic fatty liver disease. The Journal of biological chemistry. 2004;279:32345-53.

[131] Flamment M, Hajduch E, Ferre P, Foufelle F. New insights into ER stress-induced insulin resistance. Trends in endocrinology and metabolism: TEM. 2012;23:381-90.

[132] Cao SS, Kaufman RJ. Targeting endoplasmic reticulum stress in metabolic disease. Expert opinion on therapeutic targets. 2013;17:437-48.

[133] Shimomura I, Bashmakov Y, Horton JD. Increased levels of nuclear SREBP-1c associated with fatty livers in two mouse models of diabetes mellitus. The Journal of biological chemistry. 1999;274:30028-32.

[134] Shimomura I, Matsuda M, Hammer RE, Bashmakov Y, Brown MS, Goldstein JL. Decreased IRS-2 and increased SREBP-1c lead to mixed insulin resistance and sensitivity in livers of lipodystrophic and ob/ob mice. Molecular cell. 2000;6:77-86.

[135] Schmitz-Peiffer C, Craig DL, Biden TJ. Ceramide generation is sufficient to account for the inhibition of the insulin-stimulated PKB pathway in C2C12 skeletal muscle cells pretreated with palmitate. The Journal of biological chemistry. 1999;274:24202-10.

[136] Jornayvaz FR, Shulman GI. Diacylglycerol activation of protein kinase Cepsilon and hepatic insulin resistance. Cell metabolism. 2012;15:574-84.

[137] Yahagi N, Shimano H, Hasty AH, Matsuzaka T, Ide T, Yoshikawa T, et al. Absence of sterol regulatory element-binding protein-1 (SREBP-1) ameliorates fatty livers but not obesity or insulin resistance in Lep(ob)/Lep(ob) mice. The Journal of biological chemistry. 2002;277:19353-7.

[138] Dries DR, Gallegos LL, Newton AC. A single residue in the C1 domain sensitizes novel protein kinase C isoforms to cellular diacylglycerol production. The Journal of biological chemistry. 2007;282:826-30.

[139] Samuel VT, Liu ZX, Wang A, Beddow SA, Geisler JG, Kahn M, et al. Inhibition of protein kinase Cepsilon prevents hepatic insulin resistance in nonalcoholic fatty liver disease. The Journal of clinical investigation. 2007;117:739-45.

[140] Neschen S, Morino K, Hammond LE, Zhang D, Liu ZX, Romanelli AJ, et al. Prevention of hepatic steatosis and hepatic insulin resistance in mitochondrial acyl-CoA:glycerol-sn-3-phosphate acyltransferase 1 knockout mice. Cell metabolism. 2005;2:55-65.

[141] Savage DB, Choi CS, Samuel VT, Liu ZX, Zhang D, Wang A, et al. Reversal of diet-induced hepatic steatosis and hepatic insulin resistance by antisense oligonucleotide inhibitors of acetyl-CoA carboxylases 1 and 2. The Journal of clinical investigation. 2006;116:817-24.

[142] Merrill AH, Jr. De novo sphingolipid biosynthesis: a necessary, but dangerous, pathway. The Journal of biological chemistry. 2002;277:25843-6.

[143] Turinsky J, O'Sullivan DM, Bayly BP. 1,2-Diacylglycerol and ceramide levels in insulin-resistant tissues of the rat in vivo. The Journal of biological chemistry. 1990;265:16880-5.

[144] Gorska M, Dobrzyn A, Zendzian-Piotrowska M, Gorski J. Effect of streptozotocin-diabetes on the functioning of the sphingomyelin-signalling pathway in skeletal muscles of the rat. Hormone and metabolic research = Hormon- und Stoffwechselforschung = Hormones et metabolisme. 2004;36:14-21.

[145] Straczkowski M, Kowalska I, Nikolajuk A, Dzienis-Straczkowska S, Kinalska I, Baranowski M, et al. Relationship between insulin sensitivity and sphingomyelin signaling pathway in human skeletal muscle. Diabetes. 2004;53:1215-21.

[146] Chavez JA, Summers SA. A ceramide-centric view of insulin resistance. Cell metabolism. 2012;15:585-94.

[147] Stratford S, DeWald DB, Summers SA. Ceramide dissociates 3'-phosphoinositide production from pleckstrin homology domain translocation. The Biochemical journal. 2001;354:359-68.

[148] Bourbon NA, Yun J, Kester M. Ceramide directly activates protein kinase C zeta to regulate a stress-activated protein kinase signaling complex. The Journal of biological chemistry. 2000;275:35617-23.

[149] Powell DJ, Hajduch E, Kular G, Hundal HS. Ceramide disables 3-phosphoinositide binding to the pleckstrin homology domain of protein kinase B (PKB)/Akt by a PKCzeta-dependent mechanism. Molecular and cellular biology. 2003;23:7794-808.

[150] Teruel T, Hernandez R, Lorenzo M. Ceramide mediates insulin resistance by tumor necrosis factor-alpha in brown adipocytes by maintaining Akt in an inactive dephosphorylated state. Diabetes. 2001;50:2563-71.

[151] Zinda MJ, Vlahos CJ, Lai MT. Ceramide induces the dephosphorylation and inhibition of constitutively activated Akt in PTEN negative U87mg cells. Biochemical and biophysical research communications. 2001;280:1107-15.

[152] Chavez JA, Knotts TA, Wang LP, Li G, Dobrowsky RT, Florant GL, et al. A role for ceramide, but not diacylglycerol, in the antagonism of insulin signal transduction by saturated fatty acids. The Journal of biological chemistry. 2003;278:10297-303.

[153] Salinas M, Lopez-Valdaliso R, Martin D, Alvarez A, Cuadrado A. Inhibition of PKB/Akt1 by C2-ceramide involves activation of ceramide-activated protein phosphatase in PC12 cells. Molecular and cellular neurosciences. 2000;15:156-69.

[154] Teodoro-Morrison T, Schuiki I, Zhang L, Belsham DD, Volchuk A. GRP78 overproduction in pancreatic beta cells protects against high-fat-diet-induced diabetes in mice. Diabetologia. 2013;56:1057-67.

[155] Nakamura T, Furuhashi M, Li P, Cao H, Tuncman G, Sonenberg N, et al. Double-stranded RNA-dependent protein kinase links pathogen sensing with stress and metabolic homeostasis. Cell. 2010;140:338-48.

[156] Hummasti S, Hotamisligil GS. Endoplasmic reticulum stress and inflammation in obesity and diabetes. Circ Res. 2010;107:579-91.

[157] Kammoun HL, Chabanon H, Hainault I, Luquet S, Magnan C, Koike T, et al. GRP78 expression inhibits insulin and ER stress-induced SREBP-1c activation and reduces hepatic steatosis in mice. The Journal of clinical investigation. 2009;119:1201-15.

[158] Ning J, Hong T, Ward A, Pi J, Liu Z, Liu HY, et al. Constitutive role for IRE1alpha-XBP1 signaling pathway in the insulin-mediated hepatic lipogenic program. Endocrinology. 2011;152:2247-55.

[159] Wang D, Wei Y, Schmoll D, Maclean KN, Pagliassotti MJ. Endoplasmic reticulum stress increases glucose-6-phosphatase and glucose cycling in liver cells. Endocrinology. 2006;147:350-8.

[160] Lee AH, Scapa EF, Cohen DE, Glimcher LH. Regulation of hepatic lipogenesis by the transcription factor XBP1. Science. 2008;320:1492-6.

[161] Jurczak MJ, Lee AH, Jornayvaz FR, Lee HY, Birkenfeld AL, Guigni BA, et al. Dissociation of inositol-requiring enzyme (IRE1alpha)-mediated c-Jun N-terminal kinase activation from hepatic insulin resistance in conditional X-box-binding protein-1 (XBP1) knock-out mice. The Journal of biological chemistry. 2012;287:2558-67.

[162] Jurczak MJ, Lee AH, Jornayvaz FR, Lee HY, Birkenfeld AL, Guigni BA, et al. Dissociation of inositol requiring enzyme (IRE1alpha)-mediated JNK activation from hepatic insulin resistance in conditional X-box binding protein-1 (XBP1) knockout mice. The Journal of biological chemistry. 2011.

[163] Timmins JM, Ozcan L, Seimon TA, Li G, Malagelada C, Backs J, et al. Calcium/calmodulin-dependent protein kinase II links ER stress with Fas and mitochondrial apoptosis pathways. The Journal of clinical investigation. 2009;119:2925-41.

[164] Park SW, Zhou Y, Lee J, Lu A, Sun C, Chung J, et al. The regulatory subunits of PI3K, p85alpha and p85beta, interact with XBP-1 and increase its nuclear translocation. Nature medicine. 2010;16:429-37.

[165] Huang J, Tabbi-Anneni I, Gunda V, Wang L. Transcription factor Nrf2 regulates SHP and lipogenic gene expression in hepatic lipid metabolism. American journal of physiology Gastrointestinal and liver physiology. 2010;299:G1211-21.

[166] Oberkofler H, Pfeifenberger A, Soyal S, Felder T, Hahne P, Miller K, et al. Aberrant hepatic TRIB3 gene expression in insulin-resistant obese humans. Diabetologia. 2010;53:1971-5.

[167] Koo SH, Satoh H, Herzig S, Lee CH, Hedrick S, Kulkarni R, et al. PGC-1 promotes insulin resistance in liver through PPAR-alpha-dependent induction of TRB-3. Nature medicine. 2004;10:530-4.

[168] Ohoka N, Yoshii S, Hattori T, Onozaki K, Hayashi H. TRB3, a novel ER stress-inducible gene, is induced via ATF4-CHOP pathway and is involved in cell death. The EMBO journal. 2005;24:1243-55.

[169] Zhang W, Hietakangas V, Wee S, Lim SC, Gunaratne J, Cohen SM. ER stress potentiates insulin resistance through PERK-mediated FOXO phosphorylation. Genes & development. 2013;27:441-9.

[170] Tang X, Shen H, Chen J, Wang X, Zhang Y, Chen LL, et al. Activating transcription factor 6 protects insulin receptor from ER stress-stimulated desensitization via p42/44 ERK pathway. Acta pharmacologica Sinica. 2011;32:1138-47.

[171] Usui M, Yamaguchi S, Tanji Y, Tominaga R, Ishigaki Y, Fukumoto M, et al. Atf6alpha-null mice are glucose intolerant due to pancreatic beta-cell failure on a high-fat diet but partially resistant to diet-induced insulin resistance. Metabolism: clinical and experimental. 2012;61:1118-28.

[172] Bobrovnikova-Marjon E, Hatzivassiliou G, Grigoriadou C, Romero M, Cavener DR, Thompson CB, et al. PERK-dependent regulation of lipogenesis during mouse mammary gland development and adipocyte differentiation. Proceedings of the National Academy of Sciences of the United States of America. 2008;105:16314-9.

[173] Rutkowski DT, Wu J, Back SH, Callaghan MU, Ferris SP, Iqbal J, et al. UPR pathways combine to prevent hepatic steatosis caused by ER stress-mediated suppression of transcriptional master regulators. Developmental cell. 2008;15:829-40.

[174] Ozcan L, Ergin AS, Lu A, Chung J, Sarkar S, Nie D, et al. Endoplasmic reticulum stress plays a central role in development of leptin resistance. Cell metabolism. 2009;9:35-51.

[175] Sharma NK, Das SK, Mondal AK, Hackney OG, Chu WS, Kern PA, et al. Endoplasmic reticulum stress markers are associated with obesity in nondiabetic subjects. The Journal of clinical endocrinology and metabolism. 2008;93:4532-41.

[176] Boden G, Duan X, Homko C, Molina EJ, Song W, Perez O, et al. Increase in endoplasmic reticulum stress-related proteins and genes in adipose tissue of obese, insulin-resistant individuals. Diabetes. 2008;57:2438-44.

[177] Werstuck GH, Lentz SR, Dayal S, Hossain GS, Sood SK, Shi YY, et al. Homocysteine-induced endoplasmic reticulum stress causes dysregulation of the cholesterol and triglyceride biosynthetic pathways. The Journal of clinical investigation. 2001;107:1263-73.

[178] Dietschy JM, Spady DK. Measurement of rates of cholesterol synthesis using tritiated water. Journal of lipid research. 1984;25:1469-76.

[179] Wang S, Chen Z, Lam V, Han J, Hassler J, Finck BN, et al. IRE1alpha-XBP1s induces PDI expression to increase MTP activity for hepatic VLDL assembly and lipid homeostasis. Cell metabolism. 2012;16:473-86.

[180] Sriburi R, Jackowski S, Mori K, Brewer JW. XBP1: a link between the unfolded protein response, lipid biosynthesis, and biogenesis of the endoplasmic reticulum. J Cell Biol. 2004;167:35-41.

[181] Oyadomari S, Harding HP, Zhang Y, Oyadomari M, Ron D. Dephosphorylation of translation initiation factor 2alpha enhances glucose tolerance and attenuates hepatosteatosis in mice. Cell metabolism. 2008;7:520-32.

[182] Ye J, Rawson RB, Komuro R, Chen X, Dave UP, Prywes R, et al. ER stress induces cleavage of membrane-bound ATF6 by the same proteases that process SREBPs. Molecular cell. 2000;6:1355-64.

[183] Zeng L, Lu M, Mori K, Luo S, Lee AS, Zhu Y, et al. ATF6 modulates SREBP2-mediated lipogenesis. The EMBO journal. 2004;23:950-8.

[184] Wu J, Rutkowski DT, Dubois M, Swathirajan J, Saunders T, Wang J, et al. ATF6alpha optimizes long-term endoplasmic reticulum function to protect cells from chronic stress. Developmental cell. 2007;13:351-64.

[185] Yamamoto K, Takahara K, Oyadomari S, Okada T, Sato T, Harada A, et al. Induction of liver steatosis and lipid droplet formation in ATF6alpha-knockout mice burdened with pharmacological endoplasmic reticulum stress. Molecular biology of the cell. 2010;21:2975-86.

[186] Wei Y, Wang D, Topczewski F, Pagliassotti MJ. Saturated fatty acids induce endoplasmic reticulum stress and apoptosis independently of ceramide in liver cells. American journal of physiology Endocrinology and metabolism. 2006;291:E275-81.

[187] Alhusaini S, McGee K, Schisano B, Harte A, McTernan P, Kumar S, et al. Lipopolysaccharide, high glucose and saturated fatty acids induce endoplasmic reticulum stress in cultured primary human adipocytes: Salicylate alleviates this stress. Biochemical and biophysical research communications. 2010;397:472-8.

[188] Ota T, Gayet C, Ginsberg HN. Inhibition of apolipoprotein B100 secretion by lipid-induced hepatic endoplasmic reticulum stress in rodents. The Journal of clinical investigation. 2008;118:316-32.

[189] Ariyama H, Kono N, Matsuda S, Inoue T, Arai H. Decrease in membrane phospholipid unsaturation induces unfolded protein response. The Journal of biological chemistry. 2010;285:22027-35.

[190] Hu FB, van Dam RM, Liu S. Diet and risk of Type II diabetes: the role of types of fat and carbohydrate. Diabetologia. 2001;44:805-17.

[191] Xiao C, Giacca A, Carpentier A, Lewis GF. Differential effects of monounsaturated, polyunsaturated and saturated fat ingestion on glucose-stimulated insulin secretion, sensitivity and clearance in overweight and obese, non-diabetic humans. Diabetologia. 2006;49:1371-9.

[192] Wang L, Folsom AR, Zheng ZJ, Pankow JS, Eckfeldt JH, Investigators AS. Plasma fatty acid composition and incidence of diabetes in middle-aged adults: the Atherosclerosis Risk in Communities (ARIC) Study. The American journal of clinical nutrition. 2003;78:91-8.

[193] Ren LP, Chan SM, Zeng XY, Laybutt DR, Iseli TJ, Sun RQ, et al. Differing endoplasmic reticulum stress response to excess lipogenesis versus lipid oversupply in relation to hepatic steatosis and insulin resistance. PloS one. 2012;7:e30816.

[194] Fu S, Yang L, Li P, Hofmann O, Dicker L, Hide W, et al. Aberrant lipid metabolism disrupts calcium homeostasis causing liver endoplasmic reticulum stress in obesity. Nature. 2011;473:528-31.

[195] Desvergne B, Wahli W. Peroxisome proliferator-activated receptors: nuclear control of metabolism. Endocrine reviews. 1999;20:649-88.

[196] Kersten S, Desvergne B, Wahli W. Roles of PPARs in health and disease. Nature. 2000;405:421-4.

[197] A IJ, Jeannin E, Wahli W, Desvergne B. Polarity and specific sequence requirements of peroxisome proliferator-activated receptor (PPAR)/retinoid X receptor heterodimer binding to DNA. A functional analysis of the malic enzyme gene PPAR response element. The Journal of biological chemistry. 1997;272:20108-17.

[198] Leone TC, Weinheimer CJ, Kelly DP. A critical role for the peroxisome proliferator-activated receptor alpha (PPARalpha) in the cellular fasting response: the PPARalpha-null mouse as a model of fatty acid oxidation disorders. Proceedings of the National Academy of Sciences of the United States of America. 1999;96:7473-8.

[199] Patsouris D, Reddy JK, Muller M, Kersten S. Peroxisome proliferator-activated receptor alpha mediates the effects of high-fat diet on hepatic gene expression. Endocrinology. 2006;147:1508-16.

[200] Keating GM. Fenofibrate: a review of its lipid-modifying effects in dyslipidemia and its vascular effects in type 2 diabetes mellitus. American journal of cardiovascular drugs : drugs, devices, and other interventions. 2011;11:227-47.

[201] Mandard S, Muller M, Kersten S. Peroxisome proliferator-activated receptor alpha target genes. Cellular and molecular life sciences : CMLS. 2004;61:393-416.

[202] Inagaki T, Dutchak P, Zhao G, Ding X, Gautron L, Parameswara V, et al. Endocrine regulation of the fasting response by PPARalpha-mediated induction of fibroblast growth factor 21. Cell metabolism. 2007;5:415-25.

[203] Dreyer C, Krey G, Keller H, Givel F, Helftenbein G, Wahli W. Control of the peroxisomal beta-oxidation pathway by a novel family of nuclear hormone receptors. Cell. 1992;68:879-87.

[204] Castelein H, Gulick T, Declercq PE, Mannaerts GP, Moore DD, Baes MI. The peroxisome proliferator activated receptor regulates malic enzyme gene expression. The Journal of biological chemistry. 1994;269:26754-8.

[205] Miller CW, Ntambi JM. Peroxisome proliferators induce mouse liver stearoyl-CoA desaturase 1 gene expression. Proceedings of the National Academy of Sciences of the United States of America. 1996;93:9443-8.

[206] Tang C, Cho HP, Nakamura MT, Clarke SD. Regulation of human delta-6 desaturase gene transcription: identification of a functional direct repeat-1 element. Journal of lipid research. 2003;44:686-95.

[207] Matsuzaka T, Shimano H, Yahagi N, Amemiya-Kudo M, Yoshikawa T, Hasty AH, et al. Dual regulation of mouse Delta(5)- and Delta(6)-desaturase gene expression by SREBP-1 and PPARalpha. Journal of lipid research. 2002;43:107-14.

[208] Guillou H, Martin P, Jan S, D'Andrea S, Roulet A, Catheline D, et al. Comparative effect of fenofibrate on hepatic desaturases in wild-type and peroxisome proliferator-activated receptor alpha-deficient mice. Lipids. 2002;37:981-9.

[209] Bernardes A, Souza PC, Muniz JR, Ricci CG, Ayers SD, Parekh NM, et al. Molecular mechanism of peroxisome proliferator-activated receptor alpha activation by WY14643: a new mode of ligand recognition and receptor stabilization. Journal of molecular biology. 2013;425:2878-93.

[210] Muoio DM, Way JM, Tanner CJ, Winegar DA, Kliewer SA, Houmard JA, et al. Peroxisome proliferator-activated receptor-alpha regulates fatty acid utilization in primary human skeletal muscle cells. Diabetes. 2002;51:901-9.

[211] Lebensztejn DM. Application of ursodeoxycholic acid (UDCA) in the therapy of liver and biliary duct diseases in children. Medical science monitor : international medical journal of experimental and clinical research. 2000;6:632-6.

[212] Park SJ, Kim TS, Park CK, Lee SH, Kim JM, Lee KS, et al. hCG-induced endoplasmic reticulum stress triggers apoptosis and reduces steroidogenic enzyme expression through activating transcription factor 6 in Leydig cells of the testis. Journal of molecular endocrinology. 2013;50:151-66.

[213] Xie Q, Khaoustov VI, Chung CC, Sohn J, Krishnan B, Lewis DE, et al. Effect of tauroursodeoxycholic acid on endoplasmic reticulum stress-induced caspase-12 activation. Hepatology. 2002;36:592-601.

[214] Ozcan U, Yilmaz E, Ozcan L, Furuhashi M, Vaillancourt E, Smith RO, et al. Chemical chaperones reduce ER stress and restore glucose homeostasis in a mouse model of type 2 diabetes. Science. 2006;313:1137-40.

[215] Lyssiotis CA, Cantley LC. Metabolic syndrome: F stands for fructose and fat. Nature. 2013;502:181-2.

[216] Cordain L, Eaton SB, Sebastian A, Mann N, Lindeberg S, Watkins BA, et al. Origins and evolution of the Western diet: health implications for the 21st century. The American journal of clinical nutrition. 2005;81:341-54.

[217] Elliott SS, Keim NL, Stern JS, Teff K, Havel PJ. Fructose, weight gain, and the insulin resistance syndrome. The American journal of clinical nutrition. 2002;76:911-22.

[218] Lustig RH. Fructose: metabolic, hedonic, and societal parallels with ethanol. Journal of the American Dietetic Association. 2010;110:1307-21.

[219] Bray GA, Nielsen SJ, Popkin BM. Consumption of high-fructose corn syrup in beverages may play a role in the epidemic of obesity. The American journal of clinical nutrition. 2004;79:537-43.

[220] Gaby AR. Adverse effects of dietary fructose. Alternative medicine review : a journal of clinical therapeutic. 2005;10:294-306.

[221] Lim JS, Mietus-Snyder M, Valente A, Schwarz JM, Lustig RH. The role of fructose in the pathogenesis of NAFLD and the metabolic syndrome. Nature reviews Gastroenterology & hepatology. 2010;7:251-64.

[222] Goran MI, Ulijaszek SJ, Ventura EE. High fructose corn syrup and diabetes prevalence: a global perspective. Global public health. 2013;8:55-64.

[223] Faeh D, Minehira K, Schwarz JM, Periasamy R, Park S, Tappy L. Effect of fructose overfeeding and fish oil administration on hepatic de novo lipogenesis and insulin sensitivity in healthy men. Diabetes. 2005;54:1907-13.

[224] Lecoultre V, Egli L, Carrel G, Theytaz F, Kreis R, Schneiter P, et al. Effects of fructose and glucose overfeeding on hepatic insulin sensitivity and intrahepatic lipids in healthy humans. Obesity. 2013;21:782-5.

[225] Stanhope KL, Schwarz JM, Keim NL, Griffen SC, Bremer AA, Graham JL, et al. Consuming fructose-sweetened, not glucose-sweetened, beverages increases visceral adiposity and lipids and decreases insulin sensitivity in overweight/obese humans. The Journal of clinical investigation. 2009;119:1322-34.

[226] Burant CF, Takeda J, Brot-Laroche E, Bell GI, Davidson NO. Fructose transporter in human spermatozoa and small intestine is GLUT5. The Journal of biological chemistry. 1992;267:14523-6.

[227] Mayes PA. Intermediary metabolism of fructose. The American journal of clinical nutrition. 1993;58:754S-65S.

[228] Adelman RC, Ballard FJ, Weinhouse S. Purification and properties of rat liver fructokinase. The Journal of biological chemistry. 1967;242:3360-5.

[229] Samuel VT. Fructose induced lipogenesis: from sugar to fat to insulin resistance. Trends in endocrinology and metabolism: TEM. 2011;22:60-5.

[230] Dani N, Stilla A, Marchegiani A, Tamburro A, Till S, Ladurner AG, et al. Combining affinity purification by ADP-ribose-binding macro domains with mass spectrometry to define the mammalian ADP-ribosyl proteome. Proceedings of the National Academy of Sciences of the United States of America. 2009;106:4243-8.

[231] Cantley JL, Yoshimura T, Camporez JP, Zhang D, Jornayvaz FR, Kumashiro N, et al. CGI-58 knockdown sequesters diacylglycerols in lipid droplets/ER-preventing diacylglycerol-mediated hepatic insulin resistance. Proceedings of the National Academy of Sciences of the United States of America. 2013;110:1869-74.

[232] Chan SM, Sun RQ, Zeng XY, Choong ZH, Wang H, Watt MJ, et al. Activation of PPARalpha ameliorates hepatic insulin resistance and steatosis in high fructose-fed mice despite increased ER stress. Diabetes. 2013;62:2095-105.

[233] Spina RJ, Chi MM, Hopkins MG, Nemeth PM, Lowry OH, Holloszy JO. Mitochondrial enzymes increase in muscle in response to 7-10 days of cycle exercise. Journal of applied physiology. 1996;80:2250-4.

[234] Crumbley C, Wang Y, Banerjee S, Burris TP. Regulation of expression of citrate synthase by the retinoic acid receptor-related orphan receptor alpha (RORalpha). PloS one. 2012;7:e33804.

[235] Molero JC, Waring SG, Cooper A, Turner N, Laybutt R, Cooney GJ, et al. Casitas b-lineage lymphoma-deficient mice are protected against high-fat diet-induced obesity and insulin resistance. Diabetes. 2006;55:708-15.

[236] Lehninger AL, Greville GD. The enzymic oxidation of alpha- and 2-beta-hydroxybutyrate. Biochimica et biophysica acta. 1953;12:188-202.

[237] Cox CL, Stanhope KL, Schwarz JM, Graham JL, Hatcher B, Griffen SC, et al. Consumption of fructose- but not glucose-sweetened beverages for 10 weeks increases circulating concentrations of uric acid, retinol binding protein-4, and gamma-glutamyl transferase activity in overweight/obese humans. Nutrition & metabolism. 2012;9:68.

[238] Nagai S, Dubrana K, Tsai-Pflugfelder M, Davidson MB, Roberts TM, Brown GW, et al. Functional targeting of DNA damage to a nuclear pore-associated SUMO-dependent ubiquitin ligase. Science. 2008;322:597-602.

[239] Vila L, Roglans N, Alegret M, Sanchez RM, Vazquez-Carrera M, Laguna JC. Suppressor of cytokine signaling-3 (SOCS-3) and a deficit of serine/threonine (Ser/Thr) phosphoproteins involved in leptin transduction mediate the effect of fructose on rat liver lipid metabolism. Hepatology. 2008;48:1506-16.

[240] Dolan LC, Potter SM, Burdock GA. Evidence-based review on the effect of normal dietary consumption of fructose on development of hyperlipidemia and obesity in healthy, normal weight individuals. Critical reviews in food science and nutrition. 2010;50:53-84.

[241] Purnell JQ, Fair DA. Fructose ingestion and cerebral, metabolic, and satiety responses. JAMA : the journal of the American Medical Association. 2013;309:85-6.

[242] Goran MI, Dumke K, Bouret SG, Kayser B, Walker RW, Blumberg B. The obesogenic effect of high fructose exposure during early development. Nature reviews Endocrinology. 2013;9:494-500.

[243] Rizza RA. Pathogenesis of fasting and postprandial hyperglycemia in type 2 diabetes: implications for therapy. Diabetes. 2010;59:2697-707.

[244] Samuel VT, Shulman GI. Mechanisms for insulin resistance: common threads and missing links. Cell. 2012;148:852-71.

[245] Monetti M, Levin MC, Watt MJ, Sajan MP, Marmor S, Hubbard BK, et al. Dissociation of hepatic steatosis and insulin resistance in mice overexpressing DGAT in the liver. Cell metabolism. 2007;6:69-78.

[246] Groop L. Pathogenesis of type 2 diabetes: the relative contribution of insulin resistance and impaired insulin secretion. International journal of clinical practice Supplement. 2000:3-13.

[247] Turner N, Hariharan K, TidAng J, Frangioudakis G, Beale SM, Wright LE, et al. Enhancement of muscle mitochondrial oxidative capacity and alterations in insulin action are lipid species dependent: potent tissue-specific effects of medium-chain fatty acids. Diabetes. 2009;58:2547-54.

[248] Zeng XY, Wang YP, Cantley J, Iseli TJ, Molero JC, Hegarty BD, et al. Oleanolic acid reduces hyperglycemia beyond treatment period with Akt/FoxO1-induced suppression of hepatic gluconeogenesis in type-2 diabetic mice. PloS one. 2012;7:e42115.

[249] Hotamisligil GS. Endoplasmic reticulum stress and the inflammatory basis of metabolic disease. Cell. 2010;140:900-17.

[250] Wang H, Sun RQ, Zeng XY, Zhou X, Li S, Jo E, et al. Restoration of Autophagy Alleviates Hepatic ER stress and Impaired Insulin Signalling Transduction in High Fructose-Fed Male Mice. Endocrinology. 2014:en20141454.

[251] Grarup N, Stender-Petersen KL, Andersson EA, Jorgensen T, Borch-Johnsen K, Sandbaek A, et al. Association of variants in the sterol regulatory element-binding factor 1 (SREBF1) gene with type 2 diabetes, glycemia, and insulin resistance: a study of 15,734 Danish subjects. Diabetes. 2008;57:1136-42.

[252] Hirosumi J, Tuncman G, Chang L, Gorgun CZ, Uysal KT, Maeda K, et al. A central role for JNK in obesity and insulin resistance. Nature. 2002;420:333-6.

[253] Stanhope KL, Havel PJ. Fructose consumption: considerations for future research on its effects on adipose distribution, lipid metabolism, and insulin sensitivity in humans. The Journal of nutrition. 2009;139:1236S-41S.

[254] Turner N, Kowalski GM, Leslie SJ, Risis S, Yang C, Lee-Young RS, et al. Distinct patterns of tissue-specific lipid accumulation during the induction of insulin resistance in mice by high-fat feeding. Diabetologia. 2013;56:1638-48.

[255] Park SY, Cho YR, Kim HJ, Higashimori T, Danton C, Lee MK, et al. Unraveling the temporal pattern of diet-induced insulin resistance in individual organs and cardiac dysfunction in C57BL/6 mice. Diabetes. 2005;54:3530-40.

[256] Kaufman RJ, Cao S. Inositol-requiring 1/X-box-binding protein 1 is a regulatory hub that links endoplasmic reticulum homeostasis with innate immunity and metabolism. EMBO molecular medicine. 2010;2:189-92.

[257] Copps KD, White MF. Regulation of insulin sensitivity by serine/threonine phosphorylation of insulin receptor substrate proteins IRS1 and IRS2. Diabetologia. 2012;55:2565-82.

[258] Fu S, Watkins SM, Hotamisligil GS. The role of endoplasmic reticulum in hepatic lipid homeostasis and stress signaling. Cell metabolism. 2012;15:623-34.

[259] Cho EJ, Yoon JH, Kwak MS, Jang ES, Lee JH, Yu SJ, et al. Tauroursodeoxycholic acid attenuates progression of steatohepatitis in mice fed a methionine-choline-deficient diet. Digestive diseases and sciences. 2014;59:1461-74.

[260] Hussain MM, Rava P, Walsh M, Rana M, Iqbal J. Multiple functions of microsomal triglyceride transfer protein. Nutrition & metabolism. 2012;9:14.

[261] Samuel VT, Petersen KF, Shulman GI. Lipid-induced insulin resistance: unravelling the mechanism. Lancet. 2010;375:2267-77.

[262] Maersk M, Belza A, Stodkilde-Jorgensen H, Ringgaard S, Chabanova E, Thomsen H, et al. Sucrose-sweetened beverages increase fat storage in the liver, muscle, and visceral fat depot: a 6-mo randomized intervention study. The American journal of clinical nutrition. 2012;95:283-9.

[263] Liang SH, Zhang W, McGrath BC, Zhang P, Cavener DR. PERK (eIF2alpha kinase) is required to activate the stress-activated MAPKs and induce the expression of immediate-early genes upon disruption of ER calcium homoeostasis. The Biochemical journal. 2006;393:201-9.

[264] Gao Z, Hwang D, Bataille F, Lefevre M, York D, Quon MJ, et al. Serine phosphorylation of insulin receptor substrate 1 by inhibitor kappa B kinase complex. The Journal of biological chemistry. 2002;277:48115-21.

[265] Chakravarthy MV, Lodhi IJ, Yin L, Malapaka RR, Xu HE, Turk J, et al. Identification of a physiologically relevant endogenous ligand for PPARalpha in liver. Cell. 2009;138:476-88.

[266] Oosterveer MH, Grefhorst A, van Dijk TH, Havinga R, Staels B, Kuipers F, et al. Fenofibrate simultaneously induces hepatic fatty acid oxidation, synthesis, and elongation in mice. The Journal of biological chemistry. 2009;284:34036-44.

[267] Lalloyer F, Wouters K, Baron M, Caron S, Vallez E, Vanhoutte J, et al. Peroxisome proliferator-activated receptor-alpha gene level differently affects lipid metabolism and inflammation in apolipoprotein E2 knock-in mice. Arteriosclerosis, thrombosis, and vascular biology. 2011;31:1573-9.

[268] Anderlova K, Dolezalova R, Housova J, Bosanska L, Haluzikova D, Kremen J, et al. Influence of PPAR-alpha agonist fenofibrate on insulin sensitivity and selected adipose tissue-derived hormones in obese women with type 2 diabetes. Physiol Res. 2007;56:579-86.

[269] Kersten S, Seydoux J, Peters JM, Gonzalez FJ, Desvergne B, Wahli W. Peroxisome proliferator-activated receptor alpha mediates the adaptive response to fasting. The Journal of clinical investigation. 1999;103:1489-98.

[270] Arkan MC, Hevener AL, Greten FR, Maeda S, Li ZW, Long JM, et al. IKK-beta links inflammation to obesity-induced insulin resistance. Nature medicine. 2005;11:191-8.

[271] Reddy JK, Goel SK, Nemali MR, Carrino JJ, Laffler TG, Reddy MK, et al. Transcription regulation of peroxisomal fatty acyl-CoA oxidase and enoyl-CoA hydratase/3-hydroxyacyl-CoA dehydrogenase in rat liver by peroxisome proliferators. Proceedings of the National Academy of Sciences of the United States of America. 1986;83:1747-51.

[272] Wanders RJ, Waterham HR. Biochemistry of mammalian peroxisomes revisited. Annual review of biochemistry. 2006;75:295-332.

[273] Reddy JK, Rao MS. Lipid metabolism and liver inflammation. II. Fatty liver disease and fatty acid oxidation. American journal of physiology Gastrointestinal and liver physiology. 2006;290:G852-8.

[274] Ye JM, Doyle PJ, Iglesias MA, Watson DG, Cooney GJ, Kraegen EW. Peroxisome proliferator-activated receptor (PPAR)-alpha activation lowers muscle lipids and improves insulin sensitivity in high fat-fed rats: comparison with PPAR-gamma activation. Diabetes. 2001;50:411-7.

[275] Stanhope KL. Role of fructose-containing sugars in the epidemics of obesity and metabolic syndrome. Annual review of medicine. 2012;63:329-43.

[276] Yu C, Chen Y, Cline GW, Zhang D, Zong H, Wang Y, et al. Mechanism by which fatty acids inhibit insulin activation of insulin receptor substrate-1 (IRS-1)-associated phosphatidylinositol 3-kinase activity in muscle. The Journal of biological chemistry. 2002;277:50230-6.

[277] Bruce CR, Hoy AJ, Turner N, Watt MJ, Allen TL, Carpenter K, et al. Overexpression of carnitine palmitoyltransferase-1 in skeletal muscle is sufficient to enhance fatty acid oxidation and improve high-fat diet-induced insulin resistance. Diabetes. 2009;58:550-8.

[278] Achard CS, Laybutt DR. Lipid-induced endoplasmic reticulum stress in liver cells results in two distinct outcomes: adaptation with enhanced insulin signaling or insulin resistance. Endocrinology. 2012;153:2164-77.

[279] Petersen KF, Dufour S, Befroy D, Lehrke M, Hendler RE, Shulman GI. Reversal of nonalcoholic hepatic steatosis, hepatic insulin resistance, and hyperglycemia by moderate weight reduction in patients with type 2 diabetes. Diabetes. 2005;54:603-8.

[280] Volmer R, van der Ploeg K, Ron D. Membrane lipid saturation activates endoplasmic reticulum unfolded protein response transducers through their transmembrane domains. Proceedings of the National Academy of Sciences of the United States of America. 2013;110:4628-33.

[281] Surwit RS, Kuhn CM, Cochrane C, McCubbin JA, Feinglos MN. Diet-induced type II diabetes in C57BL/6J mice. Diabetes. 1988;37:1163-7.

[282] Winzell MS, Ahren B. The high-fat diet-fed mouse: a model for studying mechanisms and treatment of impaired glucose tolerance and type 2 diabetes. Diabetes. 2004;53 Suppl 3:S215-9.

[283] Jelinek D, Castillo JJ, Arora SL, Richardson LM, Garver WS. A high-fat diet supplemented with fish oil improves metabolic features associated with type 2 diabetes. Nutrition. 2013;29:1159-65.

[284] Shimomura I, Shimano H, Korn BS, Bashmakov Y, Horton JD. Nuclear sterol regulatory element-binding proteins activate genes responsible for the entire program of unsaturated fatty acid biosynthesis in transgenic mouse liver. The Journal of biological chemistry. 1998;273:35299-306.

[285] Horton JD, Shimomura I, Brown MS, Hammer RE, Goldstein JL, Shimano H. Activation of cholesterol synthesis in preference to fatty acid synthesis in liver and adipose tissue of transgenic mice overproducing sterol regulatory element-binding protein-2. The Journal of clinical investigation. 1998;101:2331-9.

[286] Horton JD, Goldstein JL, Brown MS. SREBPs: activators of the complete program of cholesterol and fatty acid synthesis in the liver. The Journal of clinical investigation. 2002;109:1125-31.

[287] Ye JM, Iglesias MA, Watson DG, Ellis B, Wood L, Jensen PB, et al. PPARalpha /gamma ragaglitazar eliminates fatty liver and enhances insulin action in fat-fed rats in the absence of hepatomegaly. American journal of physiology Endocrinology and metabolism. 2003;284:E531-40.

[288] Kim S, Sohn I, Ahn JI, Lee KH, Lee YS, Lee YS. Hepatic gene expression profiles in a long-term high-fat diet-induced obesity mouse model. Gene. 2004;340:99-109.

[289] Dentin R, Girard J, Postic C. Carbohydrate responsive element binding protein (ChREBP) and sterol regulatory element binding protein-1c (SREBP-1c): two key regulators of glucose metabolism and lipid synthesis in liver. Biochimie. 2005;87:81-6.

[290] Dobrosotskaya IY, Seegmiller AC, Brown MS, Goldstein JL, Rawson RB. Regulation of SREBP processing and membrane lipid production by phospholipids in Drosophila. Science. 2002;296:879-83.

[291] Gregor MF, Yang L, Fabbrini E, Mohammed BS, Eagon JC, Hotamisligil GS, et al. Endoplasmic reticulum stress is reduced in tissues of obese subjects after weight loss. Diabetes. 2009;58:693-700.

[292] Appenzeller-Herzog C, Hall MN. Bidirectional crosstalk between endoplasmic reticulum stress and mTOR signaling. Trends in cell biology. 2012;22:274-82.

[293] Qin L, Wang Z, Tao L, Wang Y. ER stress negatively regulates AKT/TSC/mTOR pathway to enhance autophagy. Autophagy. 2010;6:239-47.

[294] Ding WX, Yin XM. Sorting, recognition and activation of the misfolded protein degradation pathways through macroautophagy and the proteasome. Autophagy. 2008;4:141-50.

[295] Sharma M, Urano F, Jaeschke A. Cdc42 and Rac1 are major contributors to the saturated fatty acid-stimulated JNK pathway in hepatocytes. Journal of hepatology. 2012;56:192-8.

[296] Rahman SM, Qadri I, Janssen RC, Friedman JE. Fenofibrate and PBA prevent fatty acid-induced loss of adiponectin receptor and pAMPK in human hepatoma cells and in hepatitis C virus-induced steatosis. Journal of lipid research. 2009;50:2193-202.

[297] Qiu W, Zhang J, Dekker MJ, Wang H, Huang J, Brumell JH, et al. Hepatic autophagy mediates endoplasmic reticulum stress-induced degradation of misfolded apolipoprotein B. Hepatology. 2011;53:1515-25.

[298] Hoyer-Hansen M, Jaattela M. Connecting endoplasmic reticulum stress to autophagy by unfolded protein response and calcium. Cell death and differentiation. 2007;14:1576-82.

[299] Yang L, Li P, Fu S, Calay ES, Hotamisligil GS. Defective hepatic autophagy in obesity promotes ER stress and causes insulin resistance. Cell metabolism. 2010;11:467-78.

[300] Schewe DM, Aguirre-Ghiso JA. ATF6alpha-Rheb-mTOR signaling promotes survival of dormant tumor cells in vivo. Proceedings of the National Academy of Sciences of the United States of America. 2008;105:10519-24.

[301] Rebollo A, Roglans N, Alegret M, Laguna JC. Way back for fructose and liver metabolism: bench side to molecular insights. World journal of gastroenterology : WJG. 2012;18:6552-9.